

UNCLASSIFIED

AD **405 162**

DEFENSE DOCUMENTATION CENTER

FOR

SCIENTIFIC AND TECHNICAL INFORMATION

CAMERON STATION, ALEXANDRIA, VIRGINIA



UNCLASSIFIED

NOTICE: When government or other drawings, specifications or other data are used for any purpose other than in connection with a definitely related government procurement operation, the U. S. Government thereby incurs no responsibility, nor any obligation whatsoever; and the fact that the Government may have formulated, furnished, or in any way supplied the said drawings, specifications, or other data is not to be regarded by implication or otherwise as in any manner licensing the holder or any other person or corporation, or conveying any rights or permission to manufacture, use or sell any patented invention that may in any way be related thereto.

405162

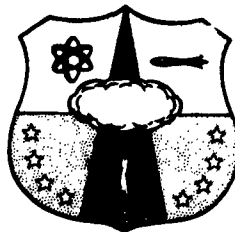
AFSWC-TDR-62-153

63-3-5
SWC
TDR
62-153

EXPERIMENTS ON THE MEASUREMENT OF THE
RESPONSE OF ROCK TO DYNAMIC LOADS

TECHNICAL DOCUMENTARY REPORT NO. AFSWC-TDR-62-153

March 1963

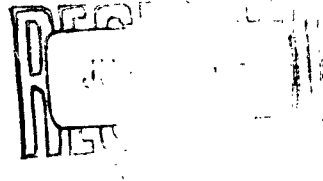


Research Directorate
AIR FORCE SPECIAL WEAPONS CENTER
Air Force Systems Command
Kirtland Air Force Base
New Mexico

This research has been funded by the Defense Atomic Support Agency
under WEB No. 13.145

Project No. 1080, Task No. 108001

(Prepared under Contract No. AF 29(601)-2821
by Rodney D. Caudle and George B. Clark,
University of Missouri School of Mines and
Metallurgy, Rolla, Missouri.)



**HEADQUARTERS
AIR FORCE SPECIAL WEAPONS CENTER
Air Force Systems Command
Kirtland Air Force Base
New Mexico**

When Government drawings, specifications, or other data are used for any purpose other than in connection with a definitely related Government procurement operation, the United States Government thereby incurs no responsibility nor any obligation whatsoever; and the fact that the Government may have formulated, furnished, or in any way supplied the said drawings, specifications, or other data, is not to be regarded by implication or otherwise as in any manner licensing the holder or any other person or corporation, or conveying any rights or permission to manufacture, use, or sell any patented invention that may in any way be related thereto.

This report is made available for study upon the understanding that the Government's proprietary interests in and relating thereto shall not be impaired. In case of apparent conflict between the Government's proprietary interests and those of others, notify the Staff Judge Advocate, Air Force Systems Command, Andrews AF Base, Washington 25, DC.

This report is published for the exchange and stimulation of ideas; it does not necessarily express the intent or policy of any higher headquarters.

Qualified requesters may obtain copies of this report from ASTIA. Orders will be expedited if placed through the librarian or other staff member designated to request and receive documents from ASTIA.

FOREWORD

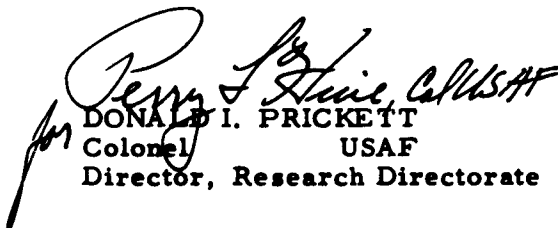
This document is the final report on a research project accomplished by the University of Missouri School of Mines and Metallurgy under Air Force Contract AF 29(601)-2821. This contract called for research in two separate phases of the rock-dynamics area. The earlier phase of the contract resulted in a study of the problems associated with protective construction in rock, particularly deep protective structures. That study is reported in AFSWC TDR-61-93, entitled Geologic Structure Stability and Deep Protective Construction. The present study is a direct outgrowth of the earlier one. The ultimate goal of the later study is the development in the laboratory of instrumentation techniques to measure those parameters which describe the response of rock to dynamic loadings such as could be produced by the detonation of a nuclear weapon. The study was made under the general direction of Dr. G. B. Clark, Director. Mr. R. D. Caudle was in charge of the experimental study and performed the numerical calculations and presented the results. Laboratory technicians and graduate assistants participated in gage and specimen construction and field experiments. The support of the Air Force in sponsoring this study is gratefully acknowledged.

ABSTRACT

The purpose of this study was the development of instrumentation techniques to measure dynamic stress and strain within rock subjected to impulse-type loads. These techniques were to be applicable to the determination of rock response to nuclear explosive loadings. Electric resistance strain gages and piezoelectric stress gages were the sensing devices utilized. Transducers were embedded in concrete test cylinders which were loaded by a plane wave generated by an HE explosive. The sensitivity of the piezoelectric gages utilized was too great for the stress intensities developed, and therefore satisfactory evaluation of the stress measuring technique was not possible. The material presented, summarizing the theoretical aspects of stress and strain measurement at an interior point in a solid, may prove valuable in future embedded gage installations.

PUBLICATION REVIEW

This report has been reviewed and is approved.


DONALD I. PRICKEIT
Colonel USAF
Director, Research Directorate

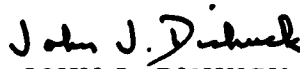

JOHN J. DISHUCK
Colonel USAF
DCS/Plans & Operations

TABLE OF CONTENTS

INTRODUCTION	1
EXPERIMENTAL PROCEDURE	3
Preparation of Embedded Strain Gages	3
Preparation of Embedded Stress Gages	7
Plane Stress Wave Generator	11
Strain Gage Instrumentation	13
Stress Gage Instrumentation	14
Oscilloscope Triggering	15
Static Test Procedure	15
Low-Level Transient Procedure	16
High Intensity Dynamic Test Procedure	17
CONCLUSIONS AND RECOMMENDATIONS	21
REFERENCES	23
APPENDIX A: DYNAMIC STRAIN MEASUREMENT WITH RESISTANCE GAGES	A.1
The Potentiometric Strain Gage Circuit	A.1
Circuit loading	A.7
Inaccuracies due to lead wires	A.10
The Electric Resistance Strain Gage	A.20
Strain transmission to gages	A.20
Local reinforcement and impedance matching	A.24
Gage-length effects	A.26
Static strain gradient	A.27
Dynamic strain gradient	A.27
Nonhomogeneous material	A.33
Gage Current	A.35
Measurement System Response	A.37
The Shunt-Calibration Method	A.38
Lead wire resistance effect	A.39
Calibration switching speed	A.41
Determination of system bandwidth	A.42
References	A.44
APPENDIX B: DYNAMIC STRESS MEASUREMENT WITH PIEZO- ELECTRIC GAGES	B.1
Piezoelectric Materials	B.1
Piezoelectric strain constant	B.3
Permittivity	B.5
Piezoelectric voltage constant	B.5
Resistivity	B.6
Internal mechanical damping	B.7
Elastic constants	B.8
Density	B.8

APPENDIX C: EXPERIMENTAL DATA	C-1
DISTRIBUTION	D-1

LIST OF ILLUSTRATIONS

Figure No.		Page
1.	Portland cement mortar discs, showing location of strain gages and piezoelectric gages	5
2.	Sketch of completed stress gage, showing PZT-4 disc, steel shell, epoxy resin covering electrodes, and RTV-40 silicone rubber isolating material	10
3.	Sketch of instrumented cylinder in test position, showing wave shaper and sand embankment	10
4.	Six-inch diameter Portland cement mortar test cylinders used in all instrumented tests. From left to right; cylinder after incomplete wave-shaper detonation; cylinder tested with layer of celotex for wave attenuation; and specimen before testing	12
5.	Oscilloscope trigger circuit used in high level transient tests	12
A.1	Variations of the basic potentiometric circuit	A-4
A.2	Effect of applied strain and ballast resistance-gage resistance ratio of a potentiometric circuit output linearity	A-6
A.3	Output of potentiometric circuit and voltage input as a function of the ratio of ballast resistance to gage resistance for varying gage currents	A-8
A.4	Output of potentiometric circuit vs. gage resistance (gage current held constant at 0.25 ma) for various applied voltages	A-9
A.5	Apparent strain error due to lead wire resistance as a function of the ratio of ballast resistance to gage resistance for various lead-wire strain-gage resistance ratios	A-13
A.6	Ratio of lead-wire resistance to strain-gage resistance as a function of wire gage for various gage resistance	A-14
A.7	Response of low-pass filter to normalized ramp voltage of finite duration showing rise time and delay time	A-17

A.8	Rise time and delay time of low-pass filter response to a finite ramp input vs. upper 3db frequency-ramp duration product	A-18
A.9	Idealized strain distribution in a single strain-sensitive filament in an adhesive layer	A-22
A.10	The effect of gage length and gage center location on the accuracy of static strain readings in regions of high-strain gradient	A-28
A.11	A comparison of frequency response curves for low-pass filter and strain gage of length L subjected to a standing or traveling wave of frequency f	A-30
A.12	Strain gage errors for various ratios of gage length to nominal maximum aggregate size	A-34
A.13	Output response of measuring system to chopper-controlled calibrating resistor	A-34
B.1	Variation of piezoelectric voltage and strain constants and planar coupling coefficient of PZT-4 with temperature	B-4
B.2	Variation of dielectric constant, frequency constant and dielectric loss angle of PZT-4 with temperature	B-4
B.3	Ageing effects in lead zirconate titanate ceramic, PZT-4	B-9
B.4	Ageing effect in lead zirconate titanate ceramic, PZT-5	B-9
B.5	Short-circuit charge output of lead zirconate titanate discs subjected to intense plane waves . . .	B-13
B.6	Short-circuit charge output of PZT discs subjected to intense plane waves plotted to an expanded pressure scale, together with "transient" and "static" test results	B-13
B.7	Influence of transducer shape and modulus on static stress concentration factor	B-22
B.8	Thin-walled elastic cylinder in an infinite medium subjected to a uniform uniaxial stress field	B-22

B.9	Influence of the wall thickness of an embedded elastic cylinder on the tangential stress concentration factor in the surrounding medium	B-27
B.10	Electrical models utilized in obtaining the piezoelectric response of an infinite plate sandwiched between two half-spaces	B-31
B.11	Response of piezoelectric plate to ramp stress wave (Plate impedance matched to surrounding medium) . . .	B-34
B.12	Simplified piezoelectric gage input circuit and modification for "Q-step" calibration	B-44
C.1 - C.24	Experimental Data	C.2 - C.13

LIST OF TABLES

Table No.	Page
I. Properties of Cured Stycast 2662	6
II. Properties of PZT-4 Ceramic	9

INTRODUCTION

The purpose of this study was to devise experimental techniques for measurement of the parameters describing the dynamic response of rock to impulse type loads to implement the Air Force protective construction research program. Although the real problem of protective construction is concerned with the high pressures and long pressure durations produced by large nuclear weapons explosions, small HE charges with resultant pressures and short durations were used in this investigation because of present limitations. The experimental techniques developed under laboratory conditions should be applicable in study of full scale problems.

Tests reported herein were to devise and perform experiments to develop an instrumentation technique to measure dynamic stress and strain on and within rock when loaded by pressure waves with wide ranges of amplitudes. Portland cement mortar was selected as the medium in which all preliminary investigations were to be made, since mechanical properties are readily reproducible, and rock-like properties are obtained. Standard 6-inch diameter by 12-inch long concrete test cylinders were utilized in all tests. In tests at high levels of transient stress, a plane wave was produced at one end of the test cylinder. Embedded electric-resistance strain gages and piezoelectric stress gages detected the radial and tangential strain and stress in the vicinity of a point on the axis of the cylinder. If accurate measurements of the strain and stress conditions at a point had been obtained, many of the questions concerning the transient behavior of the mortar, and ultimately of rock, could be solved.

The principal problems encountered in these tests were (1) devising embedded stress and strain gages which would provide reliable data at the high stress levels and short wave lengths encountered in the laboratory tests, and (2) obtaining reproducible plane waves in the mortar cylinders.

As a consequence of the problems of devising and calibrating embedded stress and strain gages, the literature surveys and analyses reported in Appendix A, "Dynamic Strain Measurement with Resistance Gages," and Appendix B, "Dynamic Stress Measurement with Piezoelectric Gages" were performed. These appendices are not intended to be comprehensive but rather to provide criteria against which data obtained by these measuring techniques could be evaluated. These sections are of particular interest since detailed description of the design and behavior of piezoelectric stress-measuring systems is not available elsewhere at the present time. The analogies of gage-length effects to electronic-filter circuit response have not been previously published, and the effect of lead-wire resistance upon calibration error using the "shunt resistance" technique has been grossly underestimated in previous analyses reported in the literature.

EXPERIMENTAL PROCEDURE

The model preparation consisted of construction of strain and stress gages, fabrication of an instrumented mortar disc, and casting the disc in a large mortar cylinder. Wave shapers were constructed from sheet explosive and DuPont line-wave generators. Experimental data were obtained from static tests, low-level transient stress tests and high-level transient stress tests.

Preparation of Embedded Strain Gages

Dentronic No. 204 foil gages were used as components of the embedded strain gages. These gages of "Advance" alloy metal foil (45% Ni., 55% Cu. approx.) have a foil thickness of 0.0001 to 0.0005 inch. Gage length is 0.25 inch, with overall dimensions of 0.60-inch long by 0.29-inch wide. The gage is attached to a laminated base consisting of layers of high-dielectric cellulose fibers impregnated with epoxy resin, providing a high modulus of elasticity. Total thickness of the foil plus backing is less than 0.002 inch. The manufacturer's listed gage factor is 2.08.

The manufacturer states that "the etching process employed by all competitive foil gage manufacturers undercuts the grid strands and produces jagged irregularities due to preferential etching along crystal or grain boundaries. This inherent flaw in etched gages causes stress concentrations. Denfoil gages show no such weakness, notably in dynamic testing." The authors did not have at their disposal the means of evaluating this statement, although it does appear to have merit. The difference among foil gages of various manufacturers of the type and gage length chosen was not expected to produce significant differences

in the results of this particular problem.

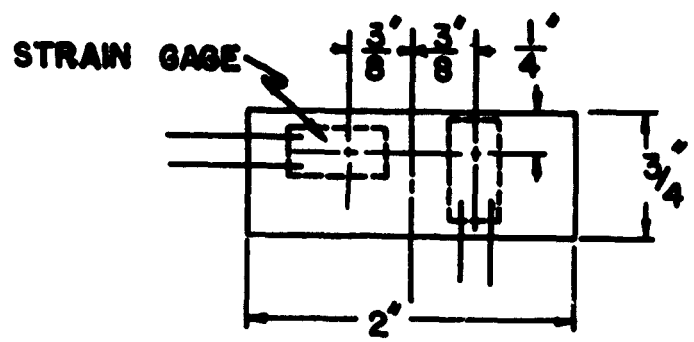
The grains of sand in the mortar chosen had an upper limit of about 0.035-inch diameter. A gage length of 0.25 inch provided better than the ten diameters recommended in Appendix A as the minimum value for accurate averaging of strain between grains.

The gages were glued between slabs of pre-cast mortar, which were later embedded, together with attached leads, in standard mortar test cylinders. Slabs of pre-cast mortar were obtained by first removing 2-inch diameter cores with a laboratory diamond core drill from cured mortar cylinders of the same composition as the final test specimens. Slabs 3/4-inch thick by 2-inch diameter cut from these mortar cores were split along a diameter to give two half-circular slabs. The diametral surface was ground on a carborundum wheel to provide a smooth surface for gage bonding. Since water was used as a coolant during drilling and cutting, the slabs were dried in an oven at 100° centigrade for 48 hours, before the foil gages were attached.

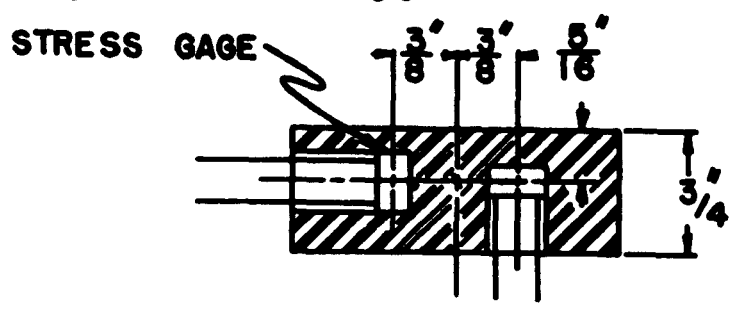
The foil strain gages were bonded to the diametral plane of one of the half-circular slabs of mortar after drying, as shown in Figure 1 (a). The adhesive used was Emerson and Duming Stycast 2662 with Catalyst 14. Stycast 2662 is an epoxy resin which is used for embeddings, as a high-temperature sealer, surface coating, or adhesive. According to the manufacturer its shrinkage during cure is negligible. Properties of cured Stycast 2662, Emerson and Cumming Tech. Bul. 7-2-11, pertinent to strain measurements are given in Table I.

The thoroughly mixed adhesive was heated to 158° F. (70° C.) in a water bath to decrease the viscosity of the mixture to facilitate removal

- (a) Diametral plane showing location of foil strain-gages.
(Ground Surface)



- (b) Diametral cross-section showing location of cylindrical piezoelectric stress gages.



- (c) Plan view of mortar disc showing gage location.

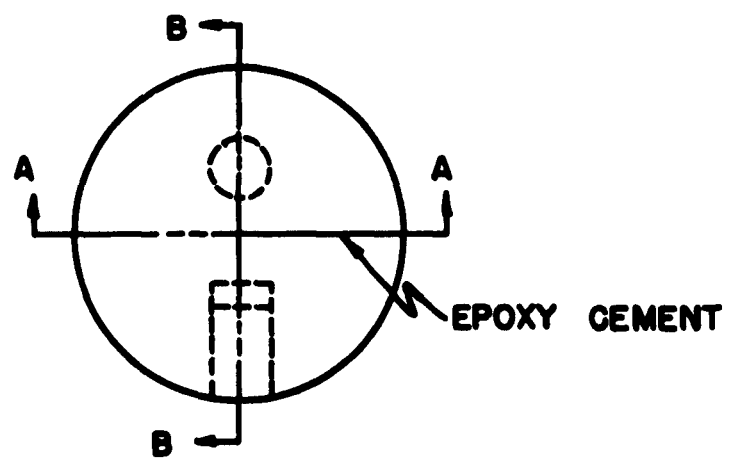


Figure 1: Portland cement mortar discs, showing location of strain gages and piezoelectric gages.

TABLE I¹Properties of Cured Stycast 2662

PHYSICAL

Specific Gravity	1.5
Flexural Strength	
at 70°F. (21°C.)	14,500 psi (1,020 Kg/cm ²)
at 300°F. (149°C.)	10,700 psi (752 Kg/cm ²)
Flexural Modulus	
at 70°F. (21°C.)	0.65 x 10 ⁶ psi (4.57 x 10 ⁴ Kg/cm ²)
at 300°F. (149°C.)	0.43 x 10 ⁶ psi (3.0 x 10 ⁴ Kg/cm ²)
Izod Impact, ft. lbs./in. of notch	0.44
Coefficient of Thermal Expansion	
per °C.	28 x 10 ⁻⁶
Water Absorption (% gain at 25°C., 24 hrs.)	0.1
Machinability - good, use carbide tools	

ELECTRICAL

<u>Frequency</u> <u>CPS</u>	<u>Temp</u> <u>°F</u>	<u>Temp</u> <u>°C</u>	<u>Dielectric</u> <u>Constant</u>	<u>Dissipation</u> <u>Factor</u>
60	70	21	3.9	.008
	300	149	4.1	.009
10 ⁶	70	21	3.5	.009
	300	149	3.6	.007
10 ⁹	70	21	3.0	.011
	300	149	3.2	.010
Dielectric Strength, volts/mil			70°F. (21°C.)	420
			300°F. (149°C.)	370
Volume Resistivity, ohm-cm.			70°F. (21°C.)	10 ¹⁶
			300°F. (149°C.)	10 ¹⁴
			500°F. (260°C.)	10 ¹¹

of trapped air bubbles. A thin layer of warm adhesive was then applied to one slab (straight from the drying oven); then two gages, one parallel and the other perpendicular to the axis of the slab, were pressed into its surface. The center of each gage was placed $3/8$ inch from the center of the diametral plane and $1/4$ inch from its upper surface. Teflon sheet was then applied over the gage surfaces and covered by a second sheet, overlying the entire area. The gage slab was then bound with elastic bands to the half-circular slab from which it had been cut previously, providing a uniform pressure over the gage surface. The gage assembly was then cured for 3 hours at 100°C . Lead wires of thermoplastic-insulated No. 32 A.W.G. solid copper were then soldered to the foil tabs. The mating-half slab was grooved to accept the wires, coated with a thin layer of adhesive, and pressed firmly against the other half slab. The assembly was returned to a 100°C . oven for 3 hours. This procedure usually provided adequate bonding of the wire insulation to the epoxy around the gages.

This procedure results in a glue-strain-gage plane less than $1/32$ -inch thick with greater tensile strength than that of the mortar mix. Since the glue line is extremely thin compared to the wave length of the transient being measured, mismatch of the modulus of elasticity and density of the adhesive do not have any appreciable effect upon the strain distribution or the gage response.

Piezoelectric gages were added to the instrumented mortar slabs at this point, if stresses as well as strains were to be measured.

Preparation of Embedded Stress Gages

The sensing element of the piezoelectric stress gages was a

Clevite 4100-4 disc 0.25-inch diameter by 0.100-inch thick. The 4100-4 element is a modified lead-zirconate-titanate polycrystalline ceramic, designated as PZT-4. It has high strain capacity and temperature stability. Nominal electromechanical specifications are given in Table II.

Lead wires were soldered to the silvered electrodes on the disc faces, and then the ceramic elements were placed in steel molds a few thousandths larger in diameter than the disc. Epoxy casting resin (Stycast 2662) 0.035-inch thick, was molded onto the two faces of the disc, to insulate the electrodes. The gages were heated to 100°C during this procedure (PZT-4 Curie temperature is above 300°C.). The gage element was then centered inside a thin-walled steel cylinder the same length as the ceramic plus epoxy ends. The steel cylinder dimensions were inside diameter 0.316 inch, outside diameter 0.377 inch and length 0.175 inch. The purpose of the steel cylinder was to isolate the stress gage from the lateral stresses, since the cross-sensitivity factor (ratio of vertical to horizontal voltage output under hydrostatic conditions) of the PZT-4 element was -0.69 as calculated in Appendix B. The cylinder wall thickness was chosen to minimize the static tangential-stress concentration factor at the mortar/steel boundary, as described in Appendix B. The space between the ceramic element and the steel shell was filled with RTV-40 silicone rubber, a low modulus, relatively inert material. The finished stress gage is illustrated in Figure 2. Overall dimensions are 0.377-inch diameter by 0.175-inch long.

The finished stress gages were cemented in 3/8-inch holes drilled in the same mortar discs in which strain gages had been mounted previously. The stress gages were mounted, one perpendicular and the other

TABLE II²Properties of PZT-4 Ceramic

Coupling coefficients - $K_{33} = 0.64$; $K_{31} = 0.30$; $K_p = 0.52$

Piezoelectric constant - $d_{33} = 255$; $d_{31} = 110$; $g_{33} = 24.0$; $g_{31} = 10.4$

Free dielectric constant - $K = 1200$

Frequency constants - $N_1 = 1650$, $N_3 = 2000$

Short-circuit elastic constants - $Y_{11}^E = 8.15$, $Y_{33}^E = 6.7$, $Y_{44}^E = 2.6$

Density, $\rho = 7.5$

Mechanical - $Q = 600$

Curie Point - $> 300^\circ$

where d = resulting strain/applied field in 10^{-12} meters/volt

g = resulting field/applied stress in 10^{-3} volt-meters/newton

$N_1 = lf_r$, cycle meters/second, where l = length of a slim expander bar

$N_3 = tf_r$, where t = thickness of a thin expander plate

Y = modulus in 10^{10} newton/meter²

ρ = density in 10^3 Kg/meter³

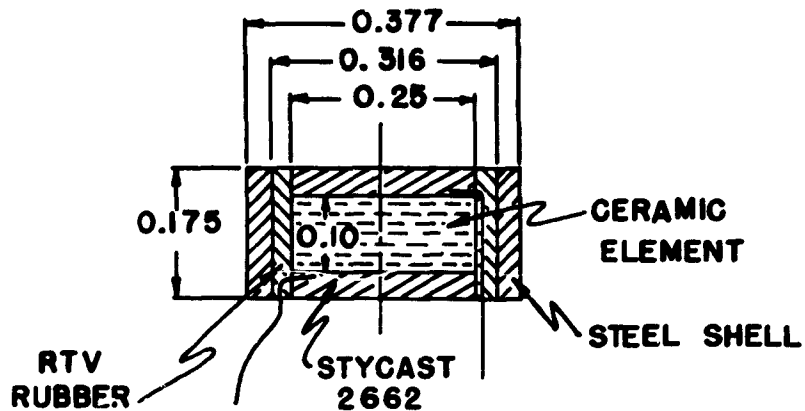


Figure 2: Sketch of completed stress gage showing PZT-4 disc, steel shell, epoxy resin covering electrodes, and RTV-40 silicone rubber isolating material.

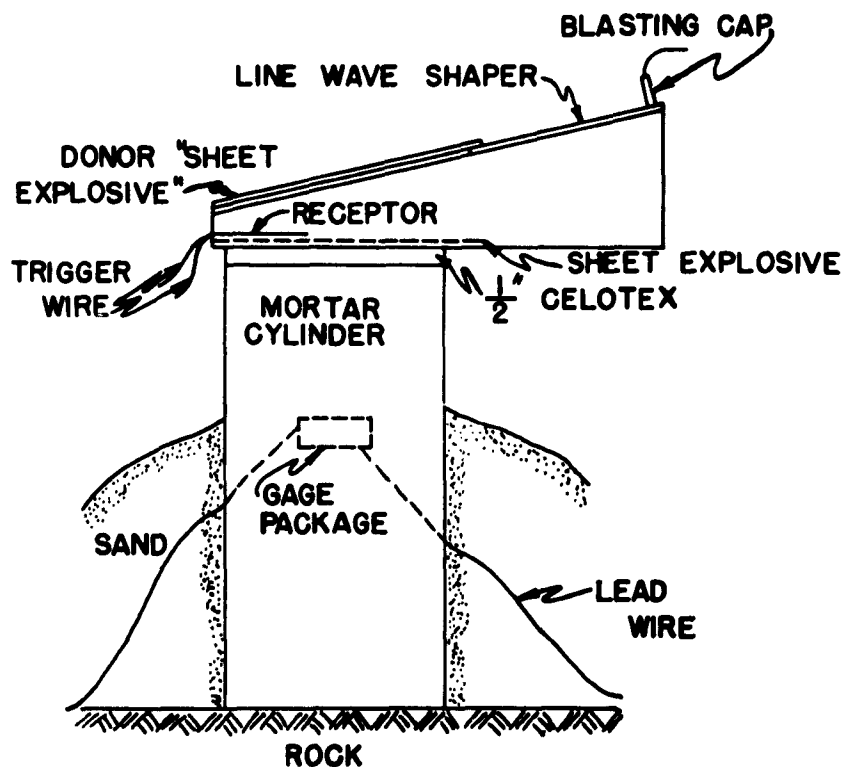


Figure 3: Sketch of instrumented cylinder in test position, showing wave shaper and sand embankment.

parallel to the disc axis. The finished instrumented mortar disc is illustrated in Figure 1. A completed disc contained two strain gages and two stress gages spaced 90 degrees apart and 3/8 inch from the disc axis for measuring simultaneously the stresses and strains parallel and perpendicular to the axis of the mortar disc.

Plane Stress Wave Generator

Two types of plane-wave generators were used during this study. During the early stages of the study, a wave shaper consisting of a conical mound of 60 per cent ammonium dynamite with an inert aluminum core was utilized. This technique provided reasonably plane waves, but the large amount of explosive required ($1\frac{1}{2}$ to $2\frac{1}{2}$ pounds) did not leave a sufficient portion of the mortar cylinder intact for evaluation.

During the latter part of the project, a plane-wave generator using a duPont line-wave generator was utilized. The plane-wave generators were fabricated as suggested in E.I duPont Bulletin No. ES-58-2A³, with the exception that the receptor explosive was a 0.084 inch thick duPont type EL-506A-2 sheet explosive (PETN combined with other ingredients to form a flexible sheet). The weight per unit area was 2.0 grams/inch².

In the early experiments utilizing this plane-wave generator, the donor explosive consisted of one 0.084 inch thickness of explosive. Under this condition complete, simultaneous detonation of the receptor explosive was erratic. The left-hand specimen of Figure 4 shows the remains of a specimen tested under those conditions. The wave-generator performance was improved by doubling the thickness of the donor explosive.

Although less than 57 grams of explosive was in contact with the

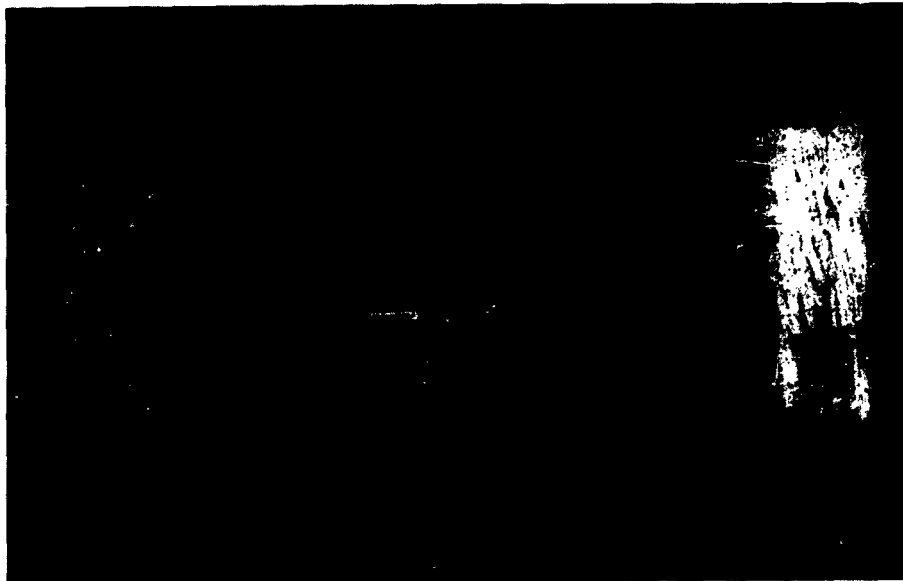


Figure 4: Six-inch diameter Portland cement mortar test cylinders used in all instrumented tests. From left to right; cylinder after incomplete wave-shaper detonation; cylinder tested with layer of celotex for wave attenuation; and specimen before testing.

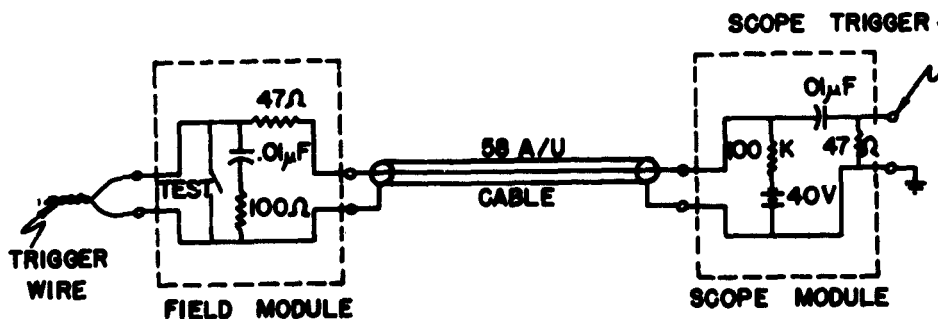


Figure 5: Oscilloscope trigger circuit used in high level transient tests.

concrete cylinders using this technique, the damage to the mortar cylinders was extremely severe, (Figures C.1 - C.4). To reduce the damage, a $\frac{1}{2}$ -inch thick sheet of celotex was glued between the wave generator and the cylinder. The remains of a test cylinder loaded in this fashion are shown at the center of Figure 4.

Strain Gage Instrumentation

The strain-gage installation consisted of embedded resistance gages, two-conductor shielded cables, potentiometric circuit input units, preamplifiers, and 530-series Tektronix oscilloscopes.

The embedded gages had 18-inch lengths of No. 32 A.W.G. insulated wire attached to them, and the two-conductor shielded cables (Belden # 8412) to the preamplifiers were 250-feet long. The potentiometric circuit consisted of a 90-volt battery power source, 3250-ohm ballast resistance, and 0.1 μ fd coupling capacitor giving a gage current of approximately 26 milliamps. From Figure A.5 it can be seen that the errors in measured strain due to lead-wire effects are negligible. The error in the calibration due to the lead-wire resistance, from equation A-41, was approximately one per cent, and was neglected for the purpose of this study.

The output of the potentiometric circuit was fed into a Model 122 Tektronix low-level preamplifier with an input impedance of 10 megohms paralleled by 50 μ f farads. The output of the preamplifier was fed directly to the input of a 530-series Tektronix 5-inch oscilloscope.

The overall bandwidth of the strain-gage system (assuming a $\frac{1}{2}$ -inch gage length) was calculated to be 0.4cps to 37Kcps from the data of Appendix A. The resulting rise time of 9.5 μ sec limits the strain pulse

rise times which can be observed without appreciable error to about 30μsec (5 per cent error).

Strain gages were calibrated using the shunt-resistance technique.

Stress Gage Instrumentation

The stress-gage instrumentation was quite similar to that used with strain gages, the only difference being that the two-conductor cables were connected directly to the oscilloscopes, without need for input units or preamplifiers. The oscilloscope input impedance of 1 megohm paralleled by 47μfd, combined with the cable shunt capacitance of 0.01 μfd, and the PZT-4 properties of Table II were utilized to obtain the stress-gage circuit voltage response as described in Appendix B:

$$E_3^* = \frac{C_g E_3}{C_g + C_c} = \frac{190 \times 10^{-12}}{10^{-8}} E_3 = 1.9 \times 10^{-2} E_3 \quad (B-22)$$

The open-circuit gage voltage E_3 for the PZT-4 ceramic element alone is theoretically 424 volts/1000 psi. Thus the voltage output of the circuit plus gage should be on the order of 10 volts/1000 psi.

The bandwidth of the system was approximately 16 cps to 300 kcps; the lower frequency limit depending upon the shunt capacitance-amplifier input resistance relationship and the upper frequency limit upon the gage transit time (as developed in Appendix B). Thus the per cent error in dc component of stress in one millisecond of observed record due to lack of low frequency response was less than

$$P = 200 \pi f_1 T = 200 \times 16 \times 1 \times 10^{-3} = 3.2 \text{ per cent} \quad (B-24)$$

The error in rise time voltage output due to a ramp input stress would be less than one per cent if the stress rise time were greater than 10μ seconds.

Oscilloscope Triggering

It was important that oscilloscope triggering be reproducible during all tests. In low-stress dynamic tests, the oscilloscope and camera were triggered by a photoelectric-cell circuit activated by the pendulum ball of the impactor. The delay-circuit capabilities of the Type-535A Tektronix oscilloscope were utilized in conventional manner to permit recording of the initial portion of the stress and strain pulses within the mortar specimen.

The triggering of oscilloscopes for the high intensity dynamic tests utilizing explosives was complicated by the fact that the oscilloscopes were located at distances up to 250 feet from the specimen. The circuit of Figure 5 was developed for this purpose. This circuit provides a positive voltage pulse output of 5-volts peak magnitude, 2-microsecond duration and less than 0.5-microsecond rise time (loaded by 1 megohm shunted by $47\mu\text{fd}$). The trigger switch consisted of two lengths of #40 enameled wire twisted together and taped to the receptor explosive sheet of the plane-wave shaper. Triggering by this method was extremely consistent.

Static Test Procedure

Embedded strain-gage performance was compared to that of surface mounted gages and standard compressometers during static tests in a universal testing machine. From these tests, the static modulus of elasticity of the Portland Cement mortar was found to be approximately

2.3×10^6 psi, while the ultimate static compressive strength was approximately 7000 psi. The embedded strain gages were found to exhibit more linear strain behavior than surface-mounted gages at low-stress magnitudes, apparently due to the presence of very small cracks on the exterior surface of the concrete specimen.

Low-Level Transient Test Procedure

The instrumented mortar test cylinders were suspended horizontally by piano wire from the laboratory ceiling and impacted on one end (the same end to which plane waves were applied in the high-intensity tests at a later date). The impact was provided by a steel ball suspended as a pendulum. The purpose of these tests was to observe the behavior of the embedded stress and strain gages and to compare their behavior with that of external strain gages. Figures C.14 to C.20 illustrate typical response to low-level transient stress. Specimen No. 15 (Figures C.14 - C.16) illustrates behavior which was typical of early tests, in which adequate tensile strength was not developed between the instrumented mortar disc and the remainder of the cylinder, indicated by the different magnitudes of tensile and compression peaks in Figure C.14. This problem was solved by moistening the discs with water before embedding them in the mortar test cylinders.

Early forms of the strain gages tested consisted of foil gages embedded in epoxy coupons which were suspended in the middle of the mortar test cylinders. The bonding of the mortar to the epoxy containing the gages was observed to be very poor, and although the static compression tests showed very accurate strain response, transient test performance was erratic. This is in contrast to the performance of

strain gages dipped in liquid epoxy, permitted to cure, and then embedded in plaster of paris models, as described by Martin.⁴ He reported no adverse effects when these models were subjected to intense shock waves (primary interest was in the compression pulse). It is possible that the bonding of plaster of paris to epoxy is considerably different than that of mortar to epoxy.

Figures C.17 to C.20 illustrate the performance of the stress and strain gages in a mortar cylinder where bonding was more satisfactory. Note the wave-form similarity of all gage responses. The presence of the high-frequency noise in the stress-gage response has not been satisfactorily explained.

Comparing the initial peak of the voltage output of the piezoelectric gage (Figure C.19) parallel to the cylinder axis, to the initial peak strain indicated by the strain gage (Figure C.18) parallel to the cylinder axis, and considering that the cavity area is 0.018 inches² whereas the gage element area is 0.049 inches², the stress-gage output of approximately 36 millivolts is about 20 per cent too low (based on the static modulus of elasticity of 2×10^6). This discrepancy may be due to the fact that the steel ring which decouples the stress gage from lateral stress, carries some of the longitudinal stress also, thereby desensitizing the gage.

High Intensity Dynamic Test Procedure

The mortar test cylinder was placed with axis vertical upon the rock floor of the Research Laboratory Block House, and with the lower end of the cylinder in a shallow puddle of water to reduce reflected energy. Gage lead wires were connected inside a water-resistant junc-

tion box to the ends of two-conductor shielded cables leading to the instrument truck parked 150-feet distant. Loose damp sand was banked around the base of the cylinder to a height of nine inches to deflect the air blast wave and reduce the strain on the gage lead wires. A make-circuit switch was taped to the receiver portion of the wave shaper and then the wave shaper complete with celotex attenuator was glued to the upper end of the mortar cylinder with contact cement. Gluing the wave shaper to the cylinder appeared to give more consistent results than by clamping.

Figures C.1 to C.4 illustrate the response of external strain gages to the duPont plane-wave generator placed in direct contact with the mortar cylinder. Note that the strains are extremely severe, well beyond static ultimate values. Rise times are comparable between these tests, although the initial peak strains show differences of 25 to 30 per cent at a point six inches from the wave shaper from test to test.

A layer of celotex glued between the wave shaper and the test cylinder reduced the loading on the cylinder as shown in Figures C.5 to C.12 and C.21 to C.24. Figures C.5 and C.6 illustrate the reduction of the strain level at the surface of the mortar cylinders.

Figure C.7 shows the behavior of a strain gage embedded parallel to the axis of the cylinder, three inches from the plane-wave generator. The loss of record after the initial compression peak was typical at this distance, and as a result gages were embedded at a greater distance from the plane wave source in subsequent tests.

Figures C.21, C.22 and C.23 illustrate the behavior of piezoelectric stress gages in the same location. Note the similarity of wave

shapes. It is believed that the difference of peak magnitudes for the first two of these stress records is due to (1) different degrees of depoling of the ceramic elements and (2) crushing of some portions of piezoelectric elements with consequent release of energy.

Figures C.11 and C.12 depict the responses of strain gages oriented parallel and perpendicular to the mortar-cylinder axis at a distance of $4\frac{1}{2}$ inches from the wave source. This is the point closest to the source, at which gage and wiring remained intact over the entire time required for the intense transient wave to travel down the mortar cylinder and reflect as a tensile wave at the base.

Figures C.8, C.9 and C.10 illustrate the varied behavior of strain gages parallel to the axis of the cylinder, six inches from the wave source. The wave shape most typical of strain-gage response is that shown in Figure C.8. The presence of the precursor in Figure C.10 has not been explained.

Figure C.23 shows the data which were obtained from the piezoelectric stress gages located at the same point. The camera did not catch the high velocity motion of the trace in the vicinity of the initial pulse.

After the experimental portion of this study had been completed, the authors' attentions were directed to work performed by Dove, Balcer and Brasier^{5,6} with internal strain gages in plastics in which it was discovered that the tensile bond of epoxy to foil gage element may be quite low, and hence high stresses may not be transmitted across the gage plane. Free-filament gages did not show this behavior to such a marked degree. Rupture of the filament-epoxy bond across the gage plane

may have occurred during some of the present experiments as a result of lateral extension of the mortar cylinders, with consequent distortion of the strain field and erroneous readings.

CONCLUSIONS AND RECOMMENDATIONS

The laboratory tests undertaken in this investigation were unsuccessful in producing any useful data on physical behavior of rock materials under high-order dynamic loading. Some useful strain measurements were obtained and an analysis and synthesis of gage theory applicable to this problem were derived, based on theory and results from other investigations.

Reasons for lack of success in obtaining data:

1. Difficulty in obtaining effective bonding between gages and mortar;
2. The sensitivity of piezoelectric gages employed too high for the pressures obtained;
3. Piezoelectric gage circuitry should be as near open-circuit condition as possible. This was not possible in these experiments;
4. Corrosion of strain gages was an apparent cause of increase in their resistance after being encased in plastic and Portland cement mortar. Corrosion may have occurred due to reaction with moisture in the plastic which is slightly hygroscopic;
5. The problem of weak bonding of epoxy adhesives to foil gage elements reported by previous investigators may have been one cause of the spread of data obtained with strain gages.

Recommendations for further work are:

1. Other plastics for encapsulating and bonding embedded gages should be considered. Types of plastics which are water proof and will not promote corrosion of the gage wires should be investigated;

2. Free-filament strain gages should be investigated as an alternative to foil gages, to obtain improved tensile strengths across the gage plane;

3. Piezoelectric materials with sensitivities much lower than those of the lead-zirconate-titanate ceramics used in this project should be studied to reduce the field problems of handling high voltages at high transient-stress levels.

REFERENCES

1. "Stycast 2662," Emerson & Cuming, Inc., Technical Bulletin 7-2-11, May, 1961
2. "Modern Piezoelectric Components," Clevite Electronic Components Bulletin No. 9244-1, Cleveland, Ohio, March, 1961.
3. "duPont Line Wave Generators," E. I. duPont de Nemours & Co., Inc., Bulletin No. ES-58-2A, Wilmington, Del.
4. Martin, C. W., "Fracture of Plaster by Explosions," Ph.D. Dissertation Iowa State University., 1962.
5. Dove, R. C., Brasier, R. I., and Baker, W. E., "Selection of Gages for Strain Measurement at Interior Points," Experimental Mechanics, Vol. 2, No. 6, June, 1962.
6. Baker, W. E. and Dove, R. C., "Measurement of Internal Strains in a Bar Subjected to Longitudinal Impact," Experimental Mechanics, Vol. 2, No. 10, Oct., 1962.

APPENDIX A
DYNAMIC STRAIN MEASUREMENT WITH
RESISTANCE GAGES

The measurement of the dynamic strain in solids by resistance strain gages requires special knowledge of the gages, of the behavior of electronic circuits, of the adhesives used, and of the material being investigated. Some of the basic information used to decide gage type, gage length, electronic circuitry, recording methods, calibration techniques, etc., which are unique to the measurement of high-intensity, short-duration strain transients is presented in this Appendix.

Special attention is directed to those sections which present new information not reported in the literature, particularly the section in which gage frequency response is related to the response of a low-pass filter, and to that section which describes lead-wire effects on calibration accuracy, using the "shunt resistance" technique.

The Potentiometric Strain-Gage Circuit

Some consideration must be given at this point to the strain-gage input circuitry. Practical reasons dictate the use of a direct-current power source, since the transient strains encountered at short distances from a shock-wave source may contain significant harmonic components above 10,000 c.p.s., where the use of a carrier system would require frequencies high enough to pose many problems. In addition to adequate high-frequency response, the bandwidth of the circuitry must extend to sufficiently low frequencies so that over the required observation time of the transient phenomena, significant errors are not introduced. One

criterion for evaluation of the system is its response to a step input. This type of input is much more severe (in terms of response required of the circuitry) than actual strain transients which can be physically achieved. The per cent error in the response at the end of a given time is related to the lower 3db frequency of the system by

$$f_1 = \frac{P}{200\pi T} \quad (A-1)$$

where: P = per cent error

f_1 = lower 3db frequency

T = time span of observation

Thus, if a circuit is to have less than one per cent error, when a step-input is applied for 1 millisecond, its lower 3db frequency must be less than 1.6 c.p.s. The actual error in transient measurement over the same time, due to low-period frequency attenuation should be less than this amount since the contribution to transient phenomena of the dc-component would normally be much less than in the case of the step-input.

This upper limit on the lower 3db frequency is significant since it permits the use of a potentiometric (ballast) circuit rather than a bridge-type strain-gage circuit. The potentiometric circuit has the advantages of circuit simplicity, operational speed and lack of balance adjustments. It has the disadvantages that calibration must be performed dynamically, that static measurements are not possible, and that the direct current power source must be a battery, since electronically filtered constant-voltage power supplies which are available commercially are not sufficiently free of hum, ripple, and noise to

permit use in low-strain-level potentiometric circuits.

The basic potentiometric-circuit components are illustrated in Figure A.1(a). The effects of lead wires are not included at this point. The incremental change of voltage at the amplifier input, due to an incremental change in strain-gage resistance, is given by:²

$$\Delta E = V \frac{R_b}{(R_g + R_b)^2} \cdot \Delta R_g \cdot \left[1 - \frac{1}{1 + \frac{R_g + R_b}{\Delta R_g}} \right] \quad (A-2)$$

where: V = voltage applied to the circuit

R_b = ballast resistance

R_g = gage resistance

This equation may be simplified by letting $R_b/R_g = a$

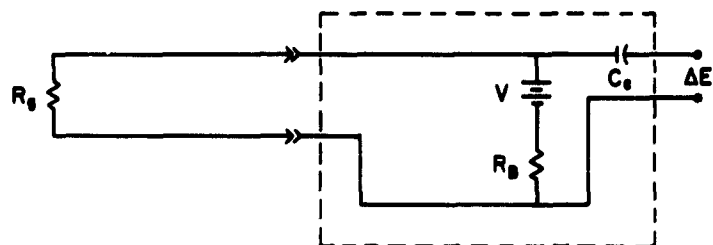
$$\Delta E = V \frac{a}{(1 + a)^2} \frac{\Delta R_g}{R_g} (1 - n) \quad (A-3)$$

$$\text{where: } n = 1 + \frac{(a + 1)R_g}{\Delta R_g}$$

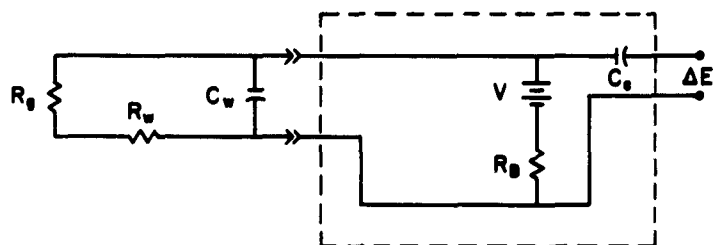
Making use of the definition of gage factor, $S = \frac{\Delta R_g/R_g}{\epsilon}$, the

change in voltage may be expressed in terms of strain.

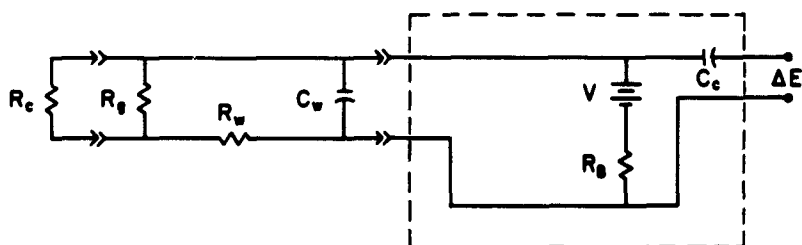
$$\Delta E = VS\epsilon \frac{a}{(1 + a)^2} (1 - n) \quad (A-4)$$



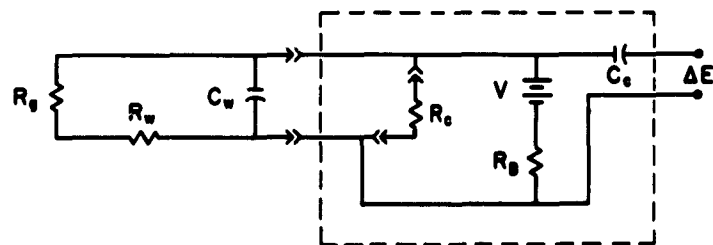
(a) Basic Potentiometric Strain Gage Circuit.



(b) Potentiometric Circuit including Lead Wire Components.



(c) Potentiometric Circuit with Calibrating Resistor Applied at Gage.



(d) Potentiometric Circuit with Calibrating Circuit in Normal Location.

Figure A.1: Variations of the basic potentiometric circuit.

$$\text{or} \quad \Delta E = I S \epsilon R_g \frac{a}{1+a} (1-n) \quad (\text{A-5})$$

where: I = gage current

The strain in terms of the observed change in voltage is

$$\epsilon = \frac{\Delta E}{I S R_g} \left(\frac{1+a}{a} \right) \frac{1}{1-n} \quad (\text{A-6})$$

The quantity 'n' represents the nonlinearity of the voltage response, and is plotted as a function of the ballast-to-gage-resistance ratio in Figure A.2, for various values of applied strain-gage factor product. It can be seen from this plot that errors are less than one per cent due to nonlinearities of the potentiometric circuit response for strains less than five per cent, where the ballast to gage resistance ratio is greater than 10 (assuming $S = 2.0$). The nonlinearity of the circuit response due to strain amplitude may therefore be disregarded for most tests of brittle materials. Thus equation (A-6) may be approximated by

$$\epsilon = \frac{dE}{I S R_g} \left(\frac{1+a}{a} \right) \quad (\text{A-7})$$

Equation (A-7) indicates that the maximum voltage output for a given strain gage subjected to a given ϵ is achieved when 'a' is a maximum, all other factors being held constant. The current I is normally adjusted to a maximum value which is a compromise between maximum sensitivity and minimum gage-heat-dissipation problems. The problem of gage heating due to the current flow is considered in more

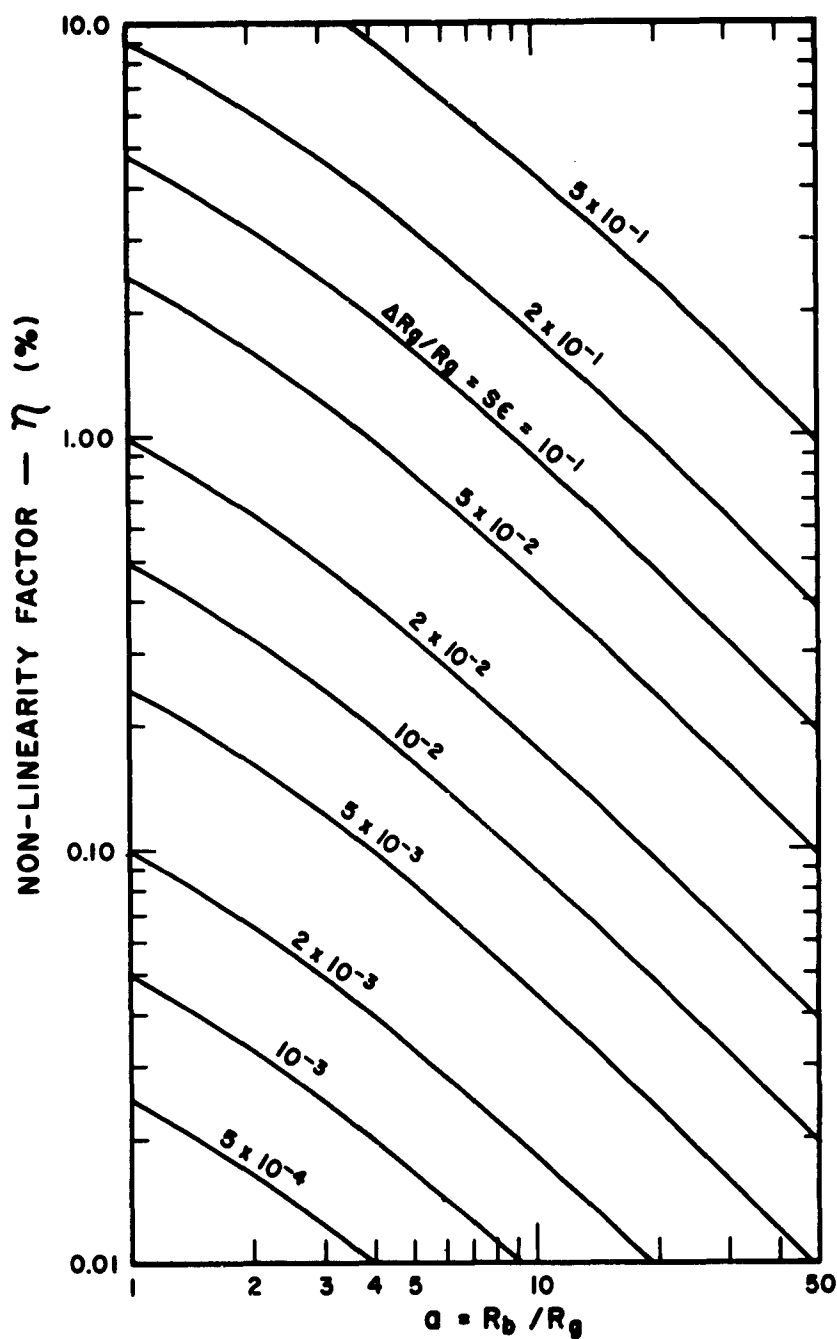


Figure A.2: Effect of applied strain and ballast resistance-gage resistance ratio of a potentiometric circuit output linearity.

detail in a separate section. Figure A.3 illustrates the effect of the ratio 'a' on circuit output and voltage input requirements. The data presented indicate that ratios of R_b to R_g greater than 10 do not provide significant increases in circuit sensitivity while requiring substantial increases in input power-supply capacity. Figure A.4 is a plot of normalized output of the potentiometric circuit versus strain-gage resistance for various values of input voltage. Curves are based on a gage current of 25 milliamperes. It appears that a 90-volt battery will provide approximately optimum sensitivity for the gage resistances which are in common usage. The benefits to be obtained in increased circuit sensitivity by an increase in gage resistance are also apparent here.

Circuit loading Equations (A-2) to (A-7) were derived assuming that the circuit into which the potentiometric circuit output feeds presents an infinite input impedance. The error introduced by this assumption is given by the equation,²

$$m = \frac{2a \frac{R_g}{R_L}}{\left[1 + a \left(1 + R_g/R_L\right)\right]^2} \quad (A-8)$$

where: R_L = input resistance of second circuit

When the ratio of ballast to strain-gage resistance is 10 or greater, the error due to loading by the next circuit is less than one per cent for values of R_L more than 15 times the gage resistance R_g . Since the input impedance of most voltage amplifiers is 10 kilohms or greater, effect of circuit-resistive loading on output impedance is

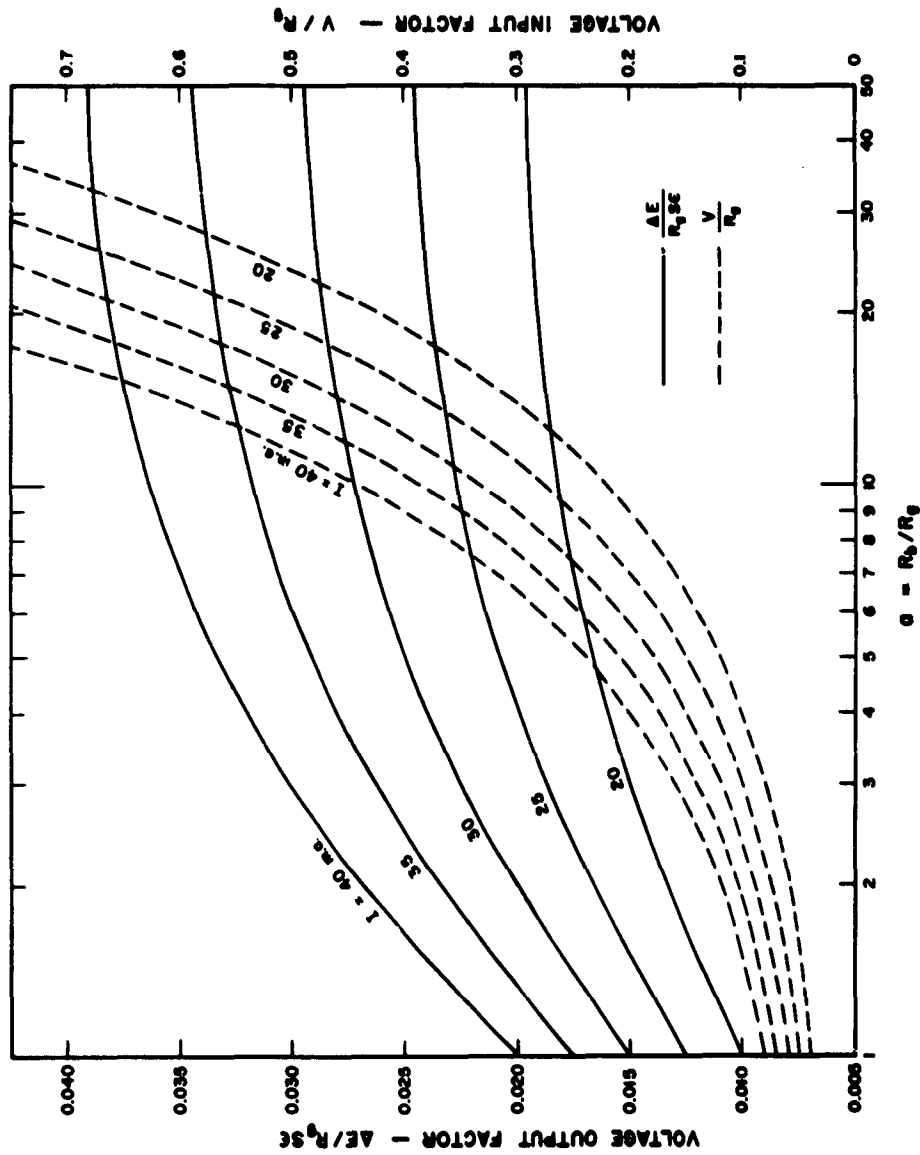


Figure A.3: Output of potentiometric circuit and voltage input as a function of the ratio of ballast resistance to gage resistance for varying gage currents.

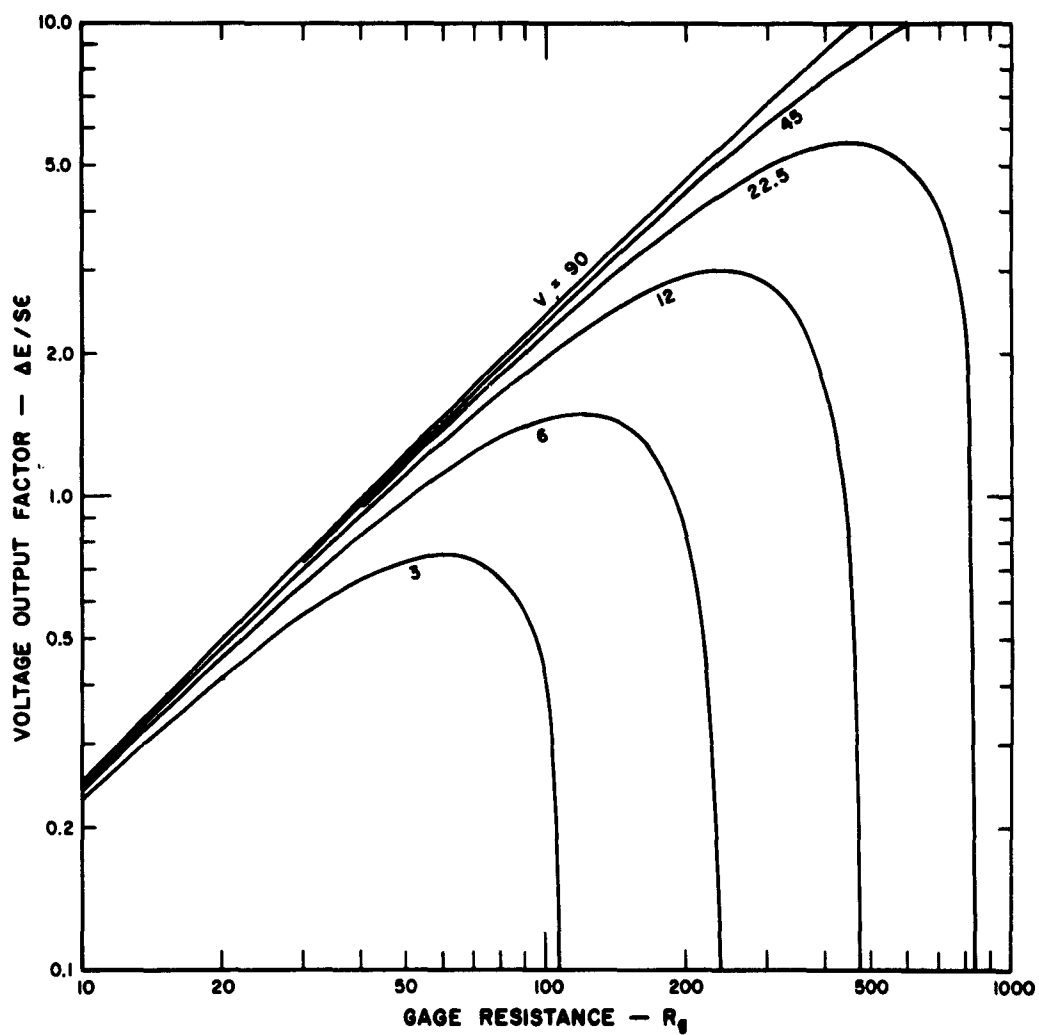


Figure A.4: Output of potentiometric circuit vs. gage resistance (gage Current held constant at 0.25 ma) for varying applied voltages.

negligible.

In many instances the high dc-voltage component across the strain gage is too great for direct coupling to ac-amplifiers or oscilloscopes.³ It is the ac-voltage component which the user of the potentiometric unit is interested in, since this portion contains the dynamic-strain signal. For this reason the capacitor C_c in Figure A.1(a) is included to remove the dc-component of voltage. This capacitor and the input resistance of the first stage of amplification form a high-pass filter, a reactive load on the potentiometric circuit at low frequencies. Typical values of $C_c = 0.1 \mu\text{farad}$ and $R_L = 1 \text{ megohm}$ give a lower 3db frequency of the potentiometric circuit

$$f_1 = \frac{1}{2\pi R_L C_c} = \frac{1}{2\pi(0.1)} = 1.6 \text{ cycles /second} \quad (\text{A-9})$$

As a result of the lower limit on frequency response, the dc-component of a transient strain signal would suffer a one per cent decrease in a time

$$T = \frac{P}{200\pi f_1} = \frac{1}{200\pi(1.6)} = 1 \text{ millisecond} \quad (\text{A-10})$$

If time spans greater than this were necessary for a complete study of the transient record, the effect of low-frequency cutoff on the results would have to be considered.

Inaccuracies due to lead wires The use of long lead wires between the strain gages and the measuring system can be a source of error, since lead-wire resistance is introduced into the system. In those instances where the lead wires are carried in a shielded cable as

two insulated, twisted wires or where coaxial cable is used, some capacitance is placed in parallel with the gage resistance. Inductance is effectively cancelled by the twist of the leads.

Lead-wire resistance is included in Figure A.1(b), a schematic of the potentiometric circuit. The voltage across the strain gage plus lead-wire resistance is given by

$$E^* = V \frac{(R_g + R_w)}{R_g + R_w + R_b} \quad (A-11)$$

The voltage output due to a change in gage resistance is given by

$$\begin{aligned} dE^* &= V \frac{R_b}{(R_g + R_w + R_b)^2} dR_g \\ &= V \frac{a}{(1 + R_w/R_g + a)^2} \frac{dR_g}{R_g} \end{aligned} \quad (A-12)$$

The effect of lead-wire resistance may be evaluated by dividing equation (A-3), the expression for voltage output neglecting lead-wire effects, by equation (A-12), which was derived including lead-wire effects, neglecting higher-order terms

$$\frac{dE}{dE^*} = \frac{(1 + R_w/R_g + a)^2}{(1 + a)^2} = 1 + \frac{2R_w/R_g}{1 + a} = 1 + b \quad (A-13)$$

$$\text{where: } b = \frac{2R_w/R_g}{1 + a}$$

The strain to which the gage responds in terms of the observed voltage may be obtained by substituting equation (A-13) into equation

(A-7). Thus

$$\epsilon = \frac{dK^*}{ISR_g} \frac{1+a}{a} (1+b) \quad (A-14)$$

The lead-wire resistance reduces the sensitivity of the strain-gage circuitry. In Figure A.5 the error due to the lead-wire resistance is plotted versus the ratio of ballast resistance to gage resistance for various values of lead-wire strain-gage resistance ratio. Figure A.6 serves as a simple source of the lead-wire strain-gage resistance ratio, when gage resistance, lead-wire gage, and lead-wire length are known. Use of these figures can be illustrated best by an example: If 'a', the ratio of ballast resistance to total resistance, = 10, and if the error due to lead resistance is to be less than one per cent, Figure A.5 indicates that R_w/R_g must be less than 6×10^{-2} . If the required total strain-gage lead length is 1000 ft. and the strain-gage resistance is 120 ohms, Figure A.6 gives a maximum wire gage to be used of 18 A.W.G.

Several points can be stated about error due to lead-wire resistance. The error increases with an increase in lead-wire gage-resistance ratio and decreases with an increase in ballast-gage resistance ratio. It is important to note that the true strain may be calculated using equation (A-14), including lead-wire effects. However, a far superior method is the calibration of the entire strain-gage system immediately before the dynamic test. The calibration techniques, including compensation for lead-wire resistance effects will be considered in a later section.

Lead-wire capacitance reduces the upper frequency limit of the

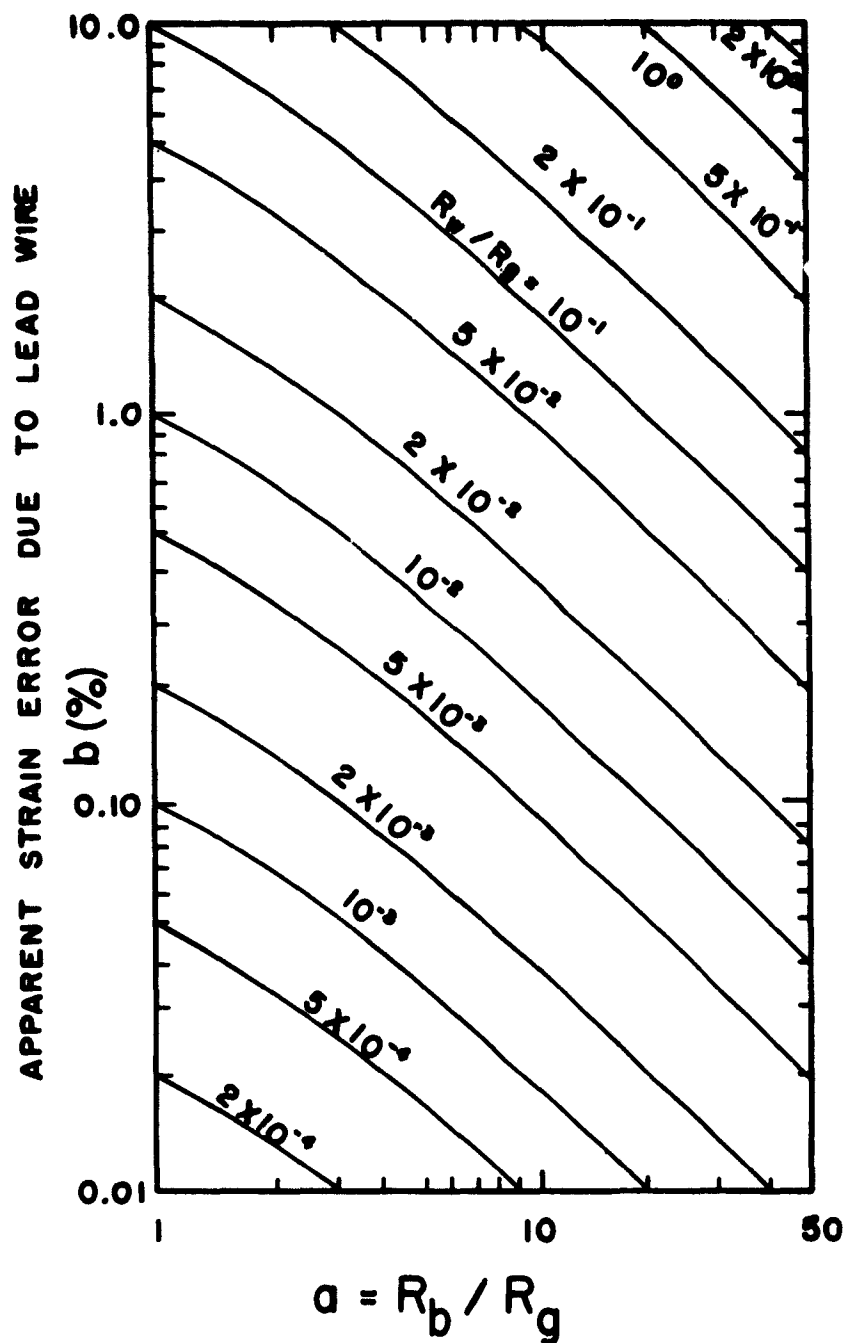


Figure A.5: Apparent strain error due to lead-wire resistance as a function of the ratio of ballast resistance to gage resistance for various lead-wire strain-gage resistance ratios.

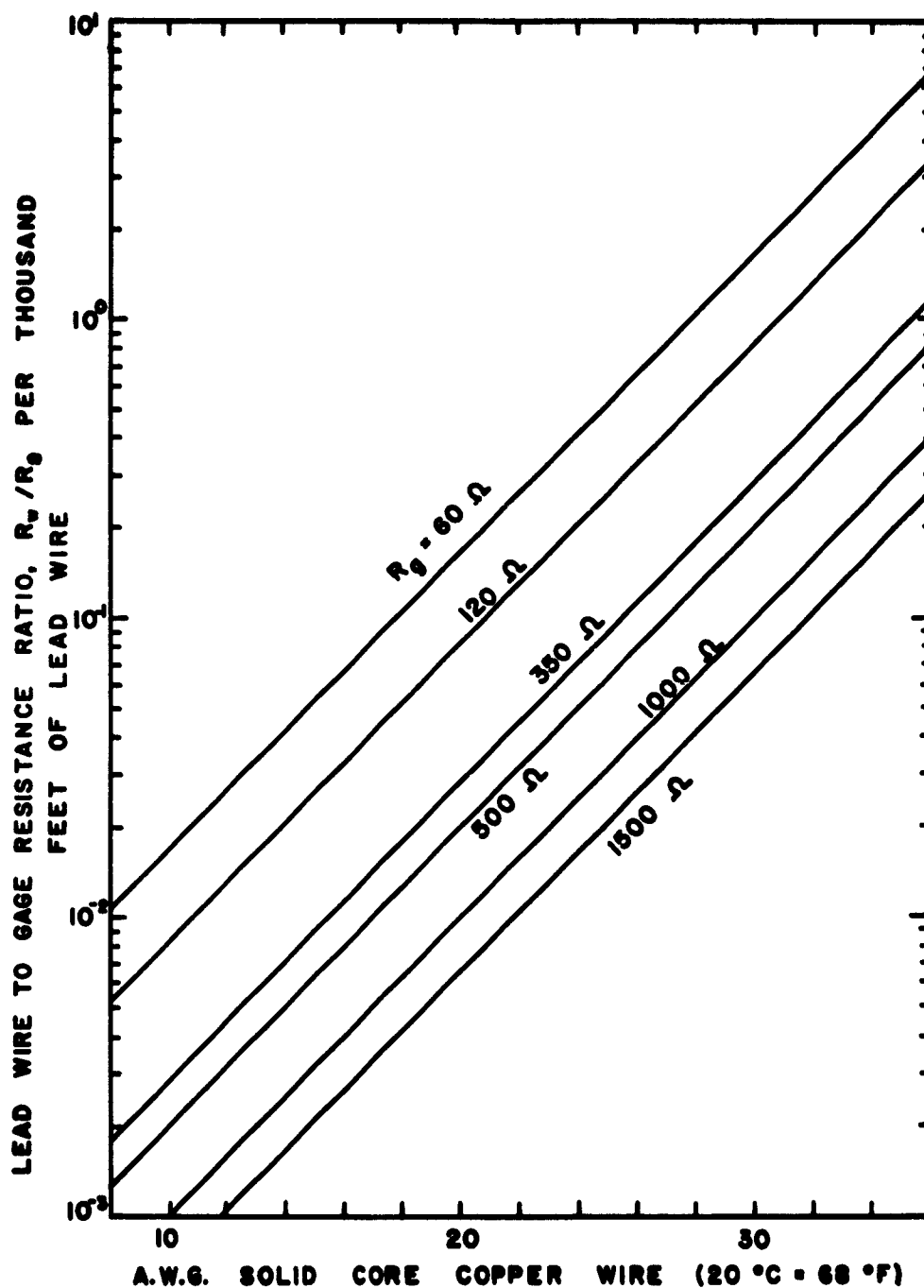


Figure A.6: Ratio of lead-wire resistance to strain-gage resistance as a function of wire gage for various gage resistances

measuring system, i.e., increasing the rise time of strain pulses. The voltage output of the potentiometric circuit due to a step change in strain-gage resistance, including lead-wire capacitance effects,⁴ may be obtained using the circuit representation of Figure A.1(b), as

$$dE^{**} = dE^{*}(1 - e^{-\frac{t}{\tau}}) \quad (A-15)$$

where: dE^{**} = output voltage in the presence of lead-wire capacitance.

dE^{*} = output voltage without capacitance (includes lead-wire resistance).

$$\tau = R_g C_w a \frac{(1 + \frac{R_w}{R_g})}{1 + a + \frac{R_w}{R_g}}$$

C_w = lead wire capacitance

Thus the time constant, τ , of the potentiometric circuit depends primarily on the strain-gage resistance and the lead-wire capacitance. The rise time of the potentiometric-circuit response (time required for circuit response to go from 0.1 to 0.9 of peak amplitude) to a step change in resistance of the strain gage is given by¹

$$T_R = 2.2\tau \quad (A-16)$$

To illustrate, a potentiometric circuit such as used in the example concerning lead-wire resistance, where $R_g = 120$, $a = 10$, and

with 1000 ft. of 18 A.W.G. wire, would have a rise time of 1.75 micro-seconds, assuming the lead-wire capacitance per foot to be 10 μfarad . Such capacitances are realized with dual-conductor cables.

The upper 3db frequency limit of the response of the potentiometric circuit to simple harmonic strain-gage resistance changes may be expressed as ¹

$$f_2 = \frac{1}{2\pi\tau} = \frac{0.35}{T_R} \quad (\text{A-17})$$

One objective of transient-strain recording is frequently the measurement of rise time of a strain pulse. The pulse shape may often be approximated by a ramp portion of finite duration followed by a portion where decay time is extremely large compared to the initial rise time. Such a case is illustrated in Figure A.7. Upon this figure are plotted the responses of low-pass circuits with various upper 3db-frequency limits to the finite ramp input of duration T. The error γ in the rise time of the circuit t_R , as compared to the ramp input rise time t_R' , is given by

$$t_R' = t_R (1 - \gamma), \quad (\text{A-18})$$

and is plotted versus the product of the upper 3db-frequency limit f_2 times T in Figure A.8. It can be seen that the error in the rise time as determined from the response is on the order of one per cent when $f_2 T = 2$. For that condition, assuming that $a = 10$, and utilising equations (A-15) and (A-17)

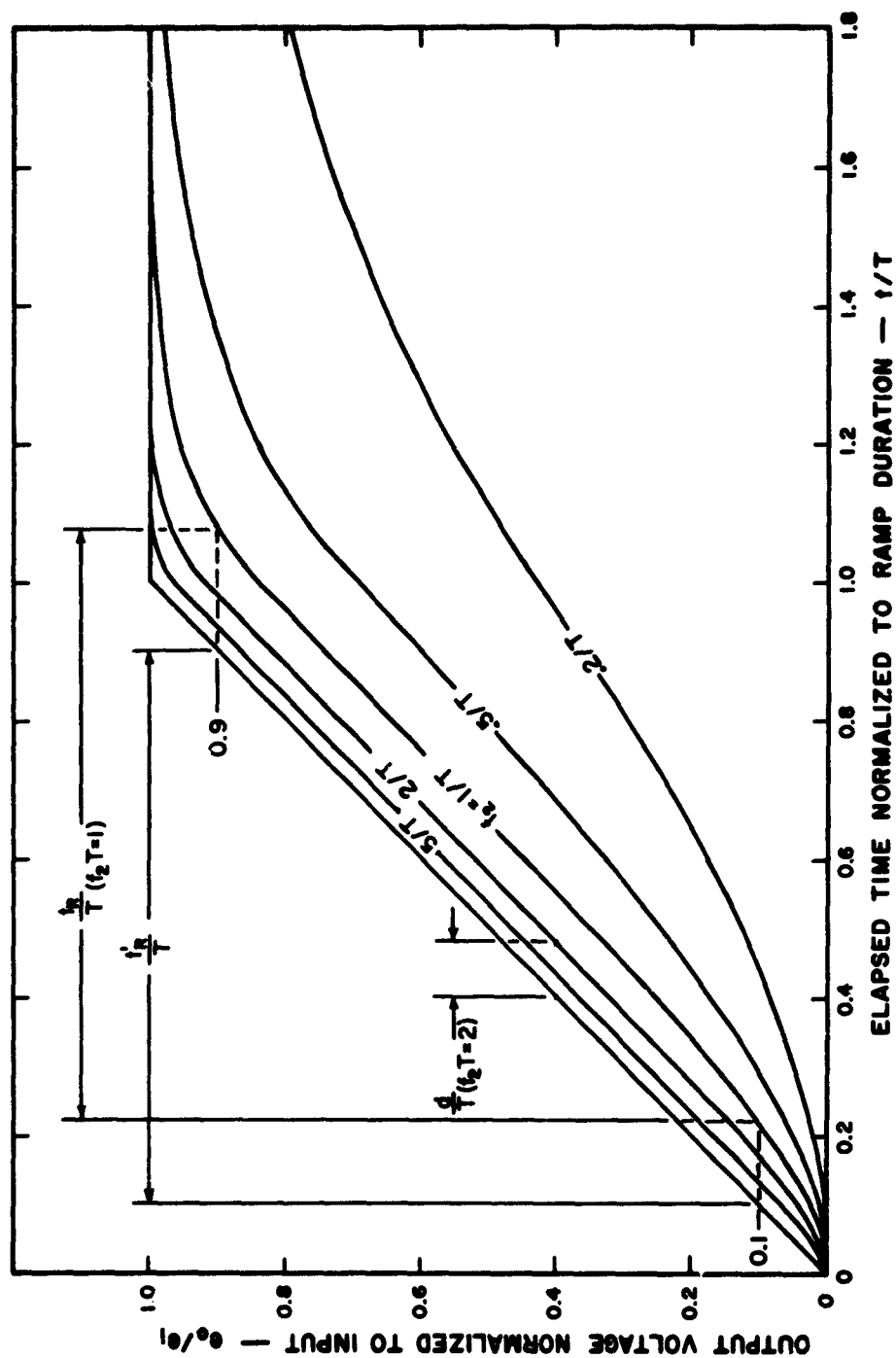


Figure A.7: Response of low-pass filter to normalized ramp voltage of finite duration showing rise time and delay time.

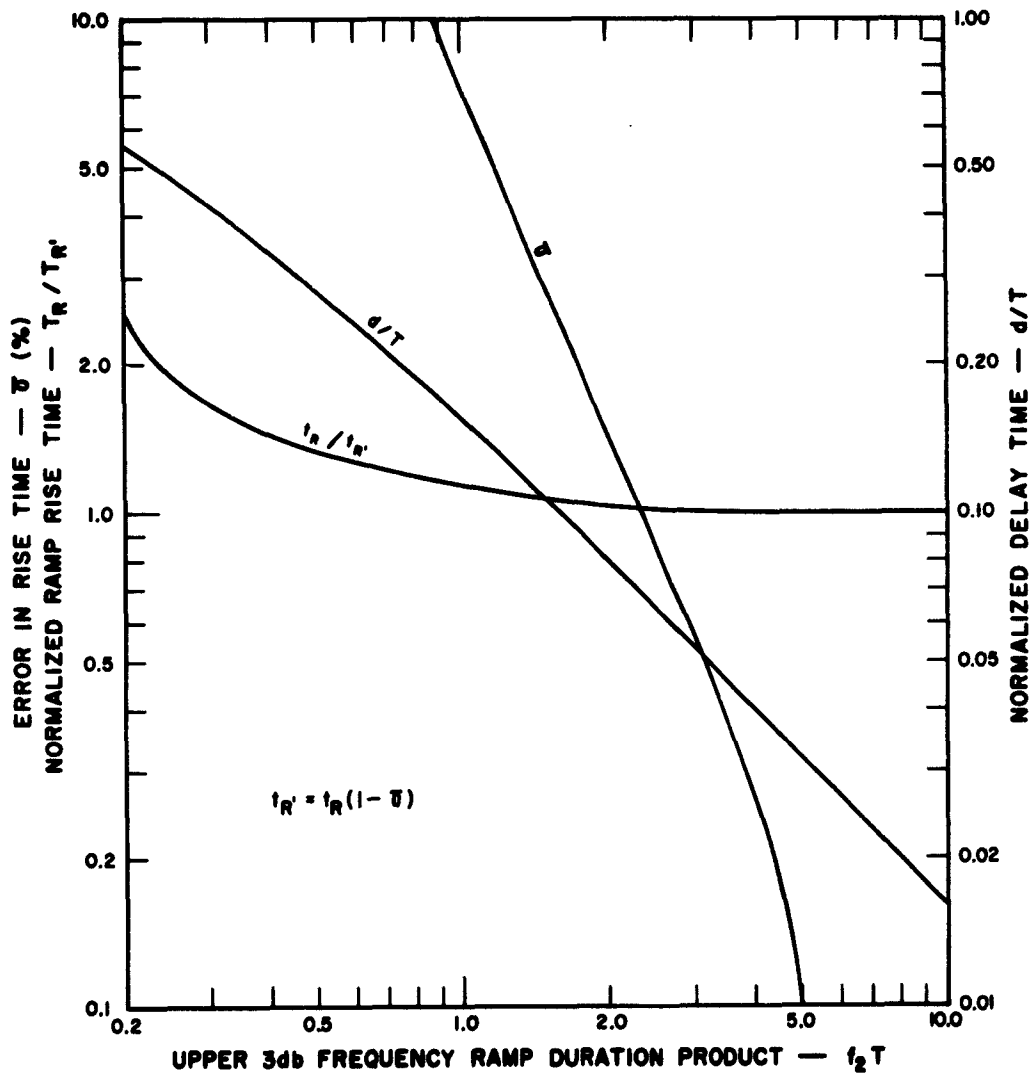


Figure A.8: Rise time and delay time of low-pass filter response to a finite ramp input vs. upper 3db frequency ramp duration product.

$$\tau_{\max} \approx R_g C_w = \frac{1}{2\pi f_2} = \frac{T}{4\pi} \quad (\text{A-19})$$

If the duration of the transient rise time being measured is on the order of 10 microseconds, equation (A-19) suggests that $R_g C_w$ must be less than 0.8 microsecond if the rise time of the response is to be accurate within one per cent. Thus upper limits on the size of the strain-gage resistance and the lead-wire capacitance are determined by the high-frequency requirements.

In addition to the lead-wire capacitance effects, capacitances due to wiring orientation, proximity to ground, etc., may add measurably to the total capacitance which determines the potentiometric-circuit high-frequency response. It is therefore difficult to calculate the frequency or transient responses of the circuit. A technique for directly determining the response during the actual calibration of the entire strain-gage instrumentation is described in a later section.

Figure A.7 also provides information on the delay time of the circuit response (the increment of time between the time when the ramp input reaches 0.4 maximum amplitude and the time when the circuit response reaches the same amplitude). The delay time normalized to ramp duration is plotted as a function of $f_2 T$ in Figure A.8. It can be seen that sizable errors in transient arrival times may be experienced if the circuit frequency response is not adequate. This may introduce some problems when wave-propagation velocities are to be determined from transient arrival times, where the effect of circuit response is disregarded.

The Electric Resistance Strain Gage

The bonded-resistance strain gage has been used for more than thirty years, but many elementary factors of its usage are still not understood. Problems of how strain is transmitted from specimen to gage, how gage current and choice of adhesive affect the gage factor have not been solved. Lack of knowledge in these areas does not seriously deter the researcher working in familiar areas; but to those extending research into heretofore unexplored regions, such lack of knowledge would be serious.

Strain transmission to gages The transmission of strain from the specimen to embedded gages is identical in principle to that experienced with surface gages. A brief summary of the effects investigated in surface-mounted gages is presented, since considerably more data have been evaluated for such gages.

Every type of strain transducer utilized is based upon transmission of strain from a surface of the specimen to the transducer. Proper use of the transducer must be based upon a knowledge of the fidelity of this transmission, its effect on transducer characteristics, and its effect upon the strains in the specimen in the vicinity of the transducer.

Strain transmission may be separated into boundary (adhesive-specimen and adhesive-strain gage) transmission and strain transmission within the adhesive. In general, strains must be transferred from the specimen to the adhesive by shear forces developed at the interface. Stein³ states "From the earliest days of the bonded resistance strain gage the problem of strain transmittal from the test specimen through

the adhesive layer to the strain sensitive element has been studied, although notably NOT in the United States."

The results of these investigations may be summarized briefly as follows: A single circular cylindrical strain-sensitive filament of length L is considered embedded in an infinite layer of adhesive applied to a uniform tensile specimen. The force distribution along the filament can be shown, as in Figure A.9, to rise approximately exponentially from zero at its ends to some constant finite value across its midsection. Since the strain in the filament is directly proportional to the force along it, it follows that the strain distribution in the filament is identical to the distribution of the applied force. As a consequence of this behavior, the effective gage length of the filament is less than the length L . The amount which it differs from the actual length is dependent upon wire diameter, adhesive-layer thickness, elastic-adhesive modulus, elastic-wire modulus, and elastic-adhesive shear modulus. This change in gage length desensitizes the gage, and reduces the effective gage factor. Least effect on gage factor is experienced by using a thin adhesive layer, fine weak wire, and rigid adhesives.

Strain-gage factors and effective gage lengths of various types of gages are determined by the manufacturer for certain conditions of specimen material, loading conditions, adhesives, curing conditions, etc. These conditions are not necessarily the same from manufacturer to manufacturer, or even gage model to model of the same manufacturer. If the shear-rigidity of the adhesive is lowered below that for which the gage was originally calibrated, other variables remaining constant,

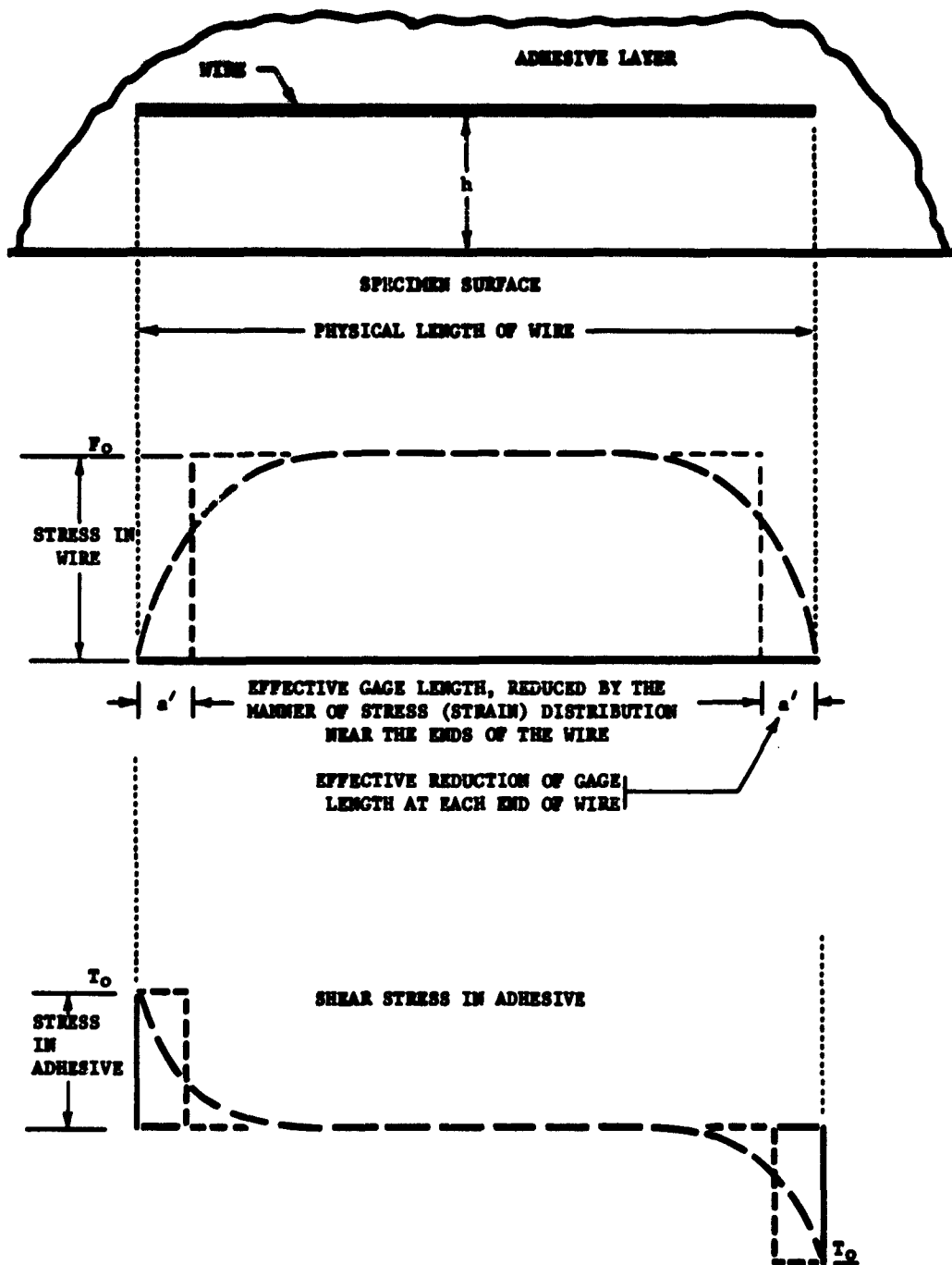


Figure A.9: Idealized strain distribution in a single strain sensitive filament in an adhesive layer. (After Stein)

the effective gage factor will be reduced. This effect is more pronounced the shorter the gage length. For this reason, a careful calibration of strain gages used in conditions other than reported by previous investigators is imperative if meaningful conclusions are to be drawn from strain-gage data.

The force distribution within the filament described above is a consequence of a distribution of shear stress within the adhesive which is zero in the center of the filament and rises exponentially to a peak at either end, as shown in Figure A.9. Therefore it is extremely important that ends of a strain gage be well bonded to the structure, and anything which increases the area of the filament at the ends of the gage, will increase gage performance. Consequently foil gages with end tabs of large area perform this function extremely well.³

The most significant fact derived from this study is that in the case of a uniform applied strain the strain-gage response approximates the average strain over the effective gage length, i.e., the relative displacements of the gage ends, divided by the effective gage length. In instances where the strain changes significantly over one gage length, such a conclusion may not be warranted. The authors are not aware of a theoretical analysis of the forces on a filament glued to a specimen subjected to a nonuniform strain.

Strain transmission to embedded strain gages may occur in the same manner as in external gages, especially when the total thickness of the gage relative to its length remains very small. However, when an embedded gage is subjected to compressive strain, some strain is

transmitted to the gage due to pressures at the ends of the gage cavity, in addition to the strain transmitted by shearing stresses in the adhesive layers on the two surfaces of the gage. Strain due to end restraint represents a greater proportion of the indicated strain, the greater the thickness-to-length ratio. When these same strain gages are subjected to tensile strain, almost all the strain transmitted to the gage must be due to shear in the adhesive surfaces. Gages designed to measure both compressive and tensile strains must use adhesives of sufficient rigidity so that the gage factor is not appreciably dependent upon strain direction.

In certain instances strains have been measured using embedded strain gages with plates attached to their ends perpendicular to the gage plane. The purpose of these plates was to force the gage strain to conform to the relative displacement over the gage length.⁵

Local reinforcement and impedance matching One primary problem which exists with either external or embedded strain gages is that of local reinforcement, with resulting changes in stress distribution and erroneous gage readings. Static photoelastic studies have revealed that surface mounted strain gages on low-modulus plastics create stress concentrations in their vicinity and consequent errors in strain reading.³ These errors are insignificant for normal test purposes in work with materials with relatively high modulus of elasticity.

The accurate use of embedded strain gages in static testing requires that the gage, the immediate adhesive layers and the material in which strains are to be investigated must have identical physical properties if strain concentrations within the material are to be

avoided. The problem is complicated by the fact that the elastic properties of the adhesive-gage combinations are not easy to ascertain, and adjusting them to fit the identity requirements would be extremely difficult in most instances. Loh⁶ considered this problem from the elastic-solid viewpoint, and found that the strain concentration due to a solid elastic cylinder in an infinite elastic mass decreased as the ratio of the length to diameter of the cylinder increased (assuming a uniaxial static-stress field parallel to the cylinder axis). At length-to-diameter ratios greater than twenty, and ratios of modulus of elasticity of gage to surroundings of one or less, the strain concentration was found to be very small.

Wilson⁷ describes a strain gage made by splitting rock cores on a diameter, attaching electrical strain gages and cementing the two halves together with Araldite D epoxy resin cement to form two-inch tapered strain-gage plugs. The cores, coated with epoxy, were pressed into tapered sockets in rock slabs which were the source of the original rock cores. During static test evaluation, strain induced in the slabs compared favorably with that detected by the gage plugs. Since the gage portion of the plugs described by Wilson actually consisted of a thin layer of adhesive and an electric strain gage in the diametral plane, it appears that the criteria set forth by Loh for cylindrical strain gages may be applicable to thin plate-like gages as well. These gages offer opportunity for adaption as dynamic-strain measuring devices.

If incident-strain pulses are to pass through embedded strain gages without reflection or diffraction effects, the velocities of

pulse travel in the media and in the strain-gage must be equal, and the gage-adhesive-media strengths must not be exceeded. This is merely another way of saying they must have identical physical properties.

Martin⁸ developed an embedded-resistance strain gage for dynamic work based on the data Loh obtained for the static stress condition. He chose a modulus of elasticity of his gage to be 1×10^6 psi for use in plaster with modulus from $.9-3.0 \times 10^6$ psi. SR-4 wrap-around A-14 and A-8 gages were dipped in Acme 4027 epoxy resin and cured at 110° centigrade. Successive coatings were built up by dipping and curing. Belden 8429 shielded, two-conductor cable, and a coating of silver paint were used to reduce electrical radiation. Completed gages, averaging about 0.025 in. thickness at the grid wire, were cast in plaster. Gages were calibrated by embedment in a pressure bar. No mention is made of difficulties with gage to plaster adhesion, gage heating, current levels, or gage curvature after coating with epoxy. The gages appear to have worked very satisfactorily and they represent the best working strain gages of their size (A-8 has 1/8-inch gage length) to date.

Gage-length effects Regardless of the method of observation, some effect of the finite gage length appears in every strain measurement. The strain-gage resistance variation is a function of the strain variations beneath its "effective" gage length. The effective gage length may be less than the geometric gage length as indicated in the strain-transmission section.

In adhesively attached strain gages, the largest possible gage length results in the greatest fidelity of strain reproduction since

pulse travel in the media and in the strain-gage must be equal, and the gage-adhesive-media strengths must not be exceeded. This is merely another way of saying they must have identical physical properties.

Martin⁸ developed an embedded-resistance strain gage for dynamic work based on the data Loh obtained for the static stress condition. He chose a modulus of elasticity of his gage to be 1×10^6 psi for use in plaster with modulus from $.9-3.0 \times 10^6$ psi. SR-4 wrap-around A-14 and A-8 gages were dipped in Acme 4027 epoxy resin and cured at 110° centigrade. Successive coatings were built up by dipping and curing. Belden 8429 shielded, two-conductor cable, and a coating of silver paint were used to reduce electrical radiation. Completed gages, averaging about 0.025 in. thickness at the grid wire, were cast in plaster. Gages were calibrated by embedment in a pressure bar. No mention is made of difficulties with gage to plaster adhesion, gage heating, current levels, or gage curvature after coating with epoxy. The gages appear to have worked very satisfactorily and they represent the best working strain gages of their size (A-8 has 1/8-inch gage length) to date.

Gage-length effects Regardless of the method of observation, some effect of the finite gage length appears in every strain measurement. The strain-gage resistance variation is a function of the strain variations beneath its "effective" gage length. The effective gage length may be less than the geometric gage length as indicated in the strain-transmission section.

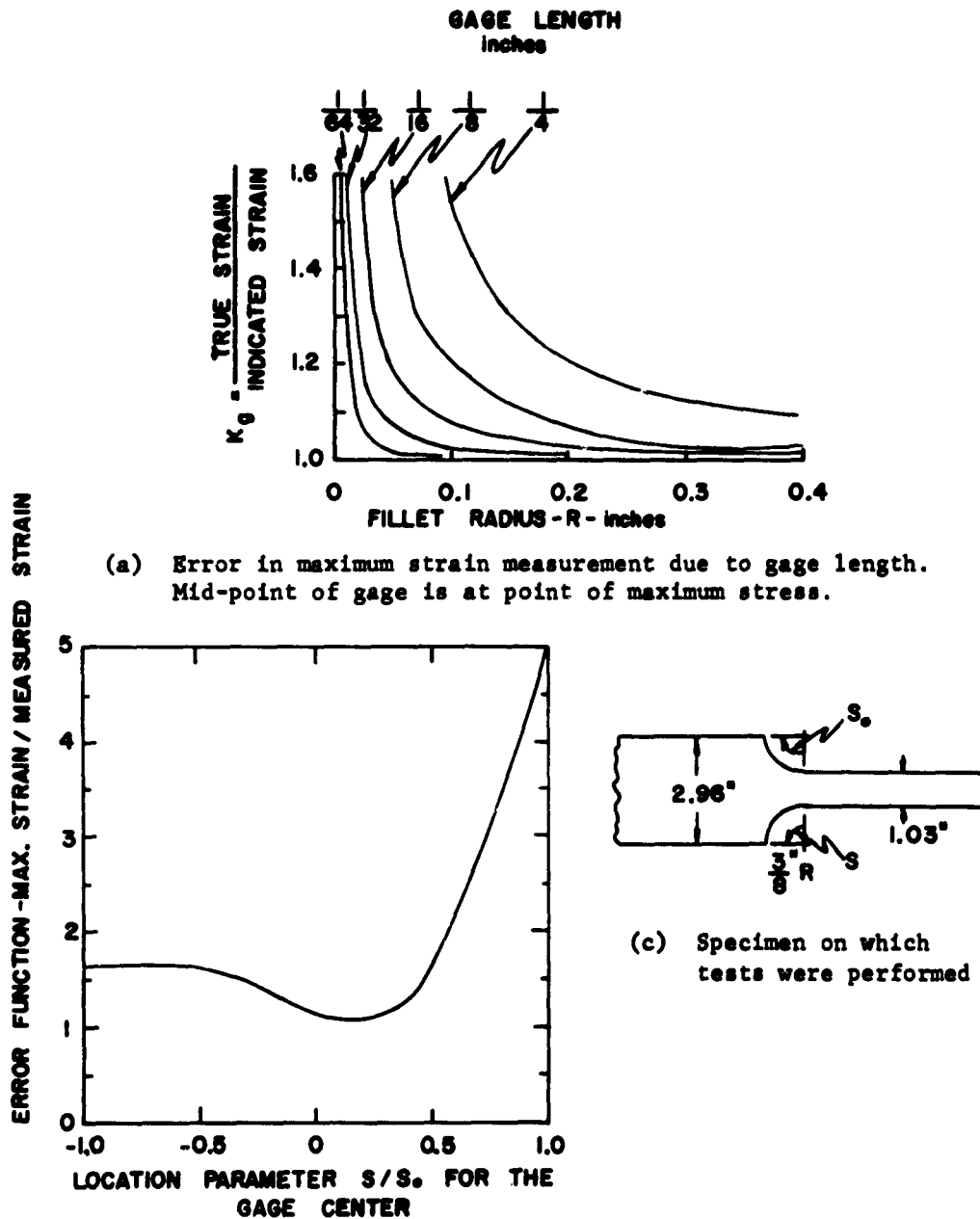
In adhesively attached strain gages, the largest possible gage length results in the greatest fidelity of strain reproduction since

strain-transmission efficiency is greater and hysteresis creep and zero shift are lower. However, the gage length is limited by (1) physical restrictions of the area allocated for gage attachment, (2) static-strain gradient, and (3) dynamic-strain gradient.³

Static strain gradient Since strain-gage response is a function of strain developed over the entire gage length, any peak strains which occur beneath the gage are "averaged" with concurrent lower strains. The effect of this phenomenon was investigated by photoelastic means⁹ and the results for a cantilever beam with circular fillet are presented in Figure A.10. It should be noted that not only is the error in indicated strain a function of gage length, but also of the position of the gage center with respect to the point of maximum strain.

Dynamic strain gradient The effect of strain-gage length has been investigated in regard to steady-state frequency response and response to transient strains, both theoretically and experimentally. However, little study has been attempted to determine the relationship between the two types of behavior.

Under steady-state sinusoidal-strain excitation, the gage length as compared with the vibration wave length will determine the time-dependent strain-gage output. In the analysis presented below, it is assumed that the strain gage reads the average strain over its length. (This is certainly true in the case of gages subjected to a uniform strain, allowing for a small reduction in gage length due to the strain transmission through a finite layer of adhesive). Its use in the case of gages subjected to gradients of strain appears to be a reasonable approximation, (especially since no other explanations have been put



(b) Error in maximum strain measurement due to location. 1/8-inch length.

Figure A.10: The effect of gage length and gage center location on the accuracy of static strain readings in regions of high strain gradient. (After Ades)

forth). When a strain gage of length L is subjected to a traveling or standing wave of wave length $\lambda = C_0/f$, where C_0 is the velocity of sound in the media, and f is the frequency of the sinusoidal strain, the gage reading is equal to the relative displacement of the ends of the gauge divided by the effective gage length.¹⁰ From Figure A.11 this gage strain ϵ_0 is

$$\begin{aligned}\epsilon_0 &= \frac{1}{L} \int_{\alpha}^{\beta} \sin \frac{2\pi x}{\lambda} dx \\ &= \frac{\lambda}{\pi L} \sin \left[\frac{\pi}{\lambda} (\alpha + \beta) \right] \sin \left[\frac{\pi}{\lambda} (\beta - \alpha) \right]\end{aligned}\quad (\text{A-20})$$

The strain at the midpoint of the gage, which the gage was presumed to measure is

$$\epsilon_1 = \sin \left[\frac{\pi}{\lambda} (\alpha + \beta) \right] \quad (\text{A-21})$$

The amplification afforded by the strain gage is

$$A_g = \frac{\epsilon_0}{\epsilon_1} = \frac{\lambda}{\pi L} \sin \left[\frac{\pi}{\lambda} (\beta - \alpha) \right] = \frac{\lambda}{\pi L} \sin \frac{\pi L}{\lambda} \quad (\text{A-22})$$

It is of interest to determine the upper 3db frequency of the strain gage, i.e., the frequency at which the apparent strain output equals $1/\sqrt{2}$ times the true strain. At the upper frequency limit

$$A_g = \frac{\lambda}{\pi L} \sin \frac{\pi L}{\lambda} = \frac{\sqrt{2}}{2} = \sin \frac{\pi}{4} \quad (\text{A-23})$$

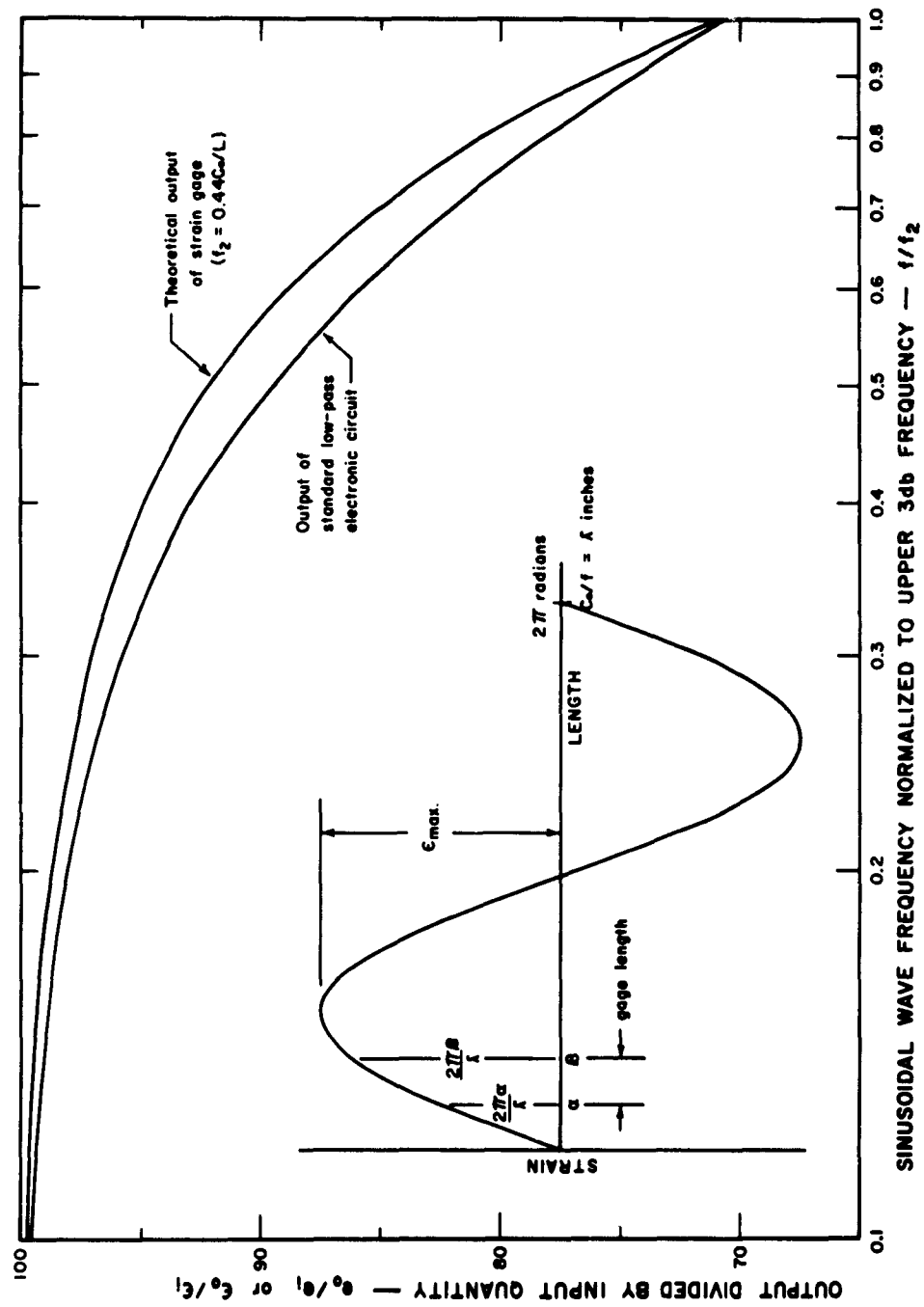


Figure A.11: A comparison of frequency response curves for low-pass filter and strain gage of length L subjected to a standing or traveling wave of frequency f .

or

$$\frac{\pi L}{\lambda_2} = 1.39 \quad (\text{A-24})$$

since $\lambda_2 = C_0/f_2$

$$f_2 = .44 \frac{C_0}{L} \quad (\text{A-25})$$

A plot of the high-frequency response of a strain gage subjected to simple harmonic strains of frequency f is presented in Figure A.11, based on equations (A-22) and (A-25). The frequency response of a low-pass electronic circuit is presented in the same figure for comparative purposes. The strain-gage response is better, for all frequencies less than f_2 , than a low-pass circuit with same 3db point.

The rise time of the response of a strain gage to a step-input strain traveling at a velocity C_0 (assuming the strain to be averaged over the length of the gage) is given by

$$T_R = 0.8 \frac{L}{C_0} \quad (\text{A-26})$$

The transient response may be linked with the sinusoidal strain-gage response by solving equations (A-25) and (A-26) simultaneously, obtaining

$$T_R = \frac{0.35}{f_2} \quad (\text{A-27})$$

This equation is identical to that relating sinusoidal to transient

response of a low-pass electronic circuit. This result, together with the frequency-response curve obtained for the strain gage in Figure A.11, suggests that other features of strain-gage response may be approximated by the low-pass circuit. In particular, the response to a finite ramp strain by a strain gage will be assumed equal to that previously derived for the potentiometric circuit, Figure A.7. This result is extremely useful since it permits evaluation of the gage length in terms of the rise time of the strain transient being recorded.

Assume a strain transient is to be recorded whose rise time is 10 microseconds, in a medium whose velocity of sound is 200,000 inches/second. If an error of less than one per cent in rise time is allowed, $f_2 T \approx 2$ from Figure A.8. Thus the upper 3db frequency $f_2 = 200$ KC, and $L = .44 C_0 / f_2 = 0.44$ in.

The effect of an adhesive layer and backing material on the strain-gage response has not been considered in this analysis. Their presence should reduce the frequency response. However, Nisbett¹¹ found that epoxy-resin bonded or nitrocellulose cemented isoelastic strain gages showed no discernable adhesive-frequency effects for harmonic strains up to 25 KC. This would suggest an upper 3db frequency for adhesive response of at least 200 KC. Using this figure and the approximate relationship¹

$$T_{Rga} = \sqrt{T_{Rg}^2 + T_{Ra}^2} \quad (A-28)$$

where: T_{Rga} = rise time of response to step input of gage plus
adhesive

T_{R_g} = rise time of gage

T_{R_a} = rise time of adhesive

the required length of gage is found from equation (A-26) to be

$$L = 2.19 \times 10^{-6} \frac{C_o}{f_2} \sqrt{4 \times 10^{10} - f_2^2} \quad (A-29)$$

If a strain transient with rise time of 10 microseconds is to be recorded with an accuracy of 2 per cent, in a medium with sound velocity equal to 200,000 inches/second, the gage length (using Figure A.8 and equation (A-29)) should be less than 0.21 in. In the identical situation but neglecting the adhesive effects, the calculated value was $L = 0.5$ inches.

Nonhomogeneous material In the study of polycrystalline materials such as rock, or in the study of concretes and mortars, where the average strains within the vicinity of a group of crystals or grains is to be determined, the problem of proper gage length must again be considered. The problem of average strain requires that the strain gage bridge across a number of the constituent particles of the non-homogeneous mass. Results of static strain-gage tests with various gage length to nominal aggregate-size ratios are presented in Figure A.12, as summarized by Stein.³ Note that approximately 3 per cent error exists in recorded strain at a ratio of gage length to maximum aggregate size of 10, and that this error shows little improvement with further increase in gage length. It is to be expected that a decrease in aggregate size should result in a smaller percentage error, holding

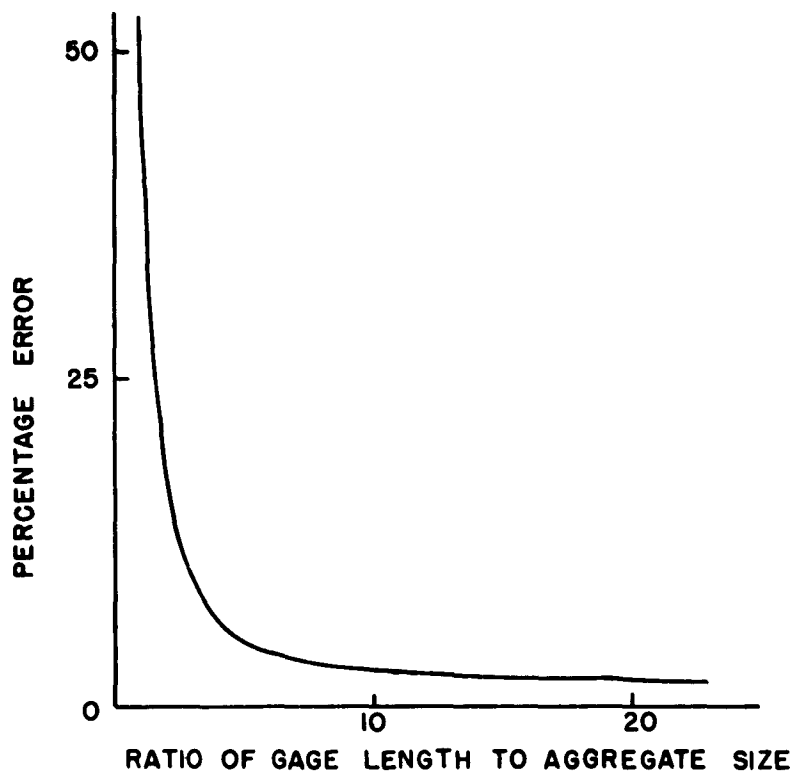


Figure A.12: Strain gage errors for various ratios of gage length to nominal maximum aggregate size includes data from Binns & Mygind, Peattie, and Cooke & Seddon. (After Stein)

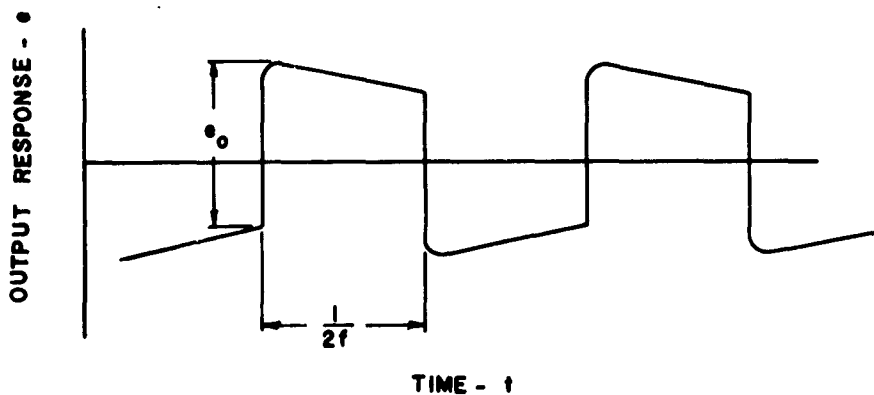


Figure A.13: Output response of measuring system to chopper controlled calibrating resistor.

gage-length aggregate-size ratio constant. A ratio equal to 10 appears to establish a lower limit on gage length.

Gage Current

The current passed through a strain gage during the measurement process has both upper and lower limits. For the maximum voltage output from a potentiometric circuit, for example, the largest currents which the gage may carry without overheating are frequently used. The effect of current upon voltage output may be determined from Figure A.3. The maximum allowable current is a function of the heat carried away from the gage,³ and has been defined as

$$I = k \sqrt{pa/\rho} \quad (A-30)$$

where k = constant for any cooling condition

p = perimeter of the gage wire

a = wire cross-sectional area

ρ = specific resistance

Experience of investigators with wire filament strain gages on metal specimens at room temperature³ suggests that an upper limit for current is given by

$$I = 800 \sqrt{d^3/\rho} \quad (A-31)$$

where: d = wire diameter

These results apply to flat-grid, Constantan-wire gages in which filament spacing is approximately ten times the wire diameter. This

formula gives safe currents of 35 and 12.5 milliamperes for the common gage-wire diameters of 0.001 and 0.0005 in., respectively. Gages with filament spacing closer than ten diameters must be de-rated; a de-rating factor of 1/20 being applied for spacings of two diameters. Foil gages have higher current-carrying capacity since their proportionally greater surface area provides better heat dissipation. (Exact values are not known, although gains of 100 per cent have been shown mathematically, and gage manufacturers claim as high as 400 per cent).

The mounting of gages on materials other than metals may result in overheating at the currents calculated above, if the heat transfer from the base material is small, such as in most plastics.

The most significant effect of gage current in dynamic testing is its effect on gage factor. In general, heat transfer from the gage approaches equilibrium rather quickly after the current is applied, and consequently the gage factor and gage resistance soon stabilize. Thus, the final temperature which the gage assumes determines its characteristics during a dynamic test. Constantan-Advance metal-wire gages of flat-grid construction have been shown to have little gage-factor variation at temperatures up to 150° centigrade,¹² while Iso-elastic gage factor is flat to only about 40° centigrade. (This is sufficient reason for preference of Advance elements for gages where some question as to gage temperature appears).

No data are available on the relation between gage current and the temperature in the vicinity of gages embedded in rock or concrete. Therefore, direct use cannot be made of available gage factor-temperature data. However, in tests of an SR-4 A-1 (120 ohm, Advance, flat-grid, wide-spaced) gage on the surface of Castolite, there was no gage

factor change at up to 20 millamperes gage current.¹³ This gage has a gage length of 13/16. Shorter gage lengths of the same type might be expected to show some effect of gage factor on temperature if resistance and current remain the same due to increased local temperature gradient. On the basis of this test, and from the other information presented, the choice of gage currents from 25-30 milliamperes appears justified for foil strain gages with copper-nickel (Advance) composition embedded in concrete, mortar, or rock for dynamic strain purposes. Further work is required in this area, however, since it is critical to meaningful interpretation of strain data.

Measurement System Response

The overall system response is dependent upon each of the components in the system: strain gage, strain gage supply circuit, and amplification circuitry. Obviously the amplification and recording equipment chosen must have adequate frequency response to depict the strain transients measured. The system rise time may be approximated by¹

$$T_R = \sqrt{\sum_{i=1}^n T_{R_i}^2} \quad (A-32)$$

where: T_{R_i} = the rise time of each component of the system

The approximate upper 3db-frequency limit may be determined from the rise time by use of equation (A-17). These approximations may be in error by as much as twenty per cent.

The approximate lower 3db-frequency limit is given by

$$f_1 = \frac{1}{\sum_{i=1}^n T_{R_i}} \quad (A-33)$$

where: f_{11} = the lower 3db-frequency limit of each component

This equation is applicable where the lower frequency limits are very low, i.e., per cent droop of response is very small.

The overall frequency response should be used together with estimates of transient strain-time history to determine the effect on the accuracy of recorded data.

The Shunt-Calibration Method

Assuming that the effective strain-gage factor has been established, the most effective calibration method for field usage is the "shunt resistance" method. In this method, a precision calibration resistor is shunted across the strain gage, while the gage is in the measuring circuit. The measuring system interprets this action as a change in gage resistance, as given by the expression

$$\Delta R_g = \frac{R_g^2}{R_g + R_c} \quad (A-34)$$

and since the effective gage factor is

$$S = \frac{\Delta R_g / R_g}{\epsilon}$$

the calibrating resistance produces an equivalent strain response in the measuring system

$$\epsilon_c = \frac{1}{S} \frac{R_g}{R_g + R_c} \quad (A-35)$$

It is important to note that since the calibrating resistance always

lowers the total resistance detected by the measuring system, the equivalent strain produced when switching the calibrating resistance into the circuit is compression. Thus, the shunt-calibration method not only gives a precise magnitude of strain in systems calibration, but also indicates the polarity of indicator response. The accuracy required of precision resistors used in the shunt technique must be equal to or greater than the accuracy demanded of the equivalent strain, as is apparent from equation (A-35). Equivalent strains are subject to the same restrictions as to magnitude before nonlinearity becomes significant as the true strains described previously. The results of Figure A-2 may be applied here to obtain a nonlinearity factor.

Lead wire resistance effect If it were possible to place the calibration resistance directly across the strain gage, as shown in Figure A.1(c), the voltage output would be

$$\begin{aligned} dE^*_c &= V \frac{R_b}{(R_g + R_w + R_b)^2} \frac{R_g^2}{R_c + R_g} \\ &= \frac{a}{(1 + R_w/R_g + a)^2} \epsilon_c \end{aligned} \quad (A-36)$$

Writing equation (A-36) in the form previously derived when considering lead-wire effects, one obtains

$$dE^*_c = I \epsilon_c S R_g \frac{a}{(1 + a)(1 + b)} \quad (A-37)$$

Thus the voltage output due to shunt resistance may be used directly to calibrate the output of the system in terms of an equivalent strain.

The shunt calibrating resistance is normally placed across the

indicator ends of the strain gage lead wires, as in Figure A.1(d) rather than across the gage itself (either for the sake of convenience or because of the inaccessibility of the strain gage). In such circumstances

$$dE' = V \frac{R_b}{(R_g + R_w + R_b)^2} \cdot \frac{(R_g + R_w)^2}{R_g + R_w + R_c} \quad (A-38)$$

$$\text{or } dE' = I \epsilon_c' S R_g \frac{a}{(1 + a)(1 + b)} \quad (A-39)$$

$$\begin{aligned} \text{where: } \epsilon_c' &= \epsilon_c \left(\frac{R_g + R_w}{R_g} \right)^2 \left(\frac{R_c + R_g}{R_c + R_g + R_w} \right) \\ &= \epsilon_c \left(1 + \frac{R_w}{R_g} \right)^2 \left(\frac{1}{1 + \frac{R_w}{R_c + R_g}} \right) \end{aligned} \quad (A-40)$$

when $R_c + R_g \gg R_w$, this equation becomes

$$\epsilon_c' = \epsilon_c \left(1 + \frac{R_w}{R_g} \right)^2 = \frac{1}{S} \left(\frac{R_g}{R_g + R_c} \right) \left(1 + \frac{R_w}{R_g} \right)^2 \quad (A-41)$$

Equation (A-41) demonstrates that the equivalent strain due to the calibrating resistor is greater when the resistance is located at the indicating instrument than when it is located directly across the strain gage.

As an example consider the circuit previously investigated, where $R_g = 120$ ohms, $a = 10$, and 1000 ft. of 18 A.W.G. wire was used. In this case the error in measured strain calculated from the observed voltage, using formula (A-7) which disregards lead-wire resistance was

1 per cent. Equation (A-41) shows that if the same system is calibrated with a shunt resistance, an error of 11 per cent will be experienced, if the equivalent strain calculation does not include lead-wire effects. Since there have been many instances where lead-wire effects were erroneously disregarded (usually on the basis of the sort of analysis leading to equation (A-14), followed by calibration in the manner just discussed, the viewpoint is expressed here that to be valid shunt resistance calibration must be based on an equivalent strain calculated from equations (A-40) or (A-41).

Calibration switching speed All the capacitive elements within the electronic portion of the measuring system have an effect on the system's frequency response. Since the dc-component is absent in the potentiometric circuit response, any calibration technique must necessarily be dynamic. The commonest form of calibration is a shunt resistance switched across the strain-gage leads by an electromechanical chopper. Since the measuring system is limited in both its upper and lower frequency response, the chopping rate must be chosen with some thought.

The ratio of incremental output-voltage change which occurs whenever the chopper contacts open or close to the incremental change which would occur if no capacitive effects were present is expressed by

$$\frac{dE''}{dE'} = \frac{f_2/f_1}{f_2/f_1 - 1} (\epsilon^{-2\pi f_1 t} - \epsilon^{-2\pi f_2 t}); t < \frac{1}{2f_c} \quad (A-40)$$

where: f_2 = system upper 3db frequency

f_1 = system lower 3db frequency

f_c = chopper frequency

Less than one per cent error in the amplitude of the incremental output voltage change occurs if $f_2 = 600f_1$. As a preliminary to calibration, the f_1 and f_2 of the total electronic system should be approximated. If the band width is greater than $600f_1$, a chopper frequency may be chosen where $f_1 < f_c < 0.5f_2$. The voltage change e_o corresponding to the calibrated resistance change (equivalent strain) is shown in Figure A.13, and should be accurate within one per cent. A good choice for chopper frequency is between f_1 and $100f_1$.

If the bandwidth of the entire strain-measuring system is narrow, i.e., below $600f_1$, a technique for choosing the chopper frequency suggested by Stein¹⁴ can be employed. This method of calibration requires accurate control of the square-wave frequency when upper and lower frequency limits are not widely separated. This technique is not normally required with the equipment which is presently available for transient strain analysis.

Determination of system bandwidth The calibration resistor may be used to determine the upper and lower 3db points of the entire measuring system exclusive of the strain gage itself. If the chopper frequency is adjusted between the limits previously suggested, and the recording system is adjusted to give time a scale so that system rise time T_s can be obtained, the upper 3db frequency is expressed by

$$f_2 = \frac{0.35}{T_s} \quad (A-41)$$

If the time scale is adjusted so that the per cent droop of the

output voltage can be observed in a given time, the lower 3db frequency is given by

$$f_1 = \frac{P}{200\pi T}$$

where: P = per cent droop

T = time period of observation

References

1. Millman, J., and Taub, H., Pulse and Digital Circuits, McGraw-Hill, 1956.
2. Murray, W. M., and Stein, P. K., Strain Gage Techniques, Mass. Inst. of Tech., Cambridge, Mass., 1958.
3. Stein, P. K., Advanced Strain Gage Technique, Stein Engr. Services, Phoenix, Arizona, 1962.
4. Pettit, J. M., Electronic Switching, Timing, and Pulse Circuits, McGraw - Hill, 1959.
5. Ehlers, O. K., et al., High Explosive Equivalence for Underground Detonation of Operation Plumbob, ERDL Tech. Rept. 1625-TR, April, 1960.
6. Loh, Y. C., "Internal Stress Gages for Cementitious Materials," SESA Proceedings, Vol. XI, No. 2, 1954.
7. Wilson, A. H., "A Laboratory Investigation of a High Modulus Bore-hole Plug Gage for the Measurement of Rock Stress," Proceedings 4th Symp. on Rock Mech., Penn. State University, 1961.
8. Martin, C. W. "Fracture of Plaster by Explosions," Ph.D. Dissertation Iowa State Univ., 1962.
9. Ades, C. S. and Lee, L. H. N., "Strain-gage Measurements in Regions of High Stress Gradient," SESA Proceedings, Vol. XVIII, No. 1, 1961.
10. Maslen, K. R., "On Effect of Gage Length on the Response of Strain Gages to Dynamic Strain," Royal Aircraft Estab. Tech. Memo, No. Instn. 294, May, 1960.
11. Nisbet, J. S., Brennan, J. N., and Tarpley, H. I. "High Frequency Strain Gage and Accelerometer Calibration," J. Of the Accous. Soc. of A., Vol. 32, No. 1, Jan. 1960.
12. Campbell, W. R., "Tests of Six Types of Bakelite-Bonded Wire Strain Gages," N.A.C.A. TN 1656, July, 1948.
13. Grocht, M. M., Landsberg, D. and Wang, "The Effect of Gage Current on Strain Measurements," SESA Proceedings, Vol. XVI, No. 2, 1959.
14. Stein, P., "Selection of Square Wave Repetition Rate for Minimum Peak-to-Peak Amplitude Error in AC Systems," Strain Gage Readings, Vol. IV, No. 6, Feb-Mar, 1962.

APPENDIX B
DYNAMIC STRESS MEASUREMENT WITH
PIEZOELECTRIC GAGES

The measurement of dynamic stress in solids by piezoelectric gages requires special knowledge of the behavior of electronic circuits, piezoelectric materials, stress isolation, and the material being investigated. Some of the basic information utilized to make decisions as to gage construction, associated electronic circuitry, calibration techniques, etc., which are unique to the measurement of high-intensity, short-duration stress transients are presented in this Appendix.

Piezoelectric Materials

Piezoelectric materials generate an electric charge when subjected to a physical stress. Conversely, a piezoelectric material undergoes a change in dimensions when a voltage is applied to it. Piezoelectric materials include (1) natural crystals such as quartz, (2) synthetic crystalline materials such as lithium sulfate, and (3) polarized ferroelectric ceramics such as barium titanate. The piezoelectric effect in a ferroelectric ceramic is obtained by applying a constant voltage to two surfaces of the material, and then removing the voltage, leaving a remnant polarization. For PZT-4 and PZT-5,* modified lead-zirconate-titanate polycrystalline ceramics, bias voltages are usually between 30,000 and 100,000 volts/inch thickness.¹

The generated charge in polarized ferroelectric ceramics is a function of the applied stress, the direction and magnitude of the induced polarization, the direction of the applied stress, and the

*Registered trademarks of the Clevite Corp.

location of the electrodes. Ferroelectric ceramics are finding increased favor over natural or synthetic crystals because of their higher sensitivity, higher dielectric constant, ease of fabrication and lower cost. However, one disadvantage of piezoelectric ceramics is change of properties with time; the material dielectric and piezoelectric constants decrease with time, and elastic stiffness and mechanical quality factors increase with time. Another disadvantage is the possibility of depolarization when subjected to high stress fields. Since in the measurement of stresses at an internal point in a body relatively little chance for re-use of gages exists, the factor of cost is important, ruling out crystal-type gages in most instances. For that reason, further discussion is limited to the ferroelectric ceramic materials.¹

A piezoelectric ceramic can be fully described by its independent elastic, piezoelectric, and dielectric constants. Those properties of greatest interest to the stress analyst are the piezoelectric strain constants d_{ij} , the piezoelectric "voltage" constants g_{ij} , the permittivity ϵ_{ij} , the resistivity, the elastic constants, and the internal mechanical damping.

Piezoelectric properties are described with regard to a mutually perpendicular axes system. Subscripts of 1, 2 and 3 applied to material constants refer to the respective axes. Subscripts 4, 5, and 6 refer to the 2-3, 1-3 and 1-2 planes, respectively. The 3-axis is always considered to lie parallel to the direction of polarization. Thus a disc polarized in the thickness direction has 1- and 2-axes equal to the radial axis.

The subscript i in the constants above refers to the direction of

the applied field in an electrically driven transducer or the measured electrical signal in a detector. The subscript j refers to the direction of the mechanical stress whether produced by, or detected by, the transducer.

Piezoelectric strain constant The piezoelectric strain constant d_{ij} (coulomb/newton) is the constant of proportionality between open-circuit charge output per unit area of a piezoelectric material and the applied stress, in the expression

$$\frac{q_i}{A_i} = d_{ij} \sigma^j \quad (B-1)$$

where: q_i = charge output (coulomb)

A_i = cross-sectional area of ceramic (meters)²

σ^j = applied stress (newtons/meter²)

The relations between applied-stress components and electrical field are linear only over limited ranges of the input signal; higher signals can cause domain reversals resulting in gross deviation. There may also be as much as 10 per cent variation of a particular piezoelectric strain constant from sample to sample of a single material.²

Temperature variation can have marked effects on the piezoelectric constants. Some barium titanate ceramics exhibit as much as 100 per cent change in d_{31} in a temperature region within twenty degrees above or below 0° centigrade. Figure B.1 shows the effect of temperature on properties of a typical lead-zirconate-titanate (PZT-4). Note that in the 0-100° centigrade region negligible change in the piezoelectric constant, d_{31} occurs. Typical values of piezoelectric strain constant

Figure B.1: Variation of piezoelectric voltage and strain constants and planar coupling coeff. of PZT-4 with temperature.
(After Crawford)

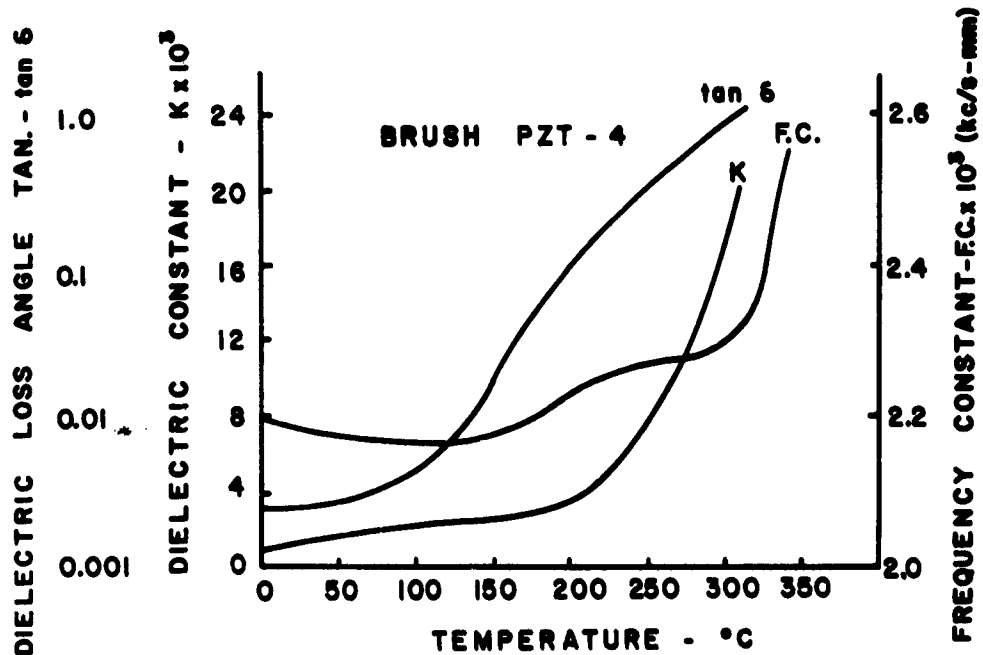
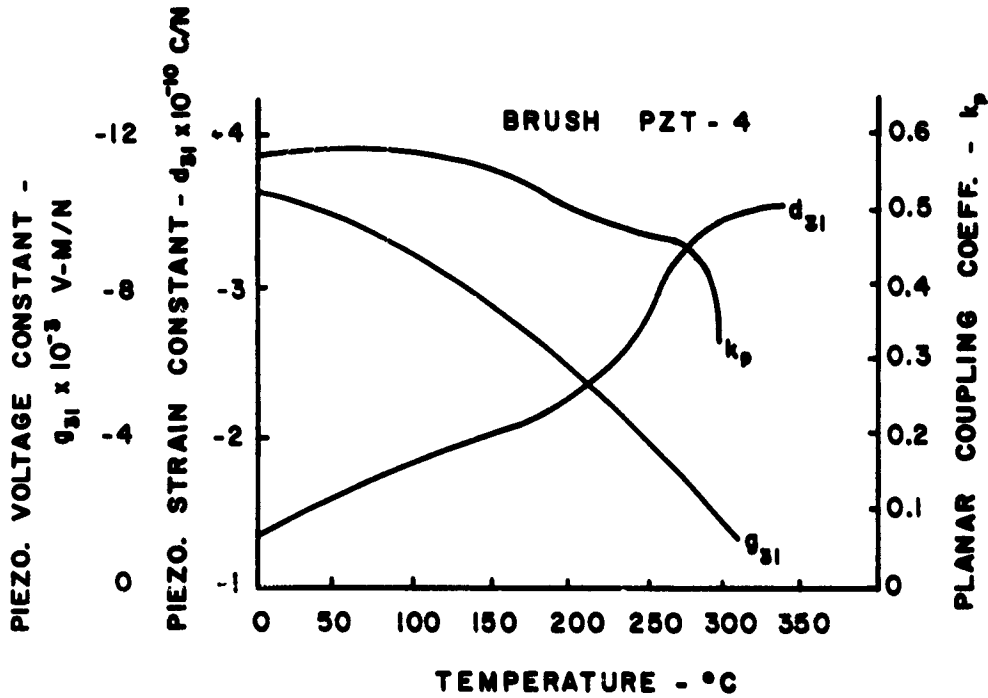


Figure B.2: Variation of dielectric constant, frequency constant and dielectric loss angle of PZT-4 with temperature.
(After Crawford)

are $d_{33} = 19$ and 310×10^{-12} coulomb/newton and $d_{31} = -78$ and -135×10^{-12} coulomb/newton for barium titanate and PZT, respectively.³ Note also that the cross-sensitivity is sufficiently large as to lead to considerable confusion where data are to be obtained in a two or three-dimensional stress field where stress components are independent.

Permittivity The permittivity ϵ_{ij} (free dielectric constant) is quite high for piezoelectric ceramics, as compared to crystals. Values range from 200 - 1250×10^{-11} farads/meter. It is customary for manufacturers to list relative dielectric constants K_1 and K_3 , obtained from ϵ_{11} and ϵ_{33} by division by the permittivity of free space $\epsilon_0 = 8.85 \times 10^{-12}$ farad/meter. High values of permittivity reduce the effect of unavoidable stray capacitances upon output voltage sensitivity, as will be seen in the section on lead wire and circuit loading effects.

The dielectric constant increases linearly over the temperature range 0° - 100° centigrade by about 20 per cent in PZT ceramics. Figure B.2 illustrates the variation of the dielectric constant K with temperature for a PZT-4 piezoelectric ceramic. Barium titanate transducers may have as much as 200 per cent fluctuation in permittivity over the same temperature range. Where transducer usage involves extreme temperature environments, the effect on the dielectric constant must be recognized.³

Piezoelectric voltage constant The open-circuit piezoelectric voltage constant g_{ij} is a derived quantity defined by the equation

$$g_{ij} = \frac{d_{ij}}{\epsilon_{ij}} \quad (\text{volt-meter/newton}) \quad (\text{B-2})$$

The voltage output from a piezoelectric material in terms of an applied stress is expressed by the relationship

$$\frac{E_i}{D_i} = g_{ij} \sigma^j \quad (B-3)$$

where: D_i = ceramic material linear dimension in the i -direction

Typical values of piezoelectric voltage constant are $g_{33} = 14.0$ and 24.0×10^{-3} volt-meters/newton and $g_{31} = -5.5$ and -10.5×10^{-3} volt-meters/newton for barium titanate and PZT materials, respectively.³

Variations of the piezoelectric voltage constant with temperature are complicated, since the voltage constant is a function of the piezoelectric strain constant and the permittivity, both of which are temperature dependent. However, the constant g_{31} of PZT-5 exhibits less fluctuation over the range 0-50° centigrade than does d_{31} . Figure B.1 illustrates the variation in g_{31} with temperature for a PZT-4 ceramic.

Resistivity The leakage resistance of most piezoelectric ceramics in use in transducer design is extremely high, with resistivities of 10^{14} ohm not uncommon. Leakage resistance decreases under conditions of increased temperature or increased humidity. Operation at humidities greater than 50 per cent may result in significant lowering of the insulation resistance. Sensitivity of resistance to humidity is related to the surface condition of the ceramic.¹ Modified lead-zirconate-titanates such as PZT-5 seem to exhibit much less resistivity-temperature effect than other ferroelectric ceramics used in transducers, maintaining a resistivity of 10^{10} ohm-cm up to the Curie point.³

Internal mechanical damping Energy loss in the piezoelectric phenomena is normally expressed in terms of the mechanical quality factor Q , the ratio of strain in-phase to strain out-of-phase with stress. The lower the value of Q , the less efficient the energy transformation as a consequence of the higher internal mechanical damping.² The Q factor of PZT ceramics varies from 600 to 75, depending upon the additives in the material. PZT-4 has a mechanical Q of 600, and may be subjected to higher stress fields than ceramics with much lower Q 's without being damaged by internal heat energy resulting from dielectric losses.³ The Q of ceramic materials is considerably less than that of quartz and other piezoelectric crystals, hence, piezoelectric ceramics are less sensitive to mounting conditions than are the piezoelectric crystals.²

Elastic constants The modulus of elasticity of ferroelectric ceramics is quite high, ranging from .35 to 1.35×10^{11} newtons/meter² ($5\text{-}20 \times 10^6$ psi).¹ Since poled piezoelectric ceramics possess an axis of rotation of infinite order in the direction of polarization and an infinite set of all planes parallel to that axis as reflection planes, only five independent compliances exist; S_{11} , S_{33} , S_{55} , S_{12} and S_{13} . The compliances are normally determined with a constant electric field (essentially short-circuit) under resonant conditions. In uniaxial loadings

$$Y_{11}^E = \frac{1}{S_{11}^E} \quad (B-4)$$

where: Y_{11}^E = modulus of elasticity (newton/m.²)

S_{11}^E = compliance (m²/newton)

superscript E denotes constant field

$$\gamma_1^E = \frac{-S_{12}^E}{S_{11}^E} \quad (B-5)$$

where: γ_1^E = Poisson's ratio

Poisson's ratio lies between 0.28 and 0.32 for the ferroelectric ceramics.² The elastic moduli of PZT-4 and PZT-5 in the direction of polarization are 9.7×10^6 and 8.5×10^6 psi, respectively.³

Density The density of ferroelectric ceramics is approximately 5.5×10^3 Kg/meter³ for barium titanates and 7.5×10^3 Kg/meter³ for lead-zirconate-titanates.³

Ageing Piezoelectric ceramics exhibit one form of behavior, ageing, which is not welcome in transducer design. By ageing is meant the gradual change of material properties with time. Figure B.3 illustrates the typical change of properties over a period of better than a year for PZT-4, a lead-zirconate-titanate material.³ The time dependency of the dielectric constant K, the frequency constant, F.C., and the planar-coupling factor K_p , suggest that individual calibration of gages developed using these materials would be necessary.

The parameters of these ceramics tend to change after major disturbances, such as after heating in the transducer manufacture or after experiencing drastic electrical excursions. These changes decrease dielectric and piezoelectric constants and mechanical compliance, and hence, decrease gage output under stress.

Figure B.3: Ageing effects in lead zirconate titanate ceramic, PZT-4.
(After Crawford)

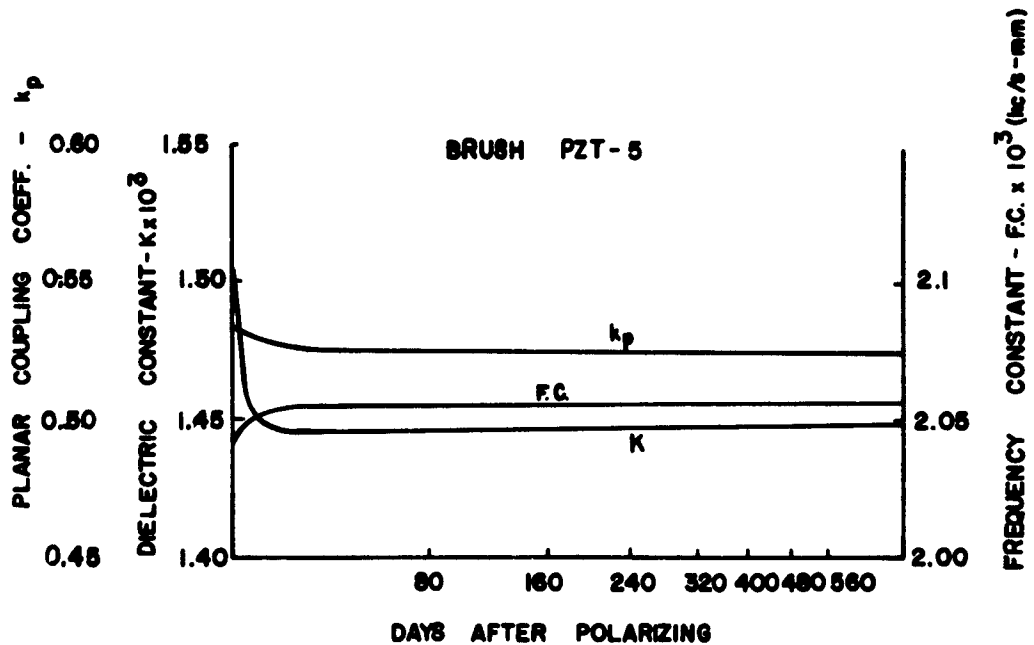
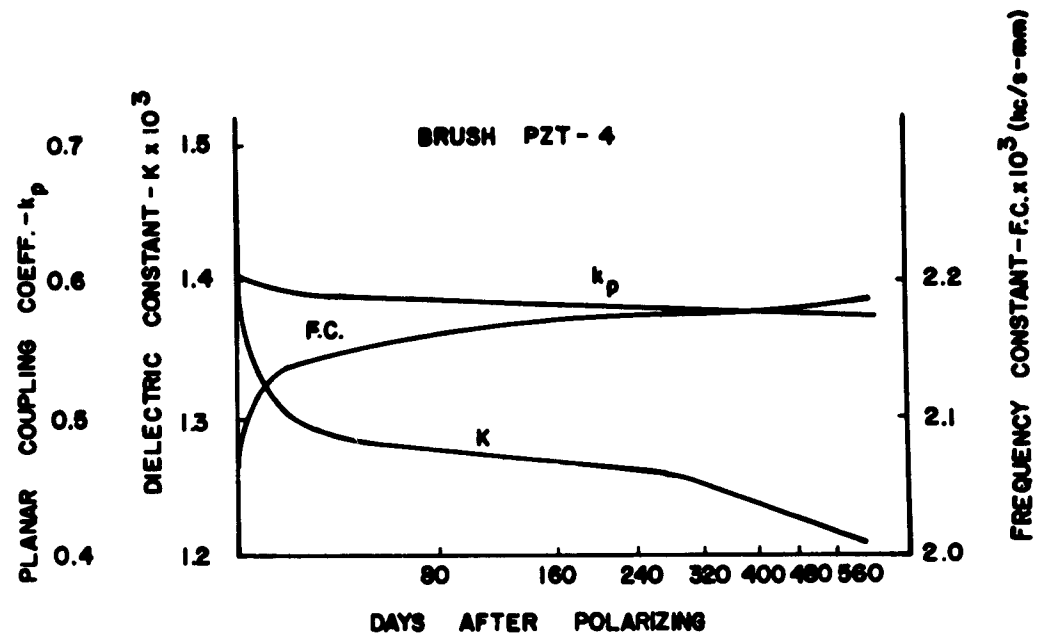


Figure B.4: Ageing effect in lead zirconate titanate ceramic, PZT-5.
(After Crawford)

Typical of the ageing effects is the change in frequency constant of barium titanate which increases by 0.54 per cent from 1 to 10 days, the rate of increase dropping to 0.42 per cent for the period from 100 to 1000 days.²

Some poled ferroelectric ceramics show relatively little significant ageing effect. Figure B.4 illustrates the behavior of a modified lead-zirconate-titanate (PZT-5) material. The dielectric constant, frequency constant and planar coupling factor are essentially constant one week after polarization.³

It is important that the piezoelectric material time dependent behavior be accounted for if quantitative results are to be relied upon.

Static strengths The compressive strengths of PZT ceramics are in the range of some of the strongest natural minerals; ceramic cylinders have been subjected to static compressive stresses of 60,000 to 100,000 psi without breaking.⁴

Static tensile strengths of about 13,000 psi were computed from bending measurements on small PZT-4 ceramic elements.⁴

Dynamic tensile strengths of the same material were determined (1) by subjecting ceramic bars to pulsed electrical excitation (resonant operation) of several milliseconds duration, increasing the excitation level until failure occurred, and (2) by continuously oscillating bars at their resonant frequency, increasing amplitude level until failure occurred. The average tensile strength under pulsed operation was 13,000 psi and under the continuous resonant frequency method was 14,000 psi. Samples used in these tests were relatively free from imperfections. Similar tests of PZT-4 ceramics showing microscopic

fissures resulted in tensile strengths of about 5000 psi.⁴

The apparent uncertainty in the true tensile strength of piezoelectric ceramics may be disregarded if a sufficiently high compressive-stress bias is applied to the transducer ceramic in the transducer design or placement.

Effect of stress-time history One question of vital importance in the accurate measurement of high-intensity stress transients by piezoelectric ceramic transducers is that of constancy of ceramic properties in the stress environment. Few approaches to this problem have been attempted. A recent study of behavior of ferroelectric ceramics under shock loading by Reynolds and Seay led to some interesting conclusions.⁵

High-intensity stress waves of 2 to 175 Kbar, were developed in BaTiO_3 and $\text{Pb}(\text{Zr}_{0.52}, \text{Ti}_{0.48})\text{O}_3$ with 1 per cent by weight Nb_2O_3 , (designated hereafter as PZT) utilizing high-explosive plane-wave generators and appropriate shock conversion techniques (impedance mismatch and elastic-plastic wave separation). In a single imposed shock wave greater than 20 Kbar (300,000 psi) magnitude, two separate plane waves were generated in and traversed through the ceramic. For waves less than 20 Kbar only a single pressure wave was induced in the ceramic.

The charge released from a 1.27 mm-thick, PZT disc as a shock wave traversed its polarization axis was detected by measuring the voltage generated across a small-valued current-detecting resistor (essentially short-circuit condition). The charge per unit area obtained from the PZT ceramic was obtained by integrating the area under the current-time curve.

Figure B.5 is a plot of the charge per unit area released as a function of the shock pressure. Note that the charge per unit area reaches a peak value of 36×10^{-6} coulomb/cm², as compared to a nominal remnant polarization of 32×10^{-6} coulomb/cm² (an excellent check on the experimental procedures). Figure B.6 illustrates that portion of the charge-pressure curve which showed linear behavior plotted on an expanded pressure scale. The charge release was linearly proportional to the applied pressure up to about 11 Kbar (160,000 psi).

The linear charge-pressure curve led to the conclusion that the primary mechanism of charge release at transient stress levels of less than 11 Kbar is a rapid, but linear reduction in the net dipole moment by the restrained compression in the propagating wave. Such a phenomenon could be reversible if unloading were sufficiently rapid. If this is the case, the charge release would be proportional to stress, an extension of the recognized piezoelectric behavior. However, this conclusion may only be applied to transients of extremely short duration, or to the stress in a wave front.

Ripperger,⁶ utilizing projectiles fired by an air gun, investigated the behavior of various ferroelectric ceramics when subjected to intense transient-stress waves with rise times of 20 microseconds or less. Barium titanate materials were depoled in all of the tests performed (levels less than 200,000 psi to 500,000 psi). One axial-mode test of PZT-1 ceramic showed linear piezoelectric response (32 kv peak) up to 1.8 msec. at which point the 0.1-inch thick disc failed mechanically. The peak stress (probably attained after the gage failed) was calculated from elastic theory to be 220,000 psi. The output voltage was measured

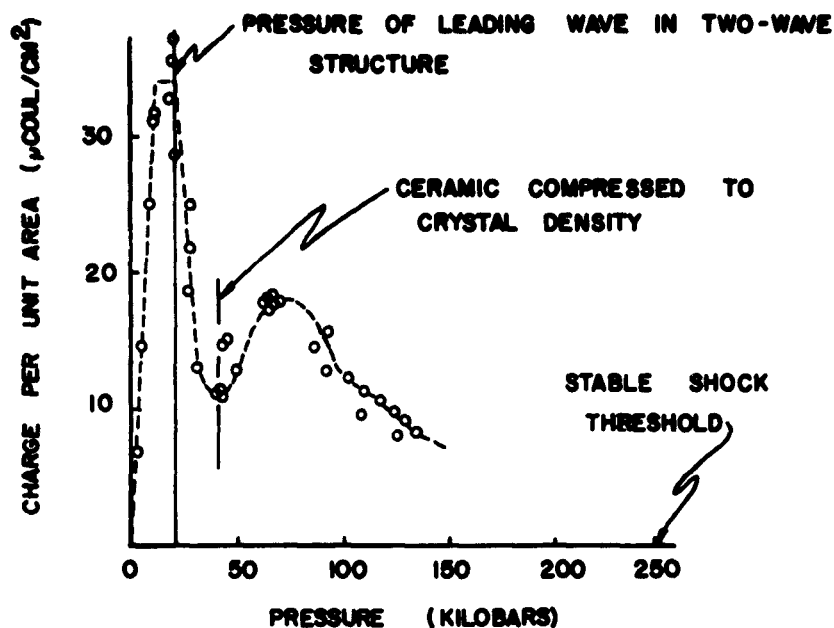


Figure B.5: Short-circuit charge output of lead zirconate titanate discs subjected to intense plane waves. (After Reynolds & Seay)

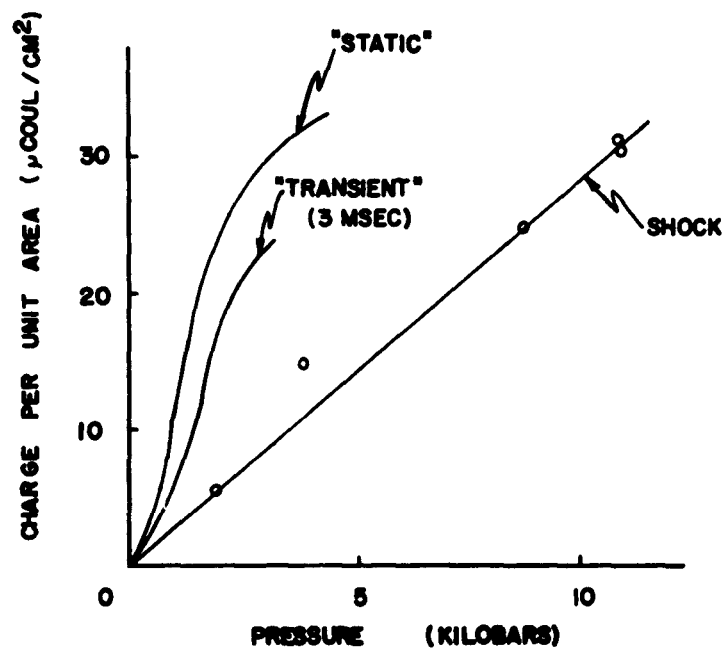


Figure B.6: Short-circuit charge output of PZT discs subjected to intense plane waves plotted to an expanded pressure scale, together with "transient" and "static" test results. (After Reynolds and Seay)

across a 210-kohm voltage divider (most probably depoling would have occurred had the ceramic material held together for sufficient time). Short-circuit tests of PZT-1 at stress levels in the neighborhood of 210,000 psi resulted in depoling.

Berlincourt and Krueger⁷ measured the short-circuit electric charge response of barium titanate and PZT ceramics to rapidly applied compressive stress with time from zero stress to peak stress of less than 3 msec. Short-circuit response was determined by measuring the voltage across a shunt capacitance three orders of magnitude greater than the test-specimen capacitance. Short-circuit response of a PZT ceramic versus applied stress is plotted in Figure B.6 as "transient stress." At very low stress levels the short-circuit charge density is a linear function of stress. From a few hundred psi to about 10,000 psi, charge flow exceeds this linear value due to depoling of the ceramic. As a result, charge effects in this range of the charge-stress curve are irreversible. The results of similar tests on the ceramic but at much slower loading rates, 250 psi/sec., are plotted in Figure B.6 as "static stress." Note that the charge output in the nonlinear range is greater, indicating that depoling is a function of time. Further proof of this is obtained from the charge response to a compressive wave front, discussed previously and plotted with the "static" and "transient" stresses for comparative purposes. One interesting feature of the "static" tests was that the short-circuit charge output was proportional to the strain of the piezoelectric element, up to about 17,000 psi applied stress. This effect was not reversible, how-

ever, due to the ceramic domain reversals.

Open-circuit voltage response to two PZT ceramics to "static" and "transient" compressive-stress loadings were also measured by Berlincourt and Krueger.⁷ Voltage output was displayed on an oscilloscope with 10^8 -ohms input resistance, giving a system RC-time constant of 10 msec. No substantial nonlinearities in voltage output with increasing "transient" stress level existed at stress levels up to 20,000 psi. The piezoelectric voltage constant was calculated to be 21.7×10^{-3} volt-meter/newton. Linearity in this instance is probably due to the fact that in the open-circuit condition charges which appear on the electrode surfaces serve to maintain a field across the ceramic supporting the original poling field and inhibiting domain switching. At the lower rates of loading, the charge gradually bleeds off through the shunt resistances and the poling field collapses. When lateral loads are applied to the ceramic, the open-circuit-voltage output becomes non-linear like the charge output in a short-circuit.

Brown⁸ investigated the effect of a two-dimensional mechanical stress on the dielectric constants of barium titanate, PZT-4 and PZT-5 ceramics. Since measurements occurred at least one minute after load application, the application of test results to transient analysis is questionable. However, the fact that the dielectric constant of all materials tested varied linearly under static loadings with durations of 1-100 minutes, at a stress of $4,000 \text{ Kg/cm}^2$, suggests that the dielectric constant may be time dependent for high-intensity short-term loading also. The dielectric constant of PZT-4 appeared to be constant for sustained stress levels up to $1,000 \text{ Kg/cm}^2$ (14,000 psi), whereas

PZT-5 shows a linear decrease in dielectric constant over the same stress range. A parallel investigation by Izhak showed that the application of a unidirectional compressional stress to ceramic barium titanate produced a rapid increase in dielectric constant followed by a gradual decrease to a steady value after a few minutes.⁸

The changes in dielectric constant described are significant since they indicate that the piezoelectric-voltage constant which is a function of the permittivity of ceramics may not be constant under varying static loads of relatively high intensity (greater than 14,000 psi in the case of PZT-4).

Krueger and Berlincourt⁹ investigated the effect of static stresses upon the piezoelectric-strain constant and the dielectric constant of PZT-4, PZT-5 and BaPb12Ti. The dielectric factor of PZT-4 changed by approximately 10 per cent and strain factor d_{33} changed 5 per cent over a range 0-19,000 psi of stress applied longitudinally. When stresses were applied laterally however, the transverse piezoelectric stress factors d_{31} and d_{32} changed by as much as 80 per cent. The other ceramic materials did not behave as well as PZT-4 under the longitudinal loadings.

PZT-4 and BaPb12Ti loaded compressively at fifteen seconds per cycle at a 10,000 psi stress level showed essentially no change in piezoelectric properties at the end of the first several cycles and not more than 8 per cent change in any property at the end of 50 stress cycles. Changes in PZT-5 properties were very severe under the same conditions. The results of these tests agree with the observations of dielectric

constant by Brown⁸ described previously under a two-dimensional stress system.

To summarize: (1) short-circuit charge release of PZT ceramics is linearly proportional to the applied stress, at stresses up to 160,000 psi, in the rise portion of a pressure wave, (2) open-circuit voltage response of PZT ceramics loaded to peak stress in 3 msec is essentially linear for stress levels to 20,000 psi. Short-circuit charge output of PZT ceramics loaded in the same manner becomes non-linear after a few hundred psi and (3) open-circuit voltage response of PZT ceramics at lower-loading rates becomes nonlinear because of the leakage of field maintaining charges from the ceramic electrodes at high-stress levels. Over the stress range 0-14,000 psi, the dielectric and piezoelectric strain constant change less than 10 per cent and 5 per cent respectively, in the case of PZT-4 (the best ceramic tested in this regard).

Piezoelectric Stress Gages

The complete stress gage consists of a transducing element; housing; isolating material, where isolation from lateral stresses is required; and a means of bonding the completed transducer to the medium in which it is embedded.

The output of the piezoelectric stress gage must be considered in regard to its physical, piezoelectric, and dielectric properties. The influence of the transducer upon the surrounding stress fields, whether static or dynamic must be minimized. Finite gage length and material nonhomogeneity affect the response of the gage and are controlling factors in the selection of transducer sizes.

Gage output Assuming that the piezoelectric gage is disc shaped, and that the gage is oriented with its axis of symmetry parallel to the direction of the stress component of interest, the charge output due to a transient longitudinal stress (assuming operation within the linear output range) is

$$q_3 = \pi r^2 d_{33} \sigma_3 \quad (B-6)$$

where: r = the disc radius

An additional charge accumulates at the transducer electrodes if stresses exist on the lateral surfaces of the cylinder. If the lateral stresses are of equal magnitude, the charge due to the ceramic cross-sensitivity is

$$\Delta q_3 = 2\pi r L_3 d_{31} \sigma_r \quad (B-7)$$

where: L_3 = disc thickness

The transducer cross-sensitivity factor is expressed by

$$K_c = \frac{\Delta q_3}{q_3} = \frac{2L_3}{r} \frac{d_{31}}{d_{33}} ; \quad \sigma_r = \sigma_3 \quad (B-8)$$

For example, a typical PZT-4 piezoelectric disc with dimensions: $r = 0.125$ in., $L_3 = 0.10$ in., and piezoelectric strain constants $d_{33} = 255 \times 10^{-12}$ coulomb/newton and $d_{31} = -110 \times 10^{-12}$ coulomb/newton, has a stress cross-sensitivity of -0.69 .¹⁰ Thus, stress gages of this particular configuration must be isolated from the lateral pressures if the charge output is to be a function of σ_3 only.

From the information presented in the section on strain-time-history effects, it is apparent that direct measurement of charge output due to high-level stress waves does not necessarily provide linear charge-stress relationships. This follows since direct-charge measurement requires an essentially short-circuit condition obtained either by (1) shunting the transducer with a capacitor several orders of magnitude larger than the transducer capacitance, or (2) shunting the transducer with an extremely small resistance; the charge output under this condition being nonlinear at high stress levels except in the special case of the wave front of a transient wave.

Another approach to the measurement of high-intensity stress waves with piezoelectric gages is to consider the open-circuit voltage response of the transducer, given by

$$E_3 = \frac{L_3 d_{33} \sigma_3}{\epsilon_{33}} = L_3 g_{33} \sigma_3 \quad (B-9)$$

The voltage output in this condition should be linear with stress, below some limiting stress level (14,000 psi in the case of PZT-4) as was shown in the section on "stress-level effects." The open-circuit voltage output can be quite large at only moderately high stress levels for common commercially available ferroelectric ceramics. For example, a transducing element fabricated of PZT-4 ceramic in the shape of a disc, where $r = 0.125$ in., $L_3 = 0.10$ in., and $g_{33} = 0.024$ volt-meters/newton, subjected to a longitudinal stress of 10,000 psi would have a theoretical voltage output of 4.24 kilovolts.¹⁰ Such voltage outputs require special techniques in measurement which provide extremely low shunt

capacitance in the connecting cables, transducer insulation, etc., and extremely high measurement circuit-input impedance.

Neither open-circuit voltage output, nor short-circuit charge output approaches to measurement of high-level transient waves appear to lead themselves to routine stress investigations. The application of modifying circuits in the measurement of output voltages from piezoelectric transducers will be discussed in the section on lead wire and circuit-loading effects.

Lower frequency limit The 3db lower-frequency limit of the individual piezoelectric transducer, in low-level stress measurement applications, is determined by the product of the transducer leakage resistance R_g and capacitance C_g , in an open-circuit test.¹

$$f_1 = \frac{1}{2\pi R_g C_g} \quad (B-10)$$

The per cent droop in the open-circuit voltage during the time of observation is given by the equation^{1,3}

$$P = 200 \pi f_1 T = \frac{100 T}{R_g C_g} \quad (B-11)$$

For example, the PZT-4 ceramic disc used as an illustration previously has a resistivity and permittivity of approximately 10^{13} ohm-cm and 10^{-8} farads/m. respectively at room temperature, giving a transducer time constant (RC-product) of 10^3 seconds with the consequence that the voltage output decay is negligible for time durations as large as 10 minutes. Such large values of leakage resistance are attainable only in

perfectly clean laboratory conditions with controlled temperature and humidity. Leakage resistance reduced by several orders of magnitude may be expected in typical situations, with resultant increase in the voltage decay per unit time.

Local reinforcement and impedance matching One primary problem which is encountered in work with embedded stress gages is that of local reinforcement, with resulting changes in stress distribution and erroneous gage readings. The accurate use of embedded stress gages in static testing requires that the gage, bonding material, and the surrounding medium must have identical physical properties, if stress concentrations within the material are to be avoided. Loh¹¹ considered this problem from the elastic-solid viewpoint, and found that the longitudinal stress-concentration factor due to a solid cylinder in an infinite mass decreases as the ratio of the length L to radius R of the cylinder decreases (assuming a uniaxial stress field parallel to the cylinder axis). At L/R ratios less than 0.2 and ratios of modulus of elasticity of gage to surroundings of one or greater, the stress-concentration factor was found to be approximately one, as illustrated in Figure B.7. Loh designed stress gages utilizing these theoretical data for static and dynamic stress measurements in concrete specimens. A circular cylindrical gage was constructed of special-alloy steel, utilizing a core and outer shell construction. The sensing element was a strain-gage element attached to the core designed to detect stress parallel to the cylinder axis. The ratio of elastic modulus of gage to surroundings between one and two, together with an L/R ratio of 5, resulted in a stress-concentration factor approximately equal to 1.2.

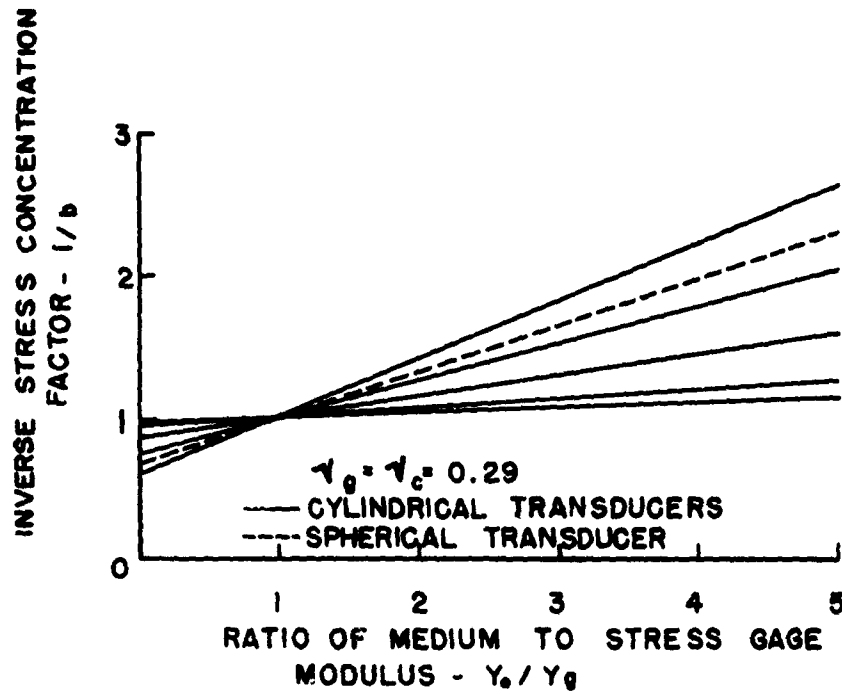


Figure B.7: Influence of transducer shape and modulus on static stress concentration factor.

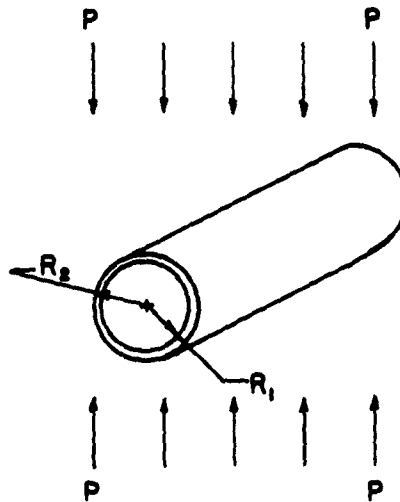


Figure B.8: Thin-walled elastic cylinder in an infinite medium subjected to a uniform uniaxial stress field.

The large L/R ratio was considered necessary to provide satisfactory material bonding of the lateral surfaces when the gages were used to measure tensile stresses. The gage natural frequency of 38,000 cps caused little time lag in the recording of dynamic stresses in small concrete cylinders with transient oscillations of about 750 cps. Indicated stresses were somewhat smaller than applied stresses, which Loh attributed to poor embedment.

Wilson¹² fabricated a cylindrical stress gage of brass for use in the measurements of static stress in rock in situ. His theoretical analysis of the stress gage was based on the stress concentrations around a spherical elastic inclusion after Sezawa and Nishimura, and Coutinho. The theoretical stress-concentration factor plotted versus the ratio of gage to surrounding medium elastic modulus is shown on Figure B.7, together with similar data for cylinders from the work of Loh for a uniaxial stress field. The stress gages designed by Wilson measured the stress component parallel to the cylinder diameter utilizing strain gages mounted in the diametral plane (hence the spherical-inclusion theory). The ratio of gage to rock modulus of elasticity was approximately 2.0. Higher values of gage modulus did not greatly improve the stress-concentration factor while reducing the gage strain.

The use of stress gages with a ratio of modulus of elasticity to surroundings greater than that of the rock has attracted favorable attention since the gage output is relatively independent of either gage or medium elastic moduli, eliminating the need for accurate moduli determinations.

Stress gages constructed using one of these "rigid inclusion"

theories have not been extremely rigid gages. It is significant that where the gages described above were most rigid relative to their surroundings, $Y_g/Y_c = 3.5$, sizable differences between theoretical and experimental stress-concentration factors were observed. However, when $1.0 \leq Y_g/Y_c \leq 1.5$, good agreement between experimental and theoretical data was obtained.¹¹ This is probably due to the strain discontinuity at the medium-inclusion boundaries which occurs with large modulus mismatch.

When a stress gage is to be used in the measurement of dynamic transient stresses, the choice of materials and construction based on the static analysis outlined above may be inadequate since the effects of wave diffraction and reflection upon the accuracy of the readings have not been considered. Wave diffraction and reflection effects are minimized when the wave velocity-density products of the surrounding medium and in the stress gages are identical. This infers that mechanical properties of the gage and surrounding material are equal. No real effort to determine the effects of transducer-media mismatch on recorded transient stresses was found in the literature. Without this information, the value of transient stress data from transducers is questionable, since neither assembled transducer or individual transducer components normally provide perfect impedance matches to the surrounding material.

It was indicated in the gage-output section that the piezoelectric cross-sensitivities of most ferroelectric ceramics are sufficiently high that they must be isolated from lateral loadings, if voltage outputs are to be proportional to longitudinal stress alone. One method

for lateral stress isolation of the sensing element is to place the element inside a laterally loose-fitting housing, which is in direct contact with the surrounding medium. However, the introduction of any foreign material into the medium to be investigated immediately provokes the question of stress field distortion, whether static or transient. Consider first the behavior of a thin, circular, elastic cylindrical housing in an infinite elastic medium subjected to a lateral static-stress field, as indicated in Figure B.8. Savin¹³ has shown that the radial and tangential stresses in the medium at the outer radius R_2 of the housing on a diameter perpendicular to the applied stress are given by

$$\sigma_{\theta}^{R_2} = \frac{P}{2} \left(2 + \frac{1}{2} \beta_{-1} - \frac{3}{2} \beta_{-3} \right) \quad (B-12)$$

$$\sigma_r^{R_2} = \frac{P}{2} \left(2\alpha_1 - \frac{1}{2} \beta_{-1} + \frac{3}{2} \beta_{-3} \right) \quad (B-13)$$

$$\text{where: } \alpha_{-1} = 2 - \frac{2(1+x)}{D_1} \left[\left(\frac{\mu}{\mu_1} - 1 \right) (3n^6 - 6n^4 + 4n^2 - 1) \right.$$

$$\left. + n^6 (n^2 - 1) \left(1 + x_1 \frac{\mu}{\mu_1} \right) \right]$$

$$\beta_{-1} = 2 - \frac{2(n^2 - 1)(1+x)}{2 \left(\frac{\mu}{\mu_1} - 1 \right) - n^2 \left[\left(\frac{\mu}{\mu_1} - 1 \right) - \left(1 + x_1 \frac{\mu}{\mu_1} \right) \right]}$$

$$\beta_{-3} = -2 + \frac{2(1+x)}{D_1} \left[\left(\frac{\mu}{\mu_1} - 1 \right) (4n^6 - 7n^4 + 4n^2 - 1) \right.$$

$$\left. + n^4 (n^4 - 1) \left(1 + x_1 \frac{\mu}{\mu_1} \right) \right]$$

$$\begin{aligned}
D_1 = & \left(x + \frac{\mu}{\mu_1}\right) n^2 \left[\left(\frac{\mu}{\mu_1} - 1\right) (3n^4 - 6n^2 + 4) \right. \\
& + n^6 \left(1 + x_1 \frac{\mu}{\mu_1}\right) \left. \right] + \left(x_1 \frac{\mu}{\mu_1} - x\right) \left[\left(\frac{\mu}{\mu_1} - 1\right) \right. \\
& + n^6 \left(1 + x_1 \frac{\mu}{\mu_1}\right) \left. \right]
\end{aligned}$$

$$n = R_2/R_1$$

R_2 = outer radius of housing

R_1 = inner radius of housing

μ = modulus of rigidity of surrounding material

μ_1 = modulus of rigidity of housing material

$$x = \frac{3 - \gamma}{1 + \gamma}$$

$$x_1 = \frac{3 - \gamma_1}{1 + \gamma_1}$$

γ = Poisson's ratio of surrounding material

γ_1 = Poisson's ratio of housing material

As an example consider a case where $\mu_1/\mu = 10$ and $\gamma_1 = \gamma = .29$ (a close approximation to a steel cylinder in a mortar matrix). A plot of tangential stress versus the ratio of cylinder wall thickness to inner diameter $H/2R_1$ is presented in Figure B.9. Note that at $H/2R_1 = 0.056$ the tangential stress-concentration factor has been reduced to 1.00 (the value which would exist if no discontinuity were present in the medium). However, the radial stress-concentration factor at the same point is 0.8, from equation B-13, whereas it would have been zero if no discontinuity were present in the medium. It is apparent that the presence of this particular steel cylinder in the elastic medium improves the tangential stress-concentration factor, reducing it from

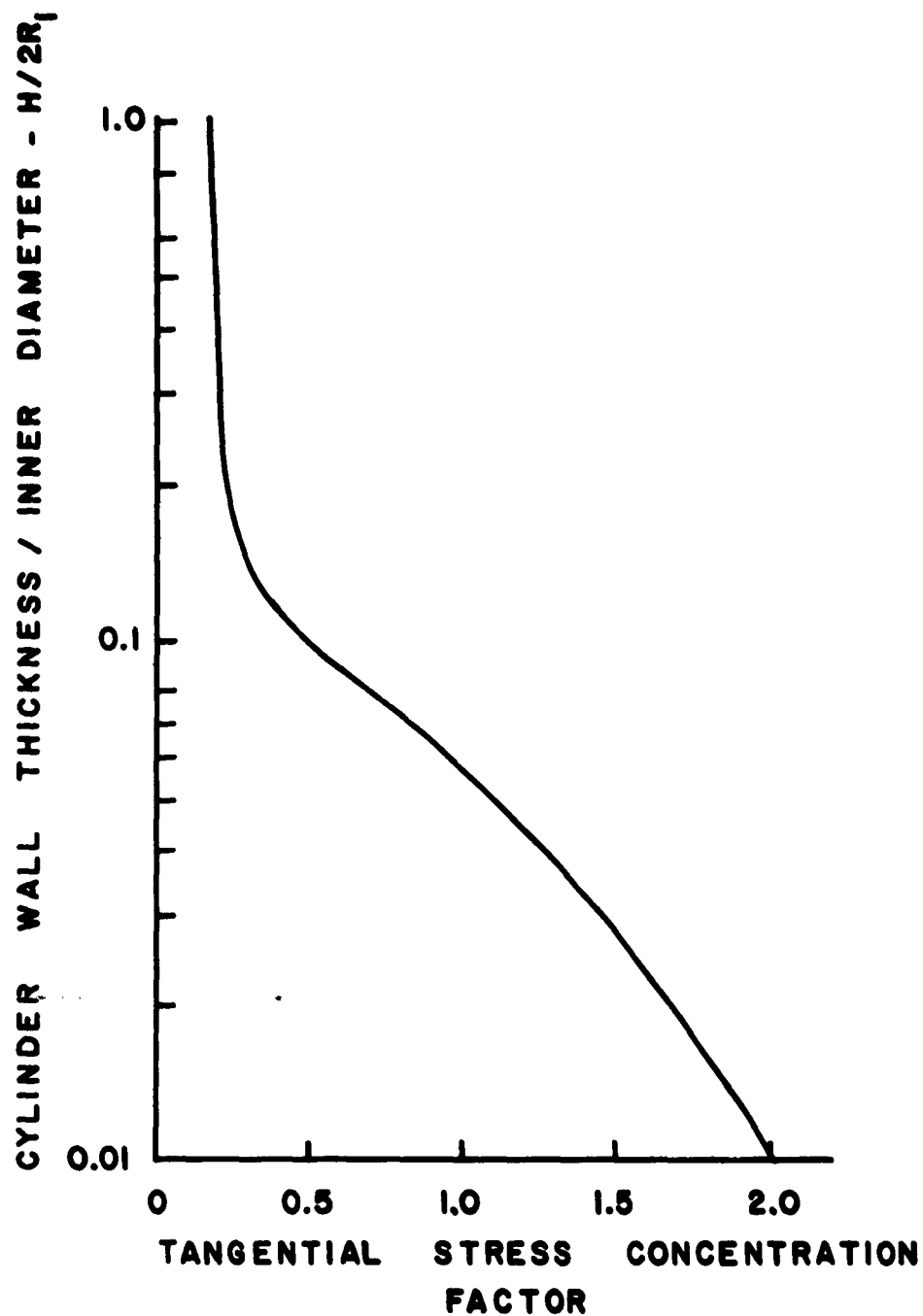


Figure B.9: Influence of the wall thickness of an embedded elastic cylinder on the tangential stress concentration factor in the surrounding medium.

a factor of 3.0 for an unlined opening to 1.0, the average value. However, the presence of a radial stress-concentration factor where none previously existed is a condition whose effect has not been evaluated. It does not appear possible to devise a lateral-stress isolation system for the stress gage which can both perform its function, and leave the surrounding static stress fields completely unaffected.

The entire lateral-stress decoupling system must consist of a housing of relatively high modulus, a stress gage of intermediate modulus, and an isolating layer of low-modulus material between gage and housing. The response of the complete transducer to a transient stress wave may be quite complex, and is worthy of further investigation. Reflections may occur at the interfaces of the components of the transducer, with the possible danger that the longitudinal stress field (the component which the stress gage was designed to measure) may be affected. In this type of transducer, the energy involved in reflected waves can be minimized by making the transducer and each of the component layers as small as possible. Whether or not this also results in true stress readings requires further investigation.

Durelli and Riley¹⁴ investigated the stress distribution in a 0.40-inch-thick Hysol 8705, urethan-rubber plate with a 5/8-inch-diameter rigid-epoxy resin-quartz-filled inclusion. The plate was subjected to long wave-front-length (rise from zero to peak) transient stresses of approximately 22 times the diameter of the inclusion from an impacting weight. The plate was also subjected to short wave-front-length waves of approximately 5-hole diameters generated by detonating a lead azide charge on an edge of the plate. Data were presented in the form of

shear-stress distributions. To permit comparison of the experimental data with the theoretical relations from Savin's work presented above, the authors calculated the maximum shear-stress concentration factors and found that the theoretical maximum static shear-stress concentration factor at the boundary of a rigid inclusion is 1.58. The maximum shear-stress concentration factor developed experimentally due to the long-wave-front stress wave was 2.3, and due to the short-wave-front wave was 2.0. It can be seen that for this extreme mismatch the static and dynamic stress-concentration factors around an obstruction vary be as much as 45 per cent. The extension of this series of experiments would be of invaluable assistance in analyzing embedded stress-gage performance.

Since stress gages to date have not been perfectly matched to their environment, and since the effect of lateral-stress decoupling by any mechanical means disturbs the stress fields in the vicinity of the gage, the voltage response of the stress gage cannot be assumed to be related to the stress-field component perpendicular to the transducer axis σ_f by Equation (B-9), since $\sigma_3 \neq \sigma_f$. However, Equation (B-9) may be modified to account for the differences between the stresses detected by the gage and the average free-field stress which would have existed at the point if no gage had been present, giving

$$E_3 = b(t, \sigma) \frac{A_3 d_{33}}{C_g} \quad \sigma_f = \frac{K_g}{C_g} \sigma_f \quad (B-14)$$

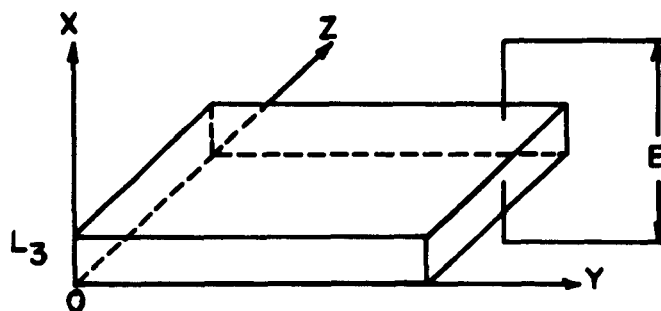
where: b = function stress-time history

σ_f = free-field stress component (psi)

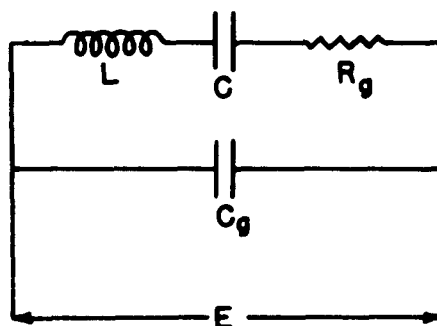
K_g = gage constant (coulomb/psi)

In materials loaded within an essentially linearly elastic range, the function $b(t-\sigma)$ may be safely approximated by a constant. However, in less ideal materials which exhibit anelastic or nonlinear elastic behavior when subjected to dynamic loadings, the dynamic-stress concentration factors can no longer be assumed independent of the stress-time history. If the stress-concentration factors are made as small as possible, the possible fluctuation of K_g will be minimized, and the assumption of a single value for use in transient investigations should not invalidate the results. Ideally K_g should be evaluated by calibration tests under conditions simulating the actual test environment as closely as possible.

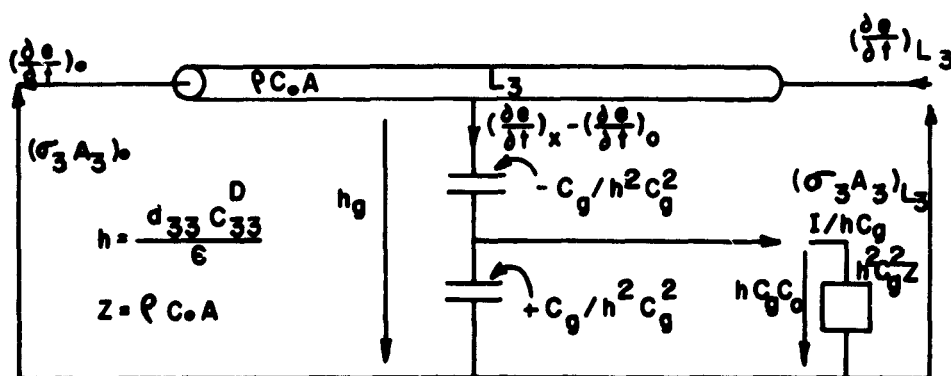
Gage length effects In the measurement of steep-fronted transient-stress waves, the finite length of the gage is one source of signal degradation as was the case for strain gages discussed previously. The problem is further complicated in piezoelectric gages by the fact that they present both finite cross-sectional area and gage length to the transient wave. As a result, perfect impedance matching is required if reflections within the transducing element are to be eliminated. Redwood¹⁵ has shown that the simple circuit of Figure B.10b is not adequate to represent the behavior of piezoelectric plates illustrated in Figure B.10a under transient loadings, although it is adequate for continuous-wave problems near the resonant frequency. Working from the equations representing a plane-compression wave in piezoelectric materials, it was shown that the open-circuit voltage response of a piezoelectric plate to a step function of force, where impedance match is perfect, is



(a) Piezoelectric plate of infinite extent polarized in the \$x\$-direction.



(b) Approximate equivalent circuit of a piezoelectric transducer.



(c) Exact equivalent circuit of a piezoelectric plate for compressional plane waves.

Figure B.10: Electrical models utilized in obtaining the piezoelectrical response of an infinite plate sandwiched between to infinite media. (After Redwood)

$$E = \frac{A_3 d_{33}}{L_3 C_g} C_0 \sigma_3 \left[t - (t - L_3/C_0)^* \right] \quad (B-15)$$

where: C_0 = wave velocity (meter/sec.)

d_{33} = piezoelectric strain constant (coulomb/newton)

($d_{33} = 255 \times 10^{-12}$ coulomb/newton for PZT-4)

t = time (sec.)

Thus, the output voltage due to a force-step function is a ramp function. The important features of this output voltage are (1) the ramp rise time is equal to the transducer transit time L/C_0 , and (2) the output-voltage amplitude is proportional to the transducer length.

It is important to note that Redwood's analysis was based on a plate of infinite extent, and therefore the results may not fit perfectly the case of transducers whose dimensions are all of the same order of magnitude. For those transducers where the thickness resonant frequency is determined primarily by the thickness dimension, plane waves may be propagated and reflected at surfaces of the piezoelectric element and still largely retain their plane nature. Thus, the infinite plate concept may provide a reasonable first approximation to voltage outputs from stress gauges loaded in the direction of the thickness dimension.

A ramp-function force input was applied by the authors to Redwood's open-circuit response function for a piezoelectric plate (represented schematically by Figure B.10c), with perfect impedance matching. The

* $[t - t_0]$ Used to denote a function equal to zero for $t < t_0$ and equal $(t - t_0)$ for $t > t_0$.

resulting output voltage

$$\begin{aligned} E = \frac{A_3 d_{33}}{2L_3 C_g} C_o \sigma_3 T \left[\frac{(t)^2}{T} - \left(\frac{t}{T} - 1\right)^2 - \left\{ \frac{t}{T} - \frac{L_3/C_o}{T} \right\} \right. \\ \left. + \left\{ \frac{t}{T} - \frac{L_3/C_o}{T} - 1 \right\}^2 \right] \end{aligned} \quad (B-16)$$

where: T = duration of the ramp portion of the force function

is plotted in nondimensional form in Figure B.11, for a number of gage transit times. Note the similarity between these results and the approximation set forth in the section on strain-gage length effects. The relationship in its nondimensional form may be applied to either case.

Redwood¹⁵ also considered a finite load impedance connected to the transducer. Since he was not interested in stress gages as such, he did not consider a transducer perfectly matched to its surroundings. The authors have considered a disc-shaped plate subjected to a step-input function. The output voltage may be expressed in transform notation as

$$\begin{aligned} \bar{E} = \frac{A_3 d_{33}}{L_3 C_g} C_o \sigma_3 \left[\frac{1}{s^2 + \frac{s}{R_T C_g} - \frac{C_o C_{33}^D A_3}{R_T} \left(\frac{d_{33}}{C_g L_3} \right)^2 (1 - e^{-SL_3/C_o})} \right] \\ \left[1 - e^{-SL_3/C_o} \right] \end{aligned} \quad (B-17)$$

where: \bar{E} = Laplace transform of output voltage

S = Laplace operator

R_T = net shunt resistance

C_{33}^D = plate thickness-elastic stiffness modulus under constant flux density. (for PZT-4, $C_{33}^D = 1.5 \times 10^{11}$ newton/meter²)

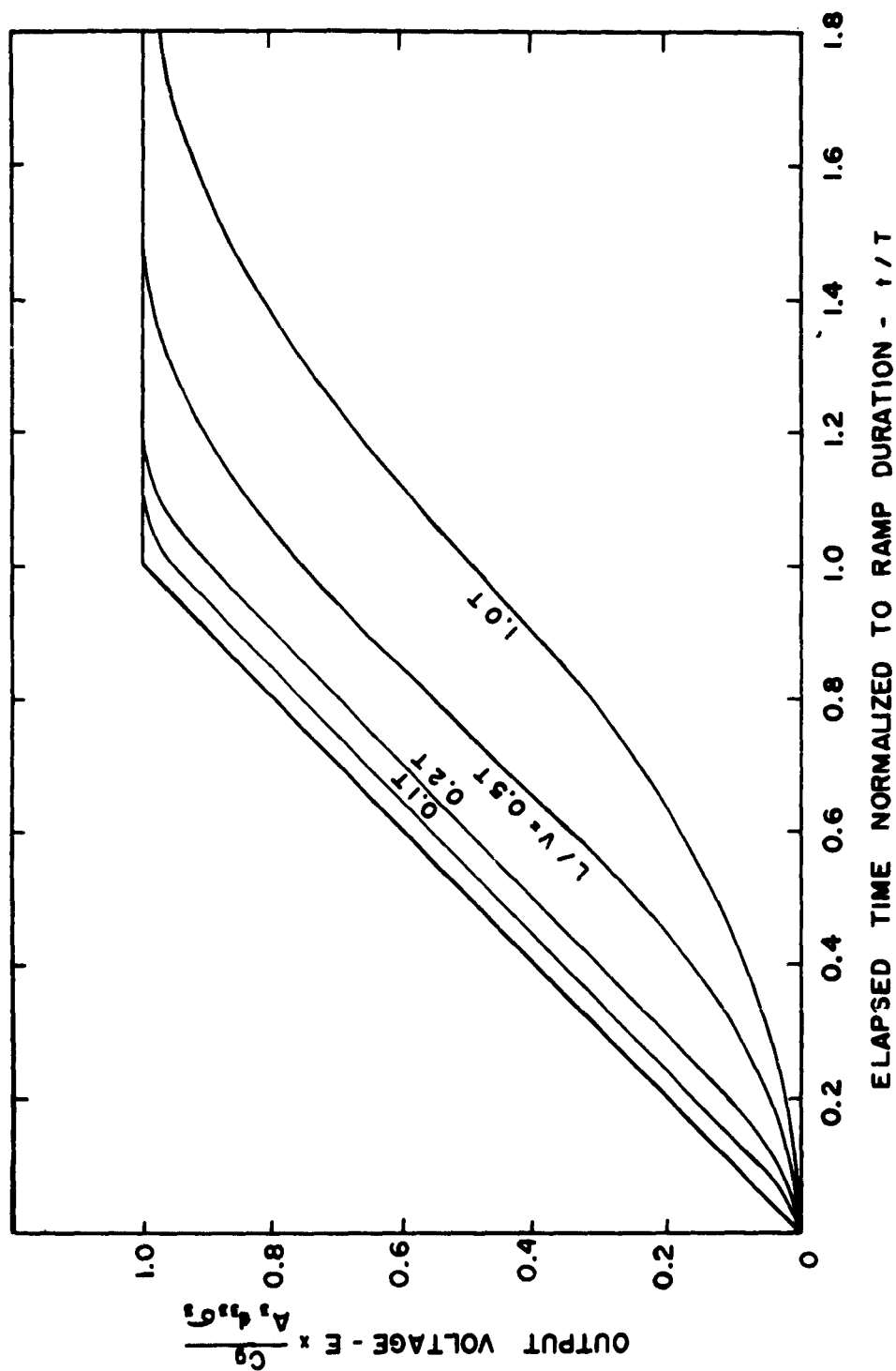


Figure 11: Response of piezoelectric plate to ramp stress wave
(Plate impedance matched to surrounding medium).

The presence of the load resistance has the effect of further degrading the output voltage. The inverse transform of this equation reduces to Equation B-14 when $R \rightarrow \infty$. It can be shown that for a typical transducer where $C_g = 100\mu\text{f}$ farad, $d_{33} = 255 \times 10^{-12}$ coulomb/newton, $C_{33}^D = 1.5 \times 10^{11}$ newton/meter², and $C_o = 4500$ meter/sec, the function is quite linear up to $t = 10^{-4}$ sec., if R_T is not less than 10^7 ohms. Resistances less than 10^7 ohms would result in increased voltage-output distortion.

In this analysis, absorption of mechanical wave energy due to the internal friction of the transducer has been neglected, although in ferroelectric ceramic materials this phenomenon may have appreciable effect on the voltage response. Although the results have been based on plane waves impinging on infinite piezoelectric plates, they are probably representative of transducer behavior under transient loadings.

Gage cross-sectional area It was indicated in Appendix A that a minimum strain-gage length can be established for accurate measurement of average strains in the vicinity of a group of crystals or grains of polycrystalline materials such as rocks, concretes, or mortars. In cylindrical stress gages, similar consideration must be given to the minimum cross-sectional area of the gage. Loh¹¹ states that the cross-sectional area of the gage should be at least 3 or 4 times the projected area of the largest aggregate. This criterion could result in a stress-gage whose diameter was less than twice that of the largest aggregate, a condition which the authors feel would not result in a reliable approximation to the average stress. For this reason it is recommended that a minimum cross-sectional area of the gage of approx-

imately 10 times the projected area of the largest aggregate should be utilized to obtain reliable average-stress results.

Resonant frequency effects The effects of transducer resonant frequency upon the high-frequency and rise-time response of transducers have been given such detailed attention by authors,¹ that some remarks as to the applicability of resonant-frequency criteria to embedded stress gages are appropriate.

The resonant frequency of a stress gauge of circular disc shape in the thickness mode may be approximated by

$$f_r \approx \frac{C_o}{2L} \quad (B-18)$$

When surface mounted gages are subjected to transient stresses containing high-frequency components, those high-frequency components, may be undesirably amplified if they are in the range of the gage resonant frequency.

Undesirable amplification of voltage-stress response due to gage resonant frequency is not experienced in embedded gages which are firmly bonded to the surrounding medium. When a gage has been properly impedance-matched to the surrounding medium, the rise time of the voltage response to a step-input stress is from equation B.14.

$$T_R = \frac{0.8L}{C_o} \approx \frac{0.8L}{2Lf_r} = \frac{0.4}{f_r} \quad (B-19)$$

From the equation relating rise time and upper 3db sinusoidal-frequency response (A-27) and equation B-18, an expression relating upper 3db frequency response and gage resonant frequency can be obtained.

$$f_2 = \frac{0.35}{T_R} \approx \frac{0.35}{0.4} f_r \approx f_r \quad (\text{B-20})$$

Thus, the resonant frequency of an embedded stress gage which has been impedance matched to its surroundings is approximately the frequency at which normalized voltage output is reduced to 0.707 of its mid frequency value, in direct contrast with the behavior associated with surface-mounted gages of all types.

Lead Wire and Circuit Loading Effects

The effect of lead-wire resistance and capacitance on piezoelectric gage output is entirely different from that developed for electric resistance type strain gages. The most common input circuit is a direct-lead-wire connection between the transducer and a voltage amplifier with high-input impedance. In this circumstance lead-wire effects and amplifier-input impedance may be lumped together in determining their effect upon the piezoelectric gage-output voltage.

Midfrequency output voltage The interlead capacitance C_c of wires leading from the pickup to the amplifier and the amplifier-input capacitance result in a shunt capacitance across the transducer, which adds directly to the self-capacitance of the pickup. The output voltage of a piezoelectric disc-shaped transducer loaded parallel to its axis is therefore expressed by

$$E_3^* = \frac{A_3 d_{33}}{C_g + C_c} \sigma_3 = \frac{K_g}{C_g + C_c} \sigma_f \quad (\text{B-21})$$

$$E_3^* = \frac{C_g}{C_g + C_c} E_3 \quad (\text{B-22})$$

Thus, the voltage sensitivity of a piezoelectric pickup is decreased by the shunt capacitance of the input circuit. An adjustable shunt capacitance of known value is frequently added to the circuit to permit precise setting of the gage sensitivity.

A typical piezoelectric stress gage was considered as an example in the Gage Output section, and found to develop 4.24 kilovolts in an open circuit condition when 10,000 psi was applied. Assuming $r = 0.125$ in, $L_3 = 0.10$ in. and a permittivity of 8.75×10^{-9} farad/meter (PZT-4), a shunt capacitance of $815\mu\mu$ farads would be required to reduce the voltage sensitivity to 5×10^{-2} volts/psi; a voltage more easily accommodated by conventional amplifiers and lead wires. This shunt capacitance is about 7.5 times that of the piezoelectric ceramic itself, and therefore could lead to some charge depletion and depoling as discussed previously, although not to the degree experienced under the short-circuit condition. This shunt capacitance may be exceeded with as little as 20 feet of twin-conductor cable used to connect the gage to an amplifier. The addition of higher shunt capacitances must be avoided as depoling under high stresses becomes more probable when the shunting capacitances become very large compared to the capacitance of the ferroelectric element. Recourse may be necessary to cathode follower-type input circuits located a short distance from the pickup, followed by long cables matched to the cathode-follower output resistance, when the stresses must be monitored at a distance.

Low frequency response The voltage sensitivity of the piezoelectric transducer and associated circuitry examined at the input to the first stage of amplification is dependent upon the circuit capaci-

tances alone, except at low frequencies where the resistances in the circuit are relatively small compared to the reactances. The lower 3db frequency of the circuit is dependent on the input resistance R_L of the amplifier, the leakage resistance R_G of the gage, and the total capacitance in the input circuit, as expressed by the relationship,

$$f_1 = \frac{1}{2\pi R_T C_T} \quad (B-23)$$

$$\text{where: } R_T = \frac{R_L R_G}{R_L + R_G}$$

$$C_T = C_g + C_c$$

Thus, the lower 3db frequency of the piezoelectric transducer circuit described above, where $C_c = 815\mu\mu$ farad, $C_g = 110\mu\mu$ farad, $R_g = 8 \times 10^{12}$ ohm, and $R_L = 100$ megohm, is $f_1 = 1.7$ cps. The per cent droop (loss of low frequencies) in the open circuit voltage during the time of observation may be expressed in the form of equation B-11, as

$$P = 200 \pi f_1 T = \frac{100T}{R_T C_T} \quad (B-24)$$

and is approximately one per cent in one millisecond for the example cited. For transient-stress observation times less than this amount, no error due to lack of low-frequency response of transducer and input circuitry would be apparent.

Measurement System Response

The overall system response is dependent upon each of the components in the system: stress gage, gage output-voltage circuitry, and amplifier

and recorder circuitry. Obviously the amplification and recording equipment should be so chosen that they do not seriously distort the output voltages over the range of stress transients to be measured. The system response may be best evaluated in terms of the rise time and per cent droop of the response to a step input stress. The system rise time may be approximated within twenty per cent by considering the rise time of all components, including gage-length effect, obtaining

$$T_R \approx \sqrt{\sum_{i=1}^n T_{R_i}^2} \quad (B-25)$$

where: T_{R_i} = the rise time of each component of the system.

The approximate per cent droop of the response may be obtained from the following expression, if individual component contributions are small.

$$P \approx \sum_{i=1}^n P_i \quad (B-26)$$

where: P_i = the per cent droop of each component in the system.

The overall system-transient response should be used together with estimates of the stress-time history to determine the effect on the accuracy of recorded data.

Stress Measurement System Calibration

The calibration of a piezoelectric stress-gage installation includes both calibration of the transducer and of the auxiliary components of

the measuring system. Calibration may be either "relative" or "absolute". A relative calibration infers that the gage factors of the stress gages being considered have been determined relative to some "standard" gage, or to some reproducible but quantitatively uncertain applied stress. Calibration can only be considered as absolute when outputs of individual gages are determined relative to known average input stresses.

Free gage calibration A number of authors have described calibration techniques utilizing fluid pressures imposed on piezoelectric gages (primarily pressure gages). Gesswein and Chertock¹⁶, in particular, describe a technique for calibrating pressure gages with a transient pressure, nulling the voltage output with the output from a standard pressure gage. If such a technique could be adapted to calibration of gages in solid media, considerable advantage could be obtained.

Free-gage calibration provides a relative sensitivity of the piezoelectric stress gages which are mounted in solids, if the mounting of the gages in the solid medium is reproducible and if the gage response in the medium is linear with stress over the test range. Due to the uncertainty as to whether these requirements are fulfilled by a particular solid, it appears that preliminary measurements are required of the output of the transducer, embedded in the medium in question, in response to a known applied stress.

In-situ gage calibration In-situ stress gage calibration may be accomplished by several means. Durelli and Riley¹⁷ used barium titanate stress gages in measuring wave propagation in soil models subjected to a traveling surface wave in a shock tube. These gages were superfi-

cially similar to the gages utilized in the present study, although designed for much lower stress levels. The gage element was a tube 1/8-inch diameter by 1/8-inch long, with a wall thickness of 20 mils; the addition of a gage shell bringing the dimensions to 5/16-inch diameter by 1/4-inch long. Gage calibration was performed in Hysol 8530/CH₂ urethane rubber or clay cylinders 2 inches in diameter and 2 3/4 inches long.¹⁴ Specimens were placed in a ballistic pendulum, and impacted with a pendulum of equal mass. The acceleration of one of the pendulums was measured during impact. From this record the average stress and average strain in the specimen at any instant of time could be determined. The response of the embedded gage to a given instantaneous stress was in all instances approximately 40 per cent greater than that of a free gage to the same stress. This should be expected since there was considerable mismatch between gage and medium. Several pertinent conclusions were reached from this study: (1) The gage must be calibrated in a sample of the material in which it is to be used; (2) The error in gage reading decreased as the modulus of elasticity of the medium was increased (gage and medium modulus approached one another); (3) The relative rigidity and density of gage to surrounding medium influence the stress field, and thus the gage response.

It is inferred that impedance matching may reduce the error in measured stress magnitudes at high-energy levels. Dynamic tests were performed with as many as 15 gages in a cylindrical clay model, 1 3/4-inch diameter by 36-inch long, subjected to shock-tube overpressures from 6.5 to 31.4 psi.¹⁴ Results from the piezoelectric gages calibrated in the manner described above were very good.

Q-step method The simplest type of piezoelectric stress-gage system calibration (called a Q-step method) consists of introducing a known step function of voltage to the input circuit. Figure B.12b shows the calibration voltage inserted in series with a shunt capacitor C_s in the input circuit. The voltage response of the piezoelectric input circuit was shown previously to be

$$E_3^* = \frac{K_g}{C_g + C_c + C_s} \sigma_f \quad (B-27)$$

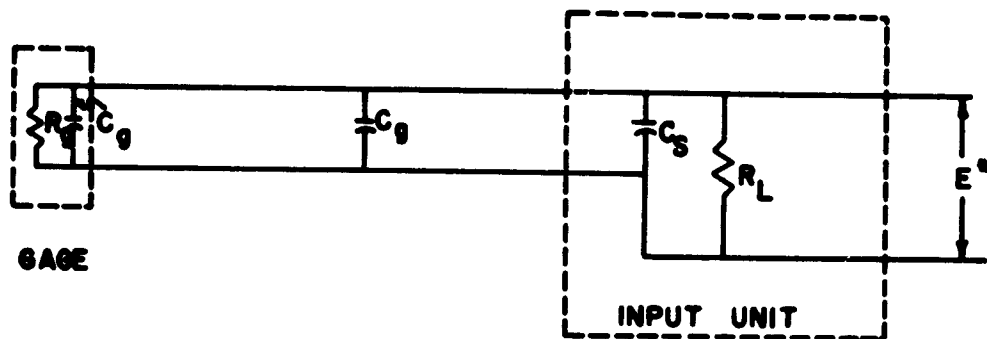
The voltage response to a calibrating voltage V_c will be equal to the voltage across the capacitances C_g and C_c in parallel, or

$$E_c = \frac{C_s}{C_g + C_c + C_s} V_c \quad (B-28)$$

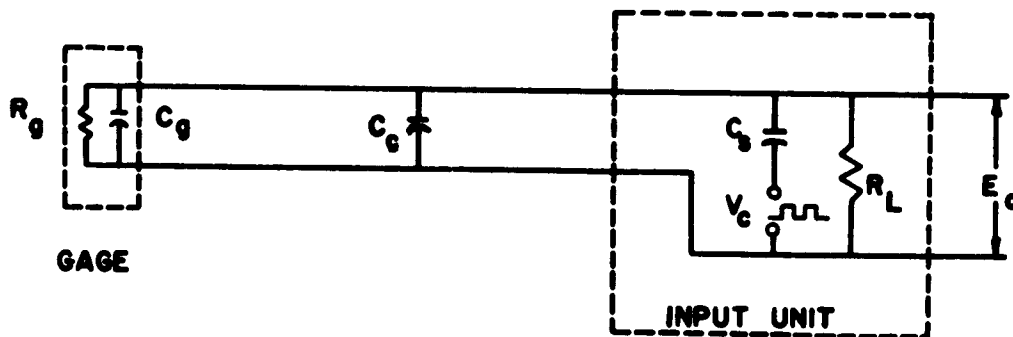
Equating equations (B-27) and (B-28), an equivalent stress in terms of the calibrating voltage is obtained

$$\sigma_e = \frac{C_s}{K_g} V_c \quad (B-29)$$

The amplitude of the measuring-system response to a calibrating voltage can be expressed in terms of an equivalent pressure, thus providing a calibration point to be utilized with actual pressure measurements. The gage capacitance does not enter directly into these calculations, and therefore its exact value is not required. Several important assumptions were necessary for the development of this technique: (1) the capacitance of the gage and circuit are constant, and (2) the



(a) Simplified piezoelectric gage input circuit.



(b) "Q-step" calibration circuit configuration.

Figure B.12: Simplified piezoelectric gage input circuit and modification for "Q-step" calibration.

gage factor K_g is known and remains constant during the calibration and test periods. The first assumption is realized with some of the PZT ceramics up to at least 14,000 psi applied stress. Determination of the gage factor K_g for stress gages embedded in solid media is not an easy task. The gage factor may vary with the amplitude and rate of loading as was discussed in the section "Local reinforcement and impedance matching."

Special mention must be made of the specifications for the calibrating voltage source, which should possess very low impedance, and be capable of developing very clean step-function voltages of a magnitude such that the voltage output obtained will be equivalent of that experienced under peak transient stress.

The rise time of the observed response is a measure of the high-frequency response of the amplifying and recording sections of the measuring system, and serves as a guide to circuit condition. The per cent droop in the observed response is identical to the per cent droop which could be expected in the measurement of a step-input strain.

Since the Q-step calibration technique relies on a prior knowledge of the gage factor K_g , it must be considered as a secondary calibrating technique, to be utilized when a value for K_g (such as obtained by in-situ calibration) can be established by other means. It can be of particular value in those instances where the variation of K_g from gage installation to installation is insignificant.

References

1. Harris, C. M., and Crede, C. E., Shock and Vibration Handbook, McGraw - Hill, 1961.
2. "IRE Standards on Piezoelectric Crystals: Measurements of Piezoelectric Ceramics, 1961," Proc. of IRE, Vol. 49, 1961.
3. Crawford, A., "Lead Zirconate-Titanate Piezoelectric Ceramics," British J. Applied Physics, Vol. 12, No. 10, 1961.
4. Gerson, R., Burlage, S. and Berlincourt, D., "Dynamic Tensile Strength of Ferroelectric Ceramic," J. Acoustical Soc. of America, Vol. 33, No. 11, 1961.
5. Reynolds, C. and Seay, G., "Two-Wave Shock Structures in the Ferroelectric Ceramics Barium Titanate and Lead Zirconate Titanate," J. Applied Physics, Vol. 33, No. 7, 1962.
6. Ripperger, E. A., "Air-Gun Studies of Ferroelectric Materials," Sandia Corporation Tech. Memo. SCTM297-57(51), OTS, Wash. D.C., Feb. 6, 1958.
7. Berlincourt, D. and Krueger, H., "Domain Processes in Lead Titanate Zirconate and Barium Titanate Ceramics," J. Applied Physics, Vol. 30, No. 11, 1959.
8. Brown, R., "Effect of Two-Dimensional Mechanical Stress on the Dielectric Properties of Poled Ceramic Barium Titanate and Lead Zirconate Titanate," Can. J. Physics, Vol. 39, 1961.
9. Krueger, H., and Berlincourt, D., "Effects of High Static Stress on the Piezoelectric Properties of Transducer Materials," J. Acoustical Soc. of America, Vol. 33, No. 10, 1961.
10. "Modern Piezoelectric Components," Clevite Electronic Components Bull. No. 9244-1, Cleveland, Ohio, March, 1961.
11. Loh, Y. C., "Internal Stress Gages for Cementitious Materials," SESA Proceedings, Vol. XI, No. 2, 1954.
12. Wilson, A. H., "A Laboratory Investigation of a High Modulus Bore-hole Plug Gage for the Measurement of Rock Stress," Proceedings 4th Symp on Rock Mech., Penn State University, 1961.
13. Savin, G. N., Stress Concentration Around Holes, Pergamon Press, London, 1961.
14. Durelli, A. J. and Riley, W. F., "Research Studies of Stress Waves in Earth and Model Media," Air Force Special Weapons Center Tech. Report, AFSWC-TR-60-4, Kirtland Air Force Base, Oct. 1959.

15. Redwood, M., "Transient Performance of a Piezoelectric Transducer," J. Acoustical Soc. of America, Vol. 33, No. 4, 1961.
16. Gesswein and Chertock, G., "A Dynamic Calibration Technique for Underwater Explosion Pressure Gages," Dept. of Navy, David Taylor Model Basin, Struc. Mech. Lab Report 1328, Sept. 1959.
17. Durelli, A. J. and Riley, W. F., "Initial Investigation of Wave Propagation in Large Soil Models," Air Force Special Weapons Center Tech. Note, AFSWC-TN-58-25, Kirtland Air Force Base, Dec., 1959.

APPENDIX C
EXPERIMENTAL DATA

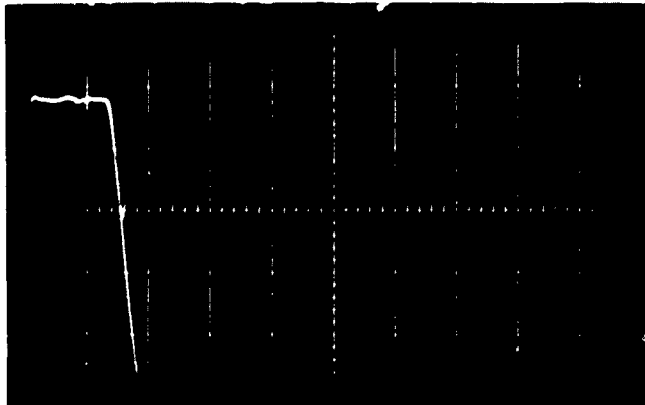


Figure C.1:

Horizontal scale: 20 μ sec/major div.	Type gage: 204 Foil
Vertical scale: 2000 μ strain/major div.	Gage factor: 2.08
Gage location: Outside - 3" from source	Gage length: 0.25 in.
Gage orientation: Parallel to axis	Wave source: Dupont W.S.
Specimen No. 14	

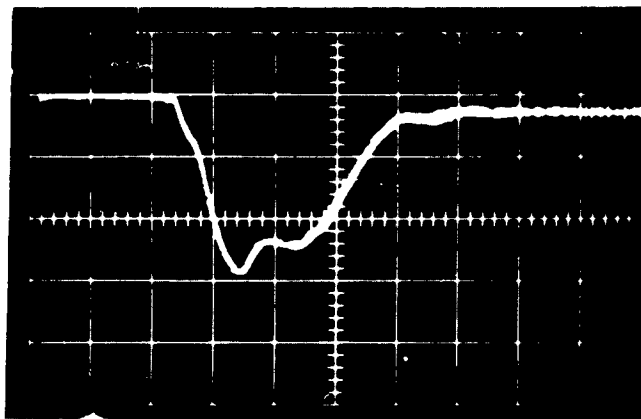


Figure C.2:

Horizontal scale: 20 μ sec/major div.	Type gage: 204 Foil
Vertical scale: 2000 μ strain/major div.	Gage factor: 2.08
Gage location: Outside - 6" from source	Gage length: 0.25 in.
Gage orientation: Parallel to axis	Wave source: Dupont W.S.
Specimen No. 17	

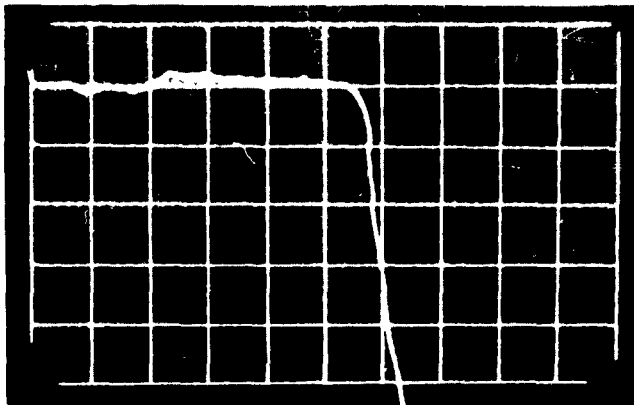


Figure C.3:

Horizontal scale: 20 μ sec/major div.
Vertical scale: 1000 μ strain/major div.
Gage location: Outside - 6" from source
Gage orientation: Parallel to axis
Specimen No. 13

Type gage: 204 Foil
Gage factor: 2.08
Gage length: 0.25 in.
Wave source: Dupont W.S.

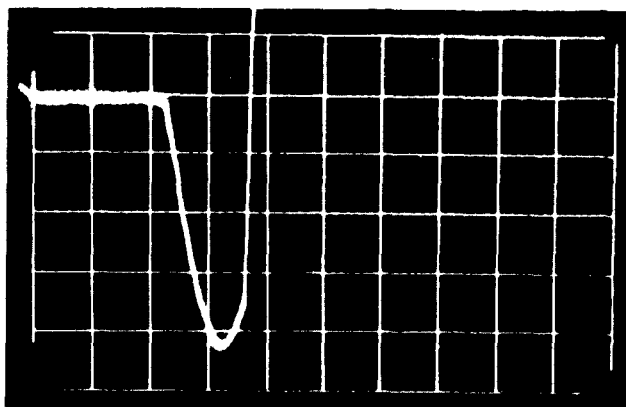


Figure C.4:

Horizontal scale: 20 μ sec/major div.
Vertical scale: 2000 μ strain/major div.
Gage location: Outside - 6" from source
Gage orientation: Parallel to axis
Specimen No. 14

Type gage: 204 Foil
Gage factor: 2.08
Gage length: 0.25 in.
Wave source: Dupont W.S.

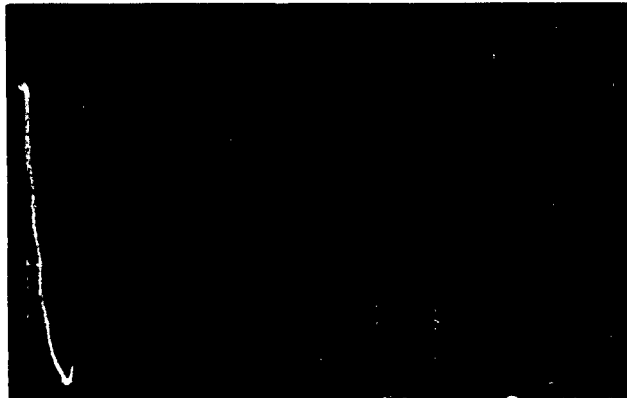


Figure C.5:

Horizontal scale: 50 μ sec/major div.
Vertical scale: 2000 μ strain/major div.
Gage location: Outside - 3" from source
Gage orientation: Parallel to axis
Specimen No. 18

Type gage: 204 Foil
Gage factor: 2.08
Gage length: 0.25 in.
Wave source: Dupont W.S./Celotex

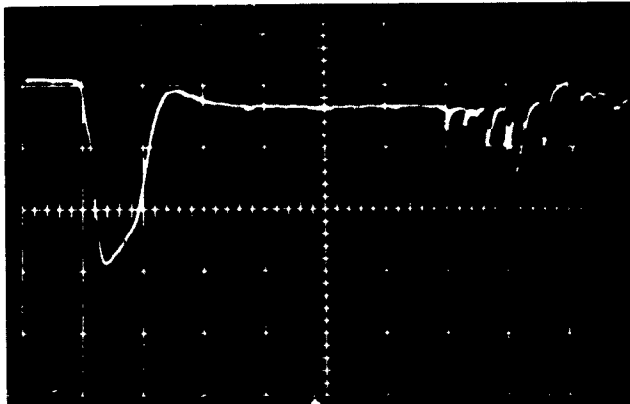


Figure C.6:

Horizontal scale: 50 μ sec/major div.
Vertical scale: 2000 μ strain/major div.
Gage location: Outside - 6" from source
Gage orientation: Parallel to axis
Specimen No. 18

Type gage: 204 Foil
Gage factor: 2.08
Gage length: 0.25 in.
Wave source: Dupont W.S./Celotex

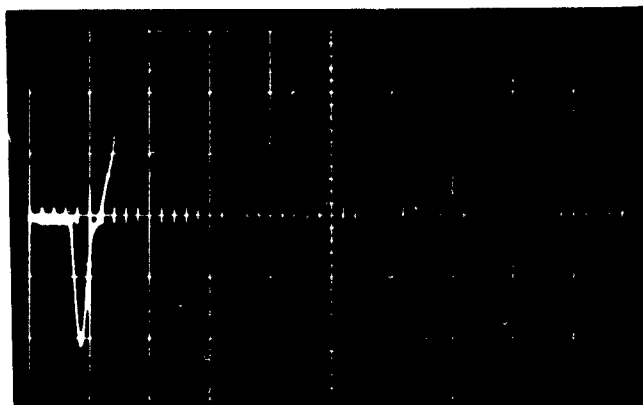


Figure C.7:

Horizontal scale: 100 μ sec/major div.
Vertical scale: 2000 μ strain/major div.
Gage location: Embedded - 3" from source
Gage orientation: Parallel to axis
Specimen No. 21

Type gage: 204 Foil
Gage factor: 2.08
Gage length: 0.25 in.
Wave source: Dupont W.S./Celotex

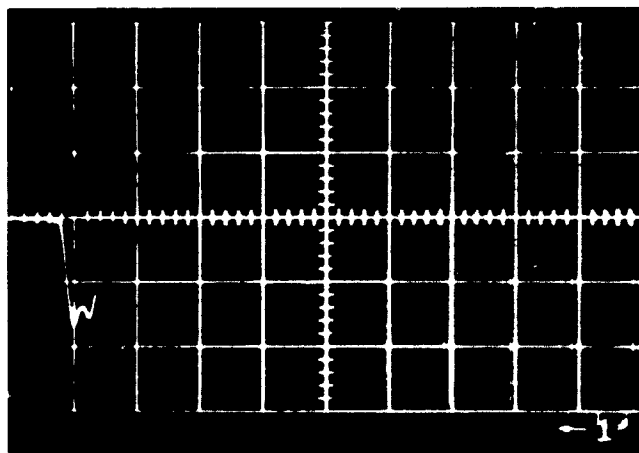


Figure C.8:

Horizontal scale: 100 μ sec/major div.
Vertical scale: 2000 μ strain/major div.
Gage location: Embedded - 6" from source
Gage orientation: Parallel to axis
Specimen No. 21

Type gage: 204 Foil
Gage factor: 2.08
Gage length: 0.25 in.
Wave source: Dupont W.S./Celotex

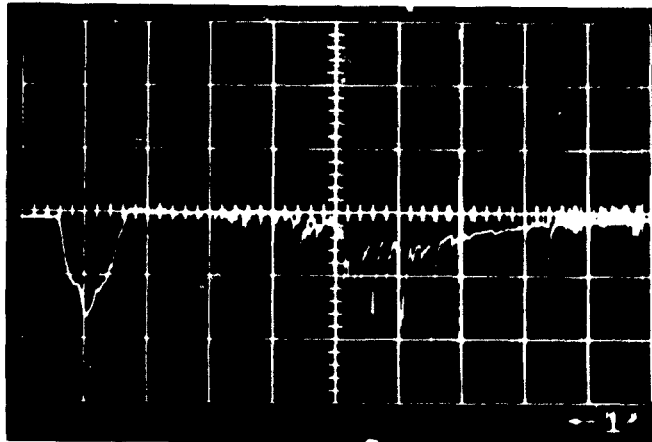


Figure C.9:

Horizontal scale: 100 μ sec/major div.	Type gage: 204 Foil
Vertical scale: 2000 μ strain/major div.	Gage factor: 2.08
Gage location: Embedded - 6" from source	Gage length: 0.25 in.
Gage orientation: Parallel to axis	Wave source: Dupont W.S./Celotex
Specimen No. 19	

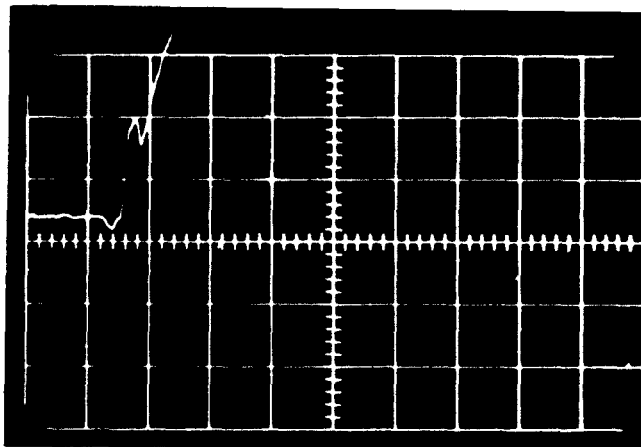


Figure C.10:

Horizontal scale: 50 μ sec/major div.	Type gage: 204 Foil
Vertical scale: 500 μ strain/major div.	Gage factor: 2.08
Gage location: Embedded - 6" from source	Gage length: 0.25 in.
Gage orientation: Perpendicular to axis	Wave source: Dupont W.S./Celotex
Specimen No. 25	

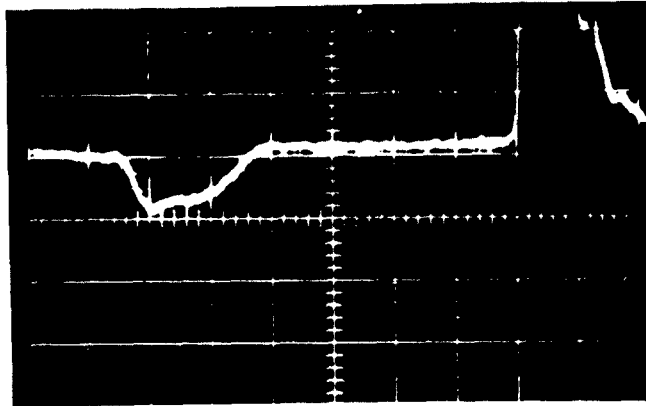


Figure C.11:

Horizontal scale: 50 μ sec/major div.	Type gage: 204 Foil
Vertical scale: 2000 μ strain/major div.	Gage factor: 2.08
Gage location: Embedded - $4\frac{1}{2}$ " from source	Gage length: 0.25 in.
Gage orientation: Parallel to axis	Wave source: Dupont W.S./Celotex
Specimen No. 23	

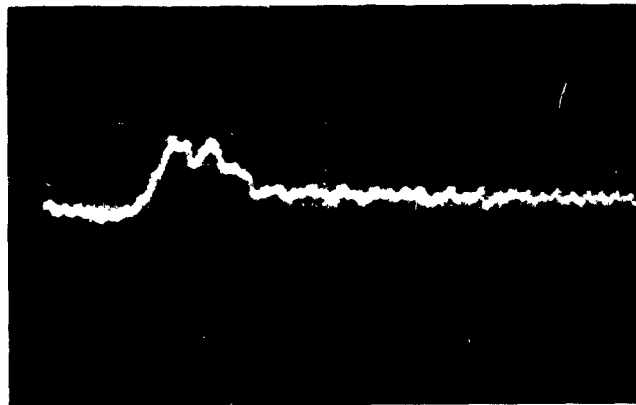


Figure C.12:

Horizontal scale: 50 μ sec/cm	Type gage: 204 Foil
Vertical scale: 500 μ strain/cm	Gage factor: 2.08
Gage location: Embedded - $4\frac{1}{2}$ " from source	Gage length: 0.25 in.
Gage orientation: Perpendicular to axis	Wave source: Dupont W.S./Celotex
Specimen No. 23	

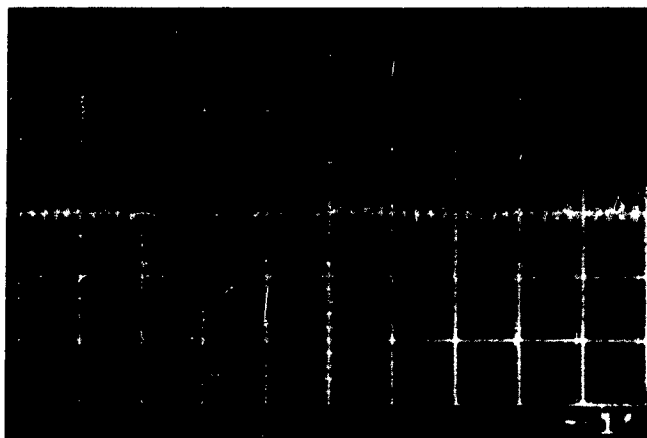


Figure C.13:

Horizontal scale: 50 μ sec/major div.	Type gage: 204 Foil
Vertical scale: 1000 μ strain/major div.	Gage factor: 2.08
Gage location: Embedded - $7\frac{1}{4}$ " from source	Gage length: 0.25 in.
Gage orientation: Parallel to axis	Wave source: Dupont W.8./Celotex
Specimen No. 22	

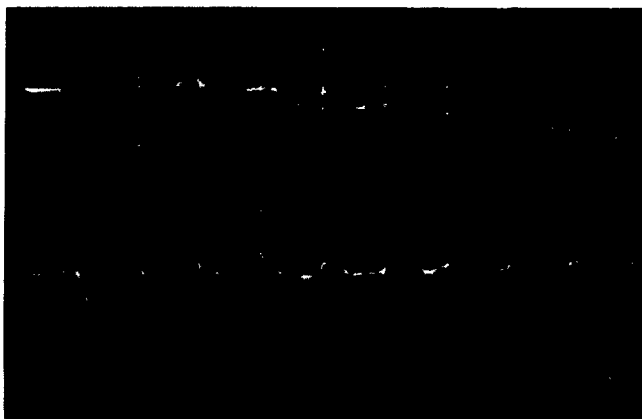


Figure C.14:

Horizontal scale: 500 μ sec/major div.	Type gage: 204 Foil
Vertical scale: U-50 μ strain/major div.	Gage factor: 2.06
L-50 μ strain/major div.	Gage length: 0.25 in.
Gage location: Embedded - 3" from source	Wave source: Pendulum Impact
Gage orientation: U-Parallel to axis	
L-Perpendicular to axis	
Specimen No. 15	



Figure C.15:

Horizontal scale:	500 μ sec/major div.	Type gage:	U-204 Foil
Vertical scale:	U-50 μ strain/major div.		L-Piezo. Stress Gage
	L-500 μ volts/major div.	Gage factor:	U-2.06
Gage location:	Embedded - 3" from source		L- \approx 100 μ q/psi
Gage orientation:	U-Parallel to axis	Gage length:	U-0.25 in.
	L-Perpendicular to axis		L-0.10 in.
Specimen No.	15	Wave source:	Pendulum Impact



Figure C.16:

Horizontal scale:	500 μ sec/major div.	Type gage:	U-204 Foil
Vertical scale:	U-50 μ strain/major div.		L-Piezo. Stress Gage
	L-2000 μ volts/major div.	Gage factor:	U-2.06
Gage location:	Embedded - 3" from source		L- \approx 100 μ q/psi
Gage orientation:	U-Parallel to axis	Gage length:	U-0.25 in.
	L-Parallel to axis		L-0.10 in.
Specimen No.	15	Wave source:	Pendulum Impact



Figure C.17:

Horizontal scale: 500 μ sec/major div.
Vertical scale: 50 μ strain/major div.
Gage location: Outside - 6" from source
Gage orientation: Parallel to axis
Specimen No. 25

Type gage: 204 Foil
Gage factor: 2.08
Gage length: 0.25 in.
Wave source: Pendulum Impact

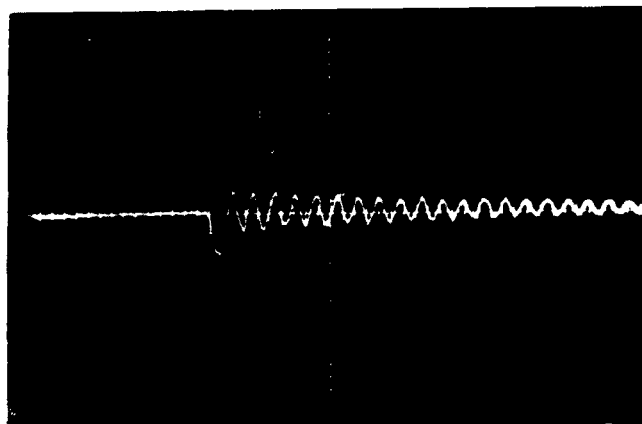


Figure C.18:

Horizontal scale: 500 μ sec/major div.
Vertical scale: 25 μ strain/major div.
Gage location: Embedded - 6" from source
Gage orientation: Parallel to axis
Specimen No. 25

Type gage: 204 Foil
Gage factor: 2.08
Gage length: 0.25 in.
Wave source: Pendulum Impact

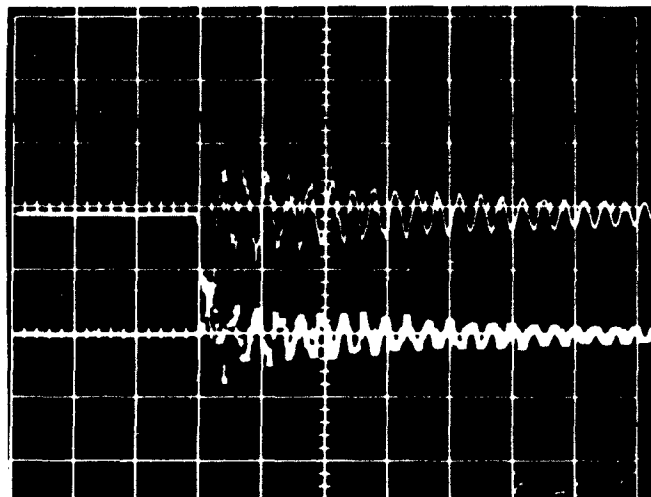


Figure C.19:

Horizontal scale: 500 μ sec/major div.

Vertical scale: U-20 mv/cm

L-20 mv/cm

Gage location: Embedded - 6" from source

Gage orientation: U-Parallel to axis

L-Perpendicular to axis

Specimen No. 25

Type gage: Piezo. Stress Gage

Gage factor: $\sim 100 \mu\mu\text{q/psi}$

Gage length: 0.10 in.

Wave source: Pendulum Impact

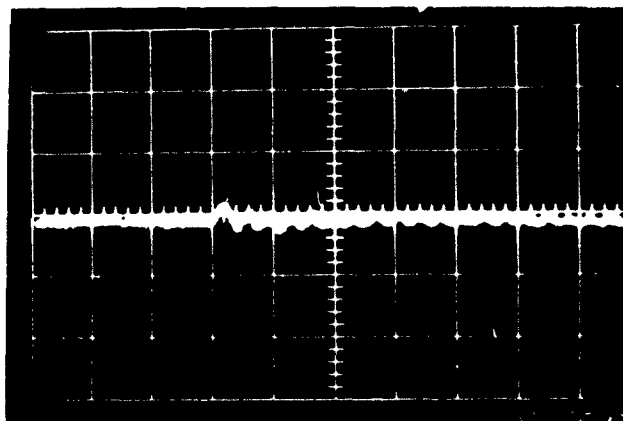


Figure C.20:

Horizontal scale: 500 μ sec/major div.Vertical scale: 25 μ strain/major div.

Gage location: Embedded - 6" from source

Gage orientation: Perpendicular to axis

Specimen No. 25

Type gage: 204 Foil

Gage factor: 2.08

Gage length: 0.25 in.

Wave source: Pendulum Impact

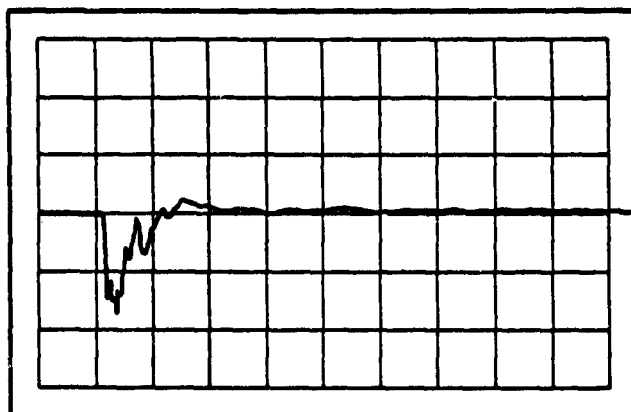


Figure C.21:

Horizontal scale: 50 μ sec/major div.
 Vertical scale: 2 volts/major div.
 Gage location: 3" from source
 Gage orientation: Parallel to axis
 Specimen No. 15

Type gage: Piezo. Stress Gage
 Gage factor $\approx 100 \mu\mu\text{q/psi}$
 Gage length: 0.10 in.
 Wave source: Dupont W.S./Celotex

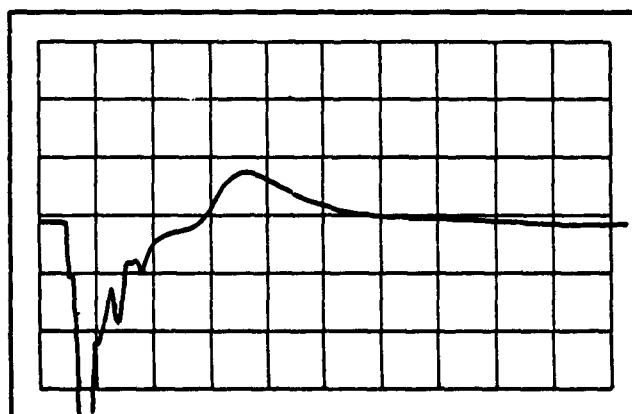


Figure C.22:

Horizontal scale: 50 μ sec/major div.
 Vertical scale: 2 volts/major div.
 Gage location: 3" from source
 Gage orientation: Parallel to axis
 Specimen No. 16

Type gage: Piezo. Stress Gage
 Gage factor: $\approx 100 \mu\mu\text{q/psi}$
 Gage length: 0.10 in.
 Wave source: Dupont W.S./Celotex

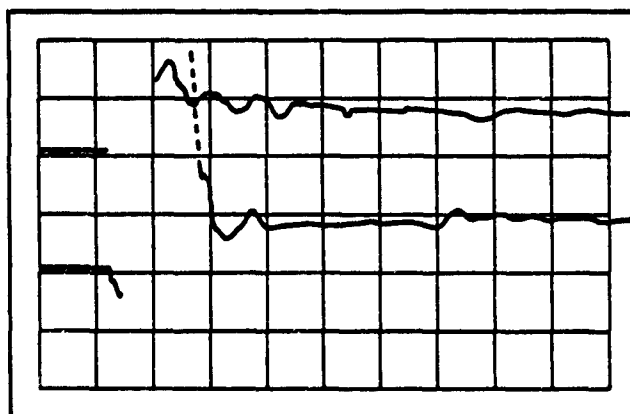


Figure C.23:

Horizontal scale: 50 μ sec/major div.

Vertical scale: U-5 volts/cm

L-2 volts/cm

Gage location: 6" from source

Gage orientation: U-Parallel to axis

L-Perpendicular to axis

Specimen No. 16

Type gage: Piezo Stress Gage

Gage factor: U \approx 100 μ q/psiL \approx 100 μ q/psi

Gage length: 0.10 in.

Wave source: Dupont W.S./Celotex

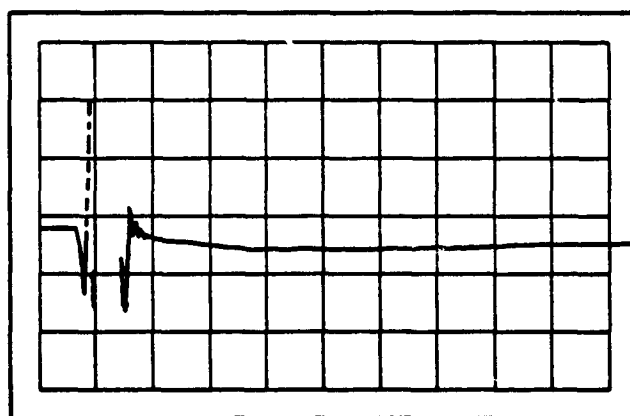


Figure C.24:

Horizontal scale: 50 μ sec/major div.

Vertical scale: 2 volts/major div.

Gage location: 3" from source

Gage orientation: Perpendicular to axis

Specimen No. 25

Type gage: Piezo. Stress Gage

Gage factor: \approx 100 μ q/psi

Gage length: 0.10 in.

Wave source: Dupont W.S./Celotex

DISTRIBUTION

No. Cys

HEADQUARTERS USAF

2. Hq USAF (AFOCE), Wash 25, DC
1 Hq USAF (AFRST), Wash 25, DC
1 Hq USAF (AFRNE-A, Maj Lowry), Wash 25, DC
1 Hq USAF (AFTAC), Wash 25, DC
1 USAF Dep, The Inspector General (AFIDI), Norton AFB, Calif
1 USAF Directorate of Nuclear Safety (AFINS), Kirtland AFB, NM
1 AFOAR, Bldg T-D, Wash 25, DC
1 AFOSR, Bldg T-D, Wash 25, DC

MAJOR AIR COMMANDS

1 AFSC, (SCT), Andrews AFB, Wash 25, DC
1 AUL, Maxwell AFB, Ala
2 USAFIT, Wright-Patterson AFB, Ohio

AFSC ORGANIZATIONS

1 AFSC Regional Office, 6331 Hollywood Blvd., Los Angeles 28, Calif
1 ASD, (ASAPRL), Wright-Patterson AFB, Ohio
3 BSD, (BSR), Norton AFB, Calif
3 SSD, (SSSC-TDC), AF Unit Post Office, Los Angeles 45, Calif
2 ESD, (ESAT), Hanscom Fld, Bedford, Mass
1 AF Msl Dev Cen, (RRRT-Tech Library), Holloman AFB, NM
1 AFMTC, (Tech Library, MU-135), Patrick AFB, Fla
2 APGC, (PGAPI), Eglin AFB, Fla
2 RADC, (Document Library), Griffiss AFB, NY
2 AEDC, (AEOI), Arnold Air Force Station, Tenn

KIRTLAND AFB ORGANIZATIONS

AFSWC, Kirtland AFB, NM

1 (SWEH)
30 (SWOI)
5 (SWRS)
1 US Naval Weapons Evaluation Facility (NWEF) (Code 404), Kirtland AFB, NM

DISTRIBUTION (cont'd)

No. Cys

OTHER AIR FORCE AGENCIES

- 2 Director, USAF Project RAND, via: Air Force Liaison Office,
The RAND Corporation, 1700 Main Street, Santa Monica, Calif

ARMY ACTIVITIES

- 2 Director, Ballistic Research Laboratories (Library), Aberdeen
Proving Ground, Md
- 1 Hq US Army Air Defense Command (ADGCB), Ent AFB, Colo
- 1 Chief of Engineers, Department of the Army (ENGEB),
Wash 25, DC
- 2 Office of the Chief, Corps of Engineers, US Army (Protective
Construction Branch), Wash 25, DC
- 1 Director, Army Research Office, Arlington Hall Sta,
Arlington, Va
- 2 Director, US Army Waterways Experiment Sta (WESRL),
P. O. Box 60, Vicksburg, Miss
- 2 Commanding Officer, US Army Engineers, Research & Develop-
ment Laboratories, Ft Belvoir, Va

NAVY ACTIVITIES

- 1 Chief, Bureau of Yards and Docks, Department of the Navy,
Wash 25, DC
- 1 Commanding Officer, Naval Research Laboratory, Wash 25, DC
- 1 Commanding Officer and Director, Naval Civil Engineering
Laboratory, Port Hueneme, Calif
- 1 Officer-in-Charge, Civil Engineering Corps Officers, US Naval
School, Naval Construction Battalion Center, Port Hueneme, Calif
- 1 Office of Naval Research, Wash 25, DC

OTHER DOD ACTIVITIES

- 1 Chief, Defense Atomic Support Agency (Document Library),
Wash 25, DC
- 2 Commander, Field Command, Defense Atomic Support Agency,
(FCAG3, Special Weapons Publication Distribution), Sandia Base,
NM
- 1 Director, Advanced Research Projects Agency, Department of
Defense, The Pentagon, Wash 25, DC

DISTRIBUTION (cont'd)

No. Cys

- 1 Director, Defense Research & Engineering, The Pentagon,
Wash 25, DC
- 10 ASTIA (TIPDR), Arlington Hall Sta, Arlington 12, Va

AEC ACTIVITIES

- 1 Sandia Corporation, (Technical Library), Sandia Base, NM
- 1 Sandia Corporation, (Technical Library), P. O. Box 969,
Livermore, Calif

OTHER

- 1 Office of Civil Defense Mobilization (OCDM), Battle Creek, Mich
- 2 South Dakota School of Mines and Technology, Department of
Mining Engineering, Rapid City, S. Dak
- 2 University of New Mexico, Air Force Shock Tube Facility,
Box 188, University Station, Albuquerque, NM
- 1 Official Record Copy, (SWRS, Mr. Peterson)
- 5 University of Missouri School of Mines and Metallurgy,
Rollo, Mo

<p>Air Force Special Weapons Center, Kirtland AF Base, New Mexico Rpt. No. AFSC-TR-62-153. EXPERIMENTS ON THE MEASUREMENT OF THE RESPONSE OF ROCK TO DYNAMIC LOADS. Final report, Mar 63, 138 p, incl illus., tables, 37 refs. Unclassified Report</p> <p>The purpose of this study was the development of instrumentation techniques to measure dynamic stress and strain within rock subjected to impulse-type loads. These techniques were to be applicable to the determination of rock response to nuclear explosive loadings. Electric resistance strain gages and piezoelectric stress gages were the sensing devices utilized. Transducers were embedded in concrete test cylinders which were loaded by a plane wave generated by an HE explosive. The sensitivity of the piezoelectric</p>	<ol style="list-style-type: none"> 1. Blast loading 2. High explosives 3. Pressure gages 4. Rocks--Effects of atomic explosions 5. Stress and strain 6. Test equipment I. AFSC Project 1080, Task 108001 II. Contract AF 29(601)-2821 III. Missouri School of Mines and Metallurgy, Rolla IV. Rodney D. Caudle V. DASA WEB No. 13.145 VI. In ASTIA collection 	<p>Air Force Special Weapons Center, Kirtland AF Base, New Mexico Rpt. No. AFSC-TR-62-153. EXPERIMENTS ON THE MEASUREMENT OF THE RESPONSE OF ROCK TO DYNAMIC LOADS. Final report, Mar 63, 138 p, incl illus., tables, 37 refs. Unclassified Report</p> <p>The purpose of this study was the development of instrumentation techniques to measure dynamic stress and strain within rock subjected to impulse-type loads. These techniques were to be applicable to the determination of rock response to nuclear explosive loadings. Electric resistance strain gages and piezoelectric stress gages were the sensing devices utilized. Transducers were embedded in concrete test cylinders which were loaded by a plane wave generated by an HE explosive. The sensitivity of the piezoelectric</p>	<ol style="list-style-type: none"> 1. Blast loading 2. High explosives 3. Pressure gages 4. Rocks--Effects of atomic explosions 5. Stress and strain 6. Test equipment I. AFSC Project 1080, Task 108001 II. Contract AF 29(601)-2821 III. Missouri School of Mines and Metallurgy, Rolla IV. Rodney D. Caudle V. DASA WEB No. 13.145 VI. In ASTIA collection
<p>Air Force Special Weapons Center, Kirtland AF Base, New Mexico Rpt. No. AFSC-TR-62-153. EXPERIMENTS ON THE MEASUREMENT OF THE RESPONSE OF ROCK TO DYNAMIC LOADS. Final report, Mar 63, 138p, incl illus., tables, 37 refs. Unclassified Report</p> <p>The purpose of this study was the development of instrumentation techniques to measure dynamic stress and strain within rock subjected to impulse-type loads. These techniques were to be applicable to the determination of rock response to nuclear explosive loadings. Electric resistance strain gages and piezoelectric stress gages were the sensing devices utilized. Transducers were embedded in concrete test cylinders which were loaded by a plane wave generated by an HE explosive. The sensitivity of the piezoelectric</p>	<ol style="list-style-type: none"> 1. Blast loading 2. High explosives 3. Pressure gages 4. Rocks--Effects of atomic explosions 5. Stress and strain 6. Test equipment I. AFSC Project 1080, Task 108001 II. Contract AF 29(601)-2821 III. Missouri School of Mines and Metallurgy, Rolla IV. Rodney D. Caudle V. DASA WEB No. 13.145 VI. In ASTIA collection 	<p>Air Force Special Weapons Center, Kirtland AF Base, New Mexico Rpt. No. AFSC-TR-62-153. EXPERIMENTS ON THE MEASUREMENT OF THE RESPONSE OF ROCK TO DYNAMIC LOADS. Final report, Mar 63, 138p, incl illus., tables, 37 refs. Unclassified Report</p> <p>The purpose of this study was the development of instrumentation techniques to measure dynamic stress and strain within rock subjected to impulse-type loads. These techniques were to be applicable to the determination of rock response to nuclear explosive loadings. Electric resistance strain gages and piezoelectric stress gages were the sensing devices utilized. Transducers were embedded in concrete test cylinders which were loaded by a plane wave generated by an HE explosive. The sensitivity of the piezoelectric</p>	<ol style="list-style-type: none"> 1. Blast loading 2. High explosives 3. Pressure gages 4. Rocks--Effects of atomic explosions 5. Stress and strain 6. Test equipment I. AFSC Project 1080, Task 108001 II. Contract AF 29(601)-2821 III. Missouri School of Mines and Metallurgy, Rolla IV. Rodney D. Caudle V. DASA WEB No. 13.145 VI. In ASTIA collection

<p>gages utilized was too great for the stress intensities developed, and therefore satisfactory evaluation of the stress measuring technique was not possible. The material presented, summarizing the theoretical aspects of stress and strain measurement at an interior point in a solid, may prove valuable in future embedded gage installations.</p>		<p>gages utilized was too great for the stress intensities developed, and therefore satisfactory evaluation of the stress measuring technique was not possible. The material presented, summarizing the theoretical aspects of stress and strain measurement at an interior point in a solid, may prove valuable in future embedded gage installations.</p>	
<p>gages utilized was too great for the stress intensities developed, and therefore satisfactory evaluation of the stress measuring technique was not possible. The material presented, summarizing the theoretical aspects of stress and strain measurement at an interior point in a solid, may prove valuable in future embedded gage installations.</p>		<p>gages utilized was too great for the stress intensities developed, and therefore satisfactory evaluation of the stress measuring technique was not possible. The material presented, summarizing the theoretical aspects of stress and strain measurement at an interior point in a solid, may prove valuable in future embedded gage installations.</p>	